

The Local Volume HI Survey (LVHIS)^{*}

Bärbel S. Koribalski¹, Jing Wang^{1,6}, P. Kamphuis^{1,7}, T. Westmeier², L. Staveley-Smith², S.-H. Oh^{2,8}, Á.R. López-Sánchez³, O. I. Wong², J. Ott⁴, W.J.G. de Blok⁵, and L. Shao¹

¹*Australia Telescope National Facility, CSIRO Astronomy & Space Science, P.O. Box 76, Epping, NSW 1710, Australia*

²*International Centre for Radio Astronomy Research (ICRAR), University of Western Australia, 35 Stirling Highway, Crawley, WA 6009, Australia*

³*Australian Astronomical Observatory, 105 Delhi Road, North Ryde, NSW 2113, Australia*

⁴*National Radio Astronomy Observatory, P.O. Box 0, 1003 Lopezville Road, Socorro, NM 87801, USA*

⁵*Netherlands Institute for Radio Astronomy, Postbus 2, 7990 AA Dwingeloo, The Netherlands*

⁶*Kavli Institute for Astronomy and Astrophysics, Peking University, Beijing 100871, China*

⁷*National Centre for Radio Astrophysics, TIFR, Ganeshkhind, Pune 411007, India*

⁸*Korea Astronomy and Space Science Institute (KASI), Daedeokdae-ro 776, Yuseong-gu, Daejeon 34055, Republic of Korea*

Received date; accepted date

ABSTRACT

The ‘*Local Volume HI Survey*’ (LVHIS) comprises deep HI spectral line and 20-cm radio continuum observations of 82 nearby, gas-rich galaxies, supplemented by multi-wavelength images. Our sample consists of all galaxies with Local Group velocities $v_{\text{LG}} < 550 \text{ km s}^{-1}$ or distances $D < 10 \text{ Mpc}$ that are detected in the HI Parkes All Sky Survey (HIPASS). Using full synthesis observations in at least three configurations of the Australia Telescope Compact Array (ATCA), we obtain detailed HI maps for a complete sample of gas-rich galaxies with $\delta \lesssim -30^\circ$. Here we present a comprehensive LVHIS galaxy atlas, including the overall gas distribution, mean velocity field, velocity dispersion and position-velocity diagrams, together with a homogeneous set of measured and derived galaxy properties. Our primary goal is to investigate the HI morphologies, kinematics and environment at high resolution and sensitivity. LVHIS galaxies represent a wide range of morphologies and sizes; our measured HI masses range from $\sim 10^7$ to $10^{10} M_\odot$, based on independent distance estimates. The LVHIS galaxy atlas (incl. FITS files) is available on-line.

Key words: surveys — galaxies: dwarf — galaxies: kinematics and dynamics — galaxies: spiral — galaxies: structure — radio lines: galaxies.

1 INTRODUCTION

The ‘*Local Volume*’ (LV), defined here as the sphere of radius 10 Mpc centered on the Local Group (LG), includes more than 500 known galaxies, many of which congregate in well-known groups. Most prominent in the southern hemisphere are the relatively loose Sculptor Group and the more compact Centaurus A Group. Together, their gas-rich members comprise about half of the ‘*Local Volume HI Survey*’ (LVHIS) galaxy sample presented here. With accurate distances available for the majority of the LV galaxies (Karachentsev et al. 2013, hereafter K13, and references therein), it is now possible to study their morphologies, dy-

namics and star formation with respect to their surroundings.

Our long-term aim is to obtain high-resolution HI maps of all LV galaxies and measure their properties in a homogeneous and unbiased way. Wang et al. (2016), for example, present HI diameters (D_{HI}) of over 500 nearby galaxies measured out to an HI mass (M_{HI}) density of $1 M_\odot \text{ pc}^{-2}$ and discuss the tightness of the $M_{\text{HI}}-D_{\text{HI}}$ relation. Large HI projects with radio interferometers, which have targeted LV galaxies, are listed in Table 1. The ‘*Faint Irregular Galaxies GMRT Survey*’ (FIGGS) by Begum et al. (2008), which contains HI results for ~ 60 dwarf irregular LV galaxies, is the largest HI study of nearby galaxies with the Giant Meterwave Radio Telescope (GMRT). The most prominent Very Large Array (VLA) HI projects are ‘*The HI Nearby Galaxy Survey*’ (THINGS; Walter et al. 2008), ‘*Little THINGS*’ (Hunter et al. 2012), and ‘*VLA-ANGST*’ (Ott et al. 2012). HI galaxy surveys with the Westerbork Synthesis Ra-

^{*} The observations were obtained with the Australia Telescope which is funded by the Commonwealth of Australia for operations as a National Facility managed by CSIRO. - E-mail: Baerbel.Koribalski@csiro.au

dio Telescope (WSRT) include the ‘*Westerbork HI Survey of Irregular and Spiral Galaxies*’ (WHISP; van der Hulst et al. 2001) and *HALOGAS* (Heald et al. 2011). Interferometric HI surveys of galaxies beyond the Local Volume include the *VLA Imaging of Virgo in Atomic Gas* (VIVA; Chung et al. 2009), ATLAS-3D, targeting 166 early-type galaxies (Serra et al. 2012), and BlueDisks (Wang et al. 2013).

The LVHIS project comprises the largest number of nearby galaxies studied with the Australia Telescope Compact Array (ATCA); an overview and HI galaxy atlas are presented in this paper. Previous publications based on LVHIS include Koribalski (2008, 2010, 2015, 2017), Bonne (2008), Koribalski & López-Sánchez (2009), van Eymeren et al. (2008, 2009c, 2010), Kirby et al. (2012), López-Sánchez et al. (2008, 2012, 2015), Johnson et al. (2015), Kamphuis et al. (2015), Wang et al. (2016, 2017), and Oh et al. (2018).

The first catalog of LV galaxies was presented by Kraan-Korteweg & Tammann (1979) and contained 179 galaxies with Local Group velocities, v_{LG} , less than 500 km s^{-1} . More recently, the LV sample defined by Karachentsev et al. (2004) included 451 galaxies with $v_{\text{LG}} < 550 \text{ km s}^{-1}$ or independent distance $D < 10 \text{ Mpc}$. A further expansion of the volume ($v_{\text{LG}} < 600 \text{ km s}^{-1}$ or $D < 11 \text{ Mpc}$) led to the most recent nearby galaxy catalog (K13; available at www.sao.ru/lv/lvgdb) which contains 869 galaxies. Of these, only 261 galaxies (30%) lie in the southern sky. Fig. 1 shows the locations of the LVHIS galaxies in the southern sky.

The HI sizes of known LV galaxies cover more than two orders of magnitude, ranging from low-mass dwarf galaxies with diameters of less than 500 pc (e.g., Leo T, Ryan-Weber et al. 2008) to grand-design spirals with HI diameters of nearly 100 kpc , e.g., Circinus (For et al. 2012) and M 83 (Koribalski 2015, 2017). Consequently, their HI masses span more than four orders of magnitudes, ranging from a few times $10^5 M_{\odot}$ to $10^{10} M_{\odot}$ (Wang et al. 2016). The majority of LV galaxies are dwarf galaxies; their morphologies — usually defined in the optical regime — range from the typically gas-poor elliptical (dE) and spheroidal (dSph) dwarfs to gas-rich irregular (dIrr), Magellanic (dM) and blue compact dwarfs (BCD). In between sit the class of dwarf transitional galaxies (dSph/dIrr), many of which show HI gas offset from their stellar disc (e.g., Phoenix, St-Germain et al. 1999).

Our primary goal is to obtain detailed HI gas distributions of LV galaxies, analyse their structure and gas kinematics, measure their overall HI extent, and search for companions. Furthermore, we investigate the influence of the galaxy environment on the shape of the outer HI disc, where gas accretion as well as effects of ram pressure stripping and tidal interactions may be detected. As an example, we refer to the multi-wavelength study of the gas dynamics and star formation in the nearby galaxy pair NGC 1512/1510 (HIPASS J0404–43) by Koribalski & López-Sánchez (2009). The HI disc of the barred spiral galaxy NGC 1512 is spectacular and among the largest in the Local Volume (Koribalski 2017). Its gas distribution and kinematics show the effects of mild interaction with the BCD companion NGC 1510. In regions of high HI column density star formation is prominent, giving rise to a well-defined spiral pattern in the outer disc.

Furthermore, three tidal dwarf galaxy candidates with HI masses around $10^7 M_{\odot}$ have been discovered within the extrapolated spiral/tidal arm of NGC 1512. Another example is the multi-wavelength study of the dIrr galaxies NGC 5408 and IC 4662 by van Eymeren et al. (2010), who find HI discs extending well beyond their stellar extent.

Our paper is structured as follows: in Section 2 we introduce the LVHIS galaxy sample, followed by a description of the ATCA observations and data reduction in Section 3. Our results are presented in Sections 4 & 5 with the latter containing short paragraphs for all LVHIS galaxies and associated galaxies. This is followed by our summary and outlook in Section 6. In the on-line Appendix we present the HI moment maps and position-velocity (pv) diagrams for the majority of LVHIS galaxies.

2 THE LVHIS GALAXY SAMPLE

The ‘*Local Volume HI Survey*’ (LVHIS)¹ comprises deep interferometric HI spectral line and 20-cm radio continuum observations of a complete sample of nearby, gas-rich galaxies and their surroundings. Following Karachentsev et al. (2004), we selected galaxies with $v_{\text{LG}} < 550 \text{ km s}^{-1}$ or, when available, independently determined distances of $D < 10 \text{ Mpc}$. To enable high-resolution HI studies of LV galaxies with the Australia Telescope Compact Array (ATCA), we also require the selected galaxies to have declinations $\delta \lesssim -30^\circ$ and be detected in the HI Parkes All Sky Survey (HIPASS). This ensures that our target galaxies are bright enough for a detailed study of their HI gas distribution and dynamics with a reasonably symmetric synthesized beam. Applying these criteria leads to an ATCA sample of 82 LV galaxies. Fig. 2 shows the HIPASS v_{LG} of all LVHIS galaxies against their best available distances.

2.1 LVHIS — Optical Galaxy Properties

The optical properties of LVHIS galaxies, as obtained from the literature, are given in Table 2. Once multi-wavelength images from the SkyMapper Southern Sky Survey and the Large Synoptic Survey Telescope (LSST) are available, it will be possible to obtain a homogeneous set of optical properties to complement the HI properties of all LVHIS galaxies. The Table 2 columns are: Col. (1+2) HIPASS and optical galaxy name; Col. (3) best available galaxy distance, D , with the reference given in Section 5 (also available from K13 and references therein); Col. (4) morphological type (from RC3, de Vaucouleurs et al. 1991, when available); Col. (5) B -band extinction, A_B , from Schlafly & Finkbeiner (2011); Col. (6) B -band magnitude from Lauberts & Valentijn (1989), using the Cousins B_T (typical uncertainties are $\pm 0.09 \text{ mag}$), when available; Col. (7) $\log L_B$ as calculated from $L_B = D^2 \times 10^{10-0.4(B_T-A_B-M_{B,\odot})} L_{\odot}$ (assuming an absolute B magnitude for the Sun of $M_{B,\odot} = 5.45 \text{ mag}$, Blanton et al. 2003); Col. (8) R -band magnitude (as above); Col. (9) $B-R$ colour; Cols. (10–12) B -band diameter at $25.5 \text{ mag arcsec}^{-2}$, inclination angle, i , and position angle, PA , from Lauberts

¹ LVHIS project webpage: www.atnf.csiro.au/research/LVHIS

Table 1. Major H I surveys of Local Volume galaxies and related surveys at other wavelengths.

Survey Name	Telescope & wavelength	No. of Galaxies	Galaxy types	Distance [Mpc]	Reference
LVHIS (south)	ATCA H I	82		<10	this paper
LVHIS (north)	WSRT H I	23		<10	PI: E. Jütte
WHISP	WSRT H I	375 (0)	dIrr+S		van der Hulst et al. (2001)
HALOGAS	WSRT H I	24 (0)	spirals	3 – 11	Heald et al. (2011)
FIGGS	GMRT H I	60 (8)	dIrr		Begum et al. (2008)
THINGS	VLA H I	34 (3)		3 – 15	Walter et al. (2008)
Little THINGS	VLA H I	41 (0)	dwarfs	<10	Hunter et al. (2012)
VLA-ANGST	VLA H I	35 (0)	dIrr+S	<4	Ott et al. (2012)
	B, R	72 (8)	dIrr	<10	Parodi et al. (2002, 2003)
LSI	AAT NIR	57 (24)		<10	Kirby et al. (2008a,b)
LSI	AAT NIR	40 (32)		<10	Young et al. (2014)
ANGST	HST optical	69 (9)	dwarfs	1 – 4	Dalcanton et al. (2009)
11HUGS	H α , R	400 (29)		1 – 11	Lee et al. (2009)
LVL	Spitzer MIR	258 (27)		<11	Dale et al. (2009)
	GALEX UV	459 (54)		<11	Lee et al. (2011)
	H α	436 (49)		<11	Kennicutt et al. (2008)
SINGS	Spitzer MIR	75 (5)		<30	Kennicutt et al. (2003)
KINGFISH	Herschel FIR	61 (4)		<30	Kennicutt et al. (2011)
HERACLES	IRAM 30-m CO	48 (0)		<30	Leroy et al. (2009)
SINGG	CTIO H α , R	93 (13)			Meurer et al. (2006)

Notes: Col. (3) gives the number of galaxies observed in the specified survey and in brackets the overlap with LVHIS.

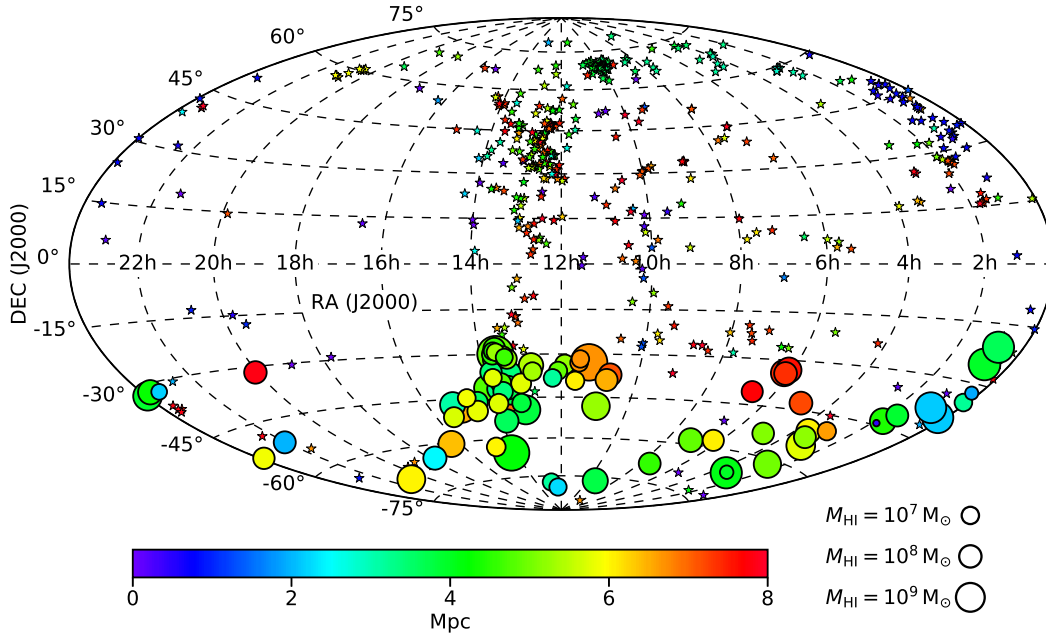


Figure 1. Aitoff distribution of Local Volume (LV) galaxies, highlighting the southern LVHIS galaxies (Dec $\lesssim -30^\circ$) presented in this paper. The H I masses of LVHIS galaxies are indicated by their symbol sizes. Other LV galaxies from the K13 sample are indicated by small stars. The symbol colours indicate the galaxy distances.

Table 2. Optical properties of LVHIS galaxies

(1) HIPASS Name	(2) Galaxy Name	(3) D [Mpc]	(4) type	(5) A_B [mag]	(6) B_T [mag]	(7) $\log L_B$ [L_\odot]	(8) R_T [mag]	(9) $(B - R)$ [mag]	(10) D_{opt} [arcsec]	(11) i [deg]	(12) PA [deg]	(13) group & no. of close neighbours
HIPASS J0008-34	ESO349-G031	3.21	IBm	0.043	15.54	6.99	14.99	0.55	150	—	—	Sculptor 3
	ESO294-G010	1.92	dS0/Im	0.021	15.66	6.49	14.44	1.22	78	40	6	Sculptor 1
HIPASS J0015-32	ESO410-G005	1.92	dS0-a	0.049	14.90	6.81	14.01	0.89	102	35	54	Sculptor 2
HIPASS J0015-39	NGC 55	2.13	SBm	0.048	8.58	9.42	7.84	0.74	2220	74	108	Sculptor 2
HIPASS J0047-20	NGC 247	3.65	SABd	0.065	9.60	9.49	8.80	0.80	1800	73	174	Sculptor 4
HIPASS J0047-25	NGC 253	3.94	SABc	0.068	8.18	10.13	6.66	1.52	1920	76	52	Sculptor 5
HIPASS J0054-37	NGC 300	2.15	Sd	0.046	8.69	9.39	7.46	1.23	1800	48	111	Sculptor 2
HIPASS J0135-41	NGC 625	3.89	SBm	0.059	11.50	8.78	10.61	0.89	390	72	92	Sculptor 2
HIPASS J0145-43	ESO245-G005	4.43	IBm	0.059	12.74	8.40	11.74	1.00	312	16	122	Sculptor 2
HIPASS J0150-44	ESO245-G007	0.42	Im	0.058	13.08	6.26	12.01	1.07	300	26	90	LG 2
HIPASS J0237-61	ESO115-G021	4.99	SBdm	0.094	13.26	8.31	12.06	1.20	510	81	44	0
HIPASS J0256-54	ESO154-G023	5.76	SBm	0.060	10.71	8.61	12.01	0.70	540	80	39	1
HIPASS J0258-49	ESO199-G007	6.6	Sd	0.078	16.44	7.27	16.00	0.44	60	66	4	1
HIPASS J0317-66	NGC 1313	4.07	SBd	0.395	9.98	9.81	8.82	0.56	720	34	39	dw-sp pair 1
HIPASS J0320-52	NGC 1311	5.22	SBm	0.078	13.23	8.35	(12.43)	(0.85)	210	73	40	3
HIPASS J0321-66	AM0319-662	3.98	dIrr	0.303	(17.6)	(6.46)	(16.70)	0.90	(72)	—	—	dw-sp pair 1
HIPASS J0333-50	IC 1959	6.05	SBm	0.040	13.22	8.47	(12.41)	0.81	228	78	147	1
HIPASS J0454-53	NGC 1705	5.11	S0	0.029	12.82	8.48	12.08	0.74	102	45	50	0
HIPASS J0457-42	ESO252-IG001 ¹	7.2	dIrr	0.046	15.28	7.80	15.04	0.24	90	75	56	1
HIPASS J0605-33	ESO364-G7029	7.6	IBm	0.163	13.60	8.57	13.23	0.37	210	44	52	NGC 2188 2
HIPASS J0607-34	AM0605-341	7.4	SBdm	0.132	(14.28)	(8.25)	(14.36)	-0.08	(48)	(76)	(110)	NGC 2188 2
HIPASS J0610-34	NGC 2188	7.4	SBm	0.118	12.10	9.13	11.39	0.71	360	77	175	NGC 2188 2
HIPASS J0615-57	ESO121-G020	6.05	Im	0.151	15.85	7.46	15.49	0.36	78	32	49	dw-dw pair 1
HIPASS J0639-40	ESO308-G022	7.7	dIrr	0.327	16.23	7.59	16.75	-0.52	78	0	—	0
HIPASS J0705-58	AM0704-582	4.90	SBm	0.435	(14.44)	(7.96)	(13.70)	(0.74)	55	45	174	0
HIPASS J0731-68	ESO059-G001	4.57	IBm	0.535	13.74	8.22	12.80	0.94	126	18	84	0
HIPASS J0926-76	NGC 2915	3.78	IO	0.997	12.93	8.56	11.90	1.03	120	60	130	0
HIPASS J1043-37	ESO376-G016	7.1	dIrr	0.212	15.44	7.79	15.24	0.20	60	37	129	1
HIPASS J1047-38	ESO318-G013	6.5	SBd	0.278	15.02	7.91	13.96	1.06	192	81	75	1
HIPASS J1057-48	ESO215-G7009	5.25	dIrr	0.801	16.03	7.53	15.02	1.01	120	60	72	0
HIPASS J1118-32	NGC 3621	6.70	Sd	0.292	9.44	10.17	8.07	1.37	1200	60	159	NGC 3621 2
HIPASS J1131-31	new	6.7	dIrr	0.253	—	—	—	—	—	—	—	NGC 3621 2
HIPASS J1132-32	new	6.7	dIrr	0.226	(17.04)	(7.11)	(16.17)	(0.87)	31	55	113	NGC 3621 3
HIPASS J1137-39	ESO320-G014	6.08	dIrr	0.519	15.85	7.62	15.17	0.68	66	35	86	0
HIPASS J1154-33	ESO379-G007	5.22	dIrr	0.270	16.60	7.08	15.50	1.10	78	32	90	3
HIPASS J1204-35	ESO379-G024	4.9	dIrr	0.270	16.58	7.04	16.37	0.21	72	41	30	2
HIPASS J1214-38	ESO321-G014	3.18	IBm	0.342	15.21	7.24	14.11	1.10	126	65	20	1
HIPASS J1219-79	IC 3104	2.27	IBm	1.486	13.65	8.03	12.04	1.61	180	55	45	2
HIPASS J1244-35	ESO381-G018	5.32	dIrr	0.228	15.79	7.41	14.84	0.95	72	54	83	wide pair 1
HIPASS J1246-33	ESO381-G020	5.44	IBm	0.238	14.24	8.05	13.50	0.74	270	66	138	wide pair 1
HIPASS J1247-77	new	3.16	Im	2.747	(17.49)	(7.30)	(16.25)	1.24	—	—	—	2
HIPASS J1305-40	CEN06	5.78	dIrr	0.372	(15.92)	(7.48)	(15.04)	0.88	(60)	—	—	(Cen A) 4
HIPASS J1305-49	NGC 4945	3.80	SBcd	0.640	9.31	9.87	7.55	1.76	1560	77	43	Cen A 3
HIPASS J1310-46A	ESO269-G058	3.80	IO	0.394	12.50	8.50	11.31	1.19	180	48	69	Cen A 8
HIPASS J1321-31	new	5.22	dSph/dIrr	0.222	(17.1)	(6.86)	—	—	(78)	—	—	(M83) 10
HIPASS J1321-36	NGC 5102	3.40	S0	0.199	9.74	9.43	8.47	1.27	720	65	48	Cen A 4
HIPASS J1324-30	AM1321-304	4.63	dIrr	0.250	(16.25)	(7.11)	—	—	(51)	—	—	M83 9
HIPASS J1324-42	NGC 5128	3.77	S0	0.416	7.60	10.45	6.29	1.31	1800	40	35	Cen A 9
HIPASS J1326-30A	IC 4247	4.97	S?	0.235	14.41	7.90	13.74	0.67	90	66	158	M83 14
HIPASS J1327-41	ESO324-G024	3.73	Im	0.409	12.91	8.32	12.13	0.78	270	41	50	Cen A 9
HIPASS J1334-45	ESO270-G017	6.95	SBm	0.404	11.69	9.35	10.03	1.66	1020	83	118	Cen A 9
HIPASS J1336-29	UGCA 365	5.25	Im	0.192	15.49	7.50	14.81	0.68	102	66	31	M83 10
HIPASS J1337-29	NGC 5236	4.92	Sc	0.241	8.22	10.37	7.34	0.88	1080	0	—	M83 9
HIPASS J1337-39	new	4.83	Im	0.271	(16.08)	(7.22)	(16.27)	(-0.19)	(36)	—	—	(Cen A) 7
HIPASS J1337-42	NGC 5237	3.40	IO	0.358	13.26	8.08	12.34	0.92	114	33	128	Cen A 8
HIPASS J1337-28	ESO444-G084	4.61	Im	0.249	15.01	7.60	15.05	-0.04	96	36	(126)	M83 8
HIPASS J1339-31	NGC 5253	3.56	Im	0.202	11.17	8.90	(10.11)	(1.06)	360	71	45	Cen A 10
HIPASS J1340-28	IC 4316	4.41	IBm	0.198	(14.97)	(7.56)	—	—	96	36	(56)	M83 9
HIPASS J1341-29	NGC 5264	4.53	IBm	0.184	12.58	8.53	11.49	1.09	210	31	(65)	M83 9
HIPASS J1345-41	ESO325-G7011	3.40	IBm	0.319	14.02	7.76	13.49	0.53	240	60	118	Cen A 6
HIPASS J1348-37	new	5.75	dIrr	0.281	(17.00)	(7.01)	(16.45)	(0.55)	—	—	—	Cen A 5
HIPASS J1348-53	ESO174-G7001	3.6	Im?	1.817	(14.44)	(8.24)	(14.20)	(0.24)	180	71	170	Cen A 0
HIPASS J1349-36	ESO383-G087	3.45	SBdm	0.260	11.00	8.96	10.11	0.89	360	24	(93)	Cen A 3
HIPASS J1351-47	new	5.73	dIrr	0.523	(16.51)	(7.30)	(15.83)	(0.68)	—	—	—	Cen A 2
HIPASS J1403-41	NGC 5408	4.81	IBm	0.248	12.59	8.61	11.96	0.63	156	52	62	Cen A 3
HIPASS J1413-65	Circinus	4.2	Sb	5.279	8.90	9.86	—	—	714	65	210	1
HIPASS J1428-46	UKS1424-460	3.58	IBm	0.472	—	—	—	—	(21)	(69)	—	Cen A 2
HIPASS J1434-49	ESO222-G010	5.8	dIrr	0.978	(14.82)	(8.17)	(14.57)	(0.25)	60	60	8	3
HIPASS J1441-62	new	6.0	dIrr	4.909	—	—	—	—	—	—	—	1
HIPASS J1443-44	ESO272-G025	5.9	dIrr	0.595	14.79	8.04	14.00	0.79	84	50	62	3
HIPASS J1501-48	ESO223-G009	6.49	Im	0.942	(12.28)	(9.27)	(12.53)	(-0.25)	240	41	135	4
HIPASS J1514-46	ESO274-G001	3.09	Sd	0.914	12.00	8.85	10.97	1.03	900	80	38	2
HIPASS J1526-51	new	5.7	dIrr	2.299	—	—	—	—	—	—	—	2
HIPASS J1620-60	ESO137-G018	6.40	Sc	0.888	12.23	9.26	11.03	1.20	240	68	29	0
HIPASS J1747-64	IC 4662	2.44	IBm	0.254	12.33	8.12	11.01	1.32	180	58	104	1
HIPASS J2003-31	ESO461-G036	7.83	dIrr	1.100	17.06	7.58	(16.35)	(0.71)	72	60	22	0
HIPASS J2052-69	IC 5052	6.03	SBd	0.184	11.58	9.18	10.91	0.67	390	79	142	0
HIPASS J2202-51	IC 5152	1.97	Im	0.91	11.03	8.72	10.19	0.84	360	48	100	Sculptor 1
HIPASS J2326-32	UGCA 438	2.18	IBm	0.053	13.89	7.32	13.19	0.70	102	28	(138)	Sculptor 1
HIPASS J2343-31	UGCA 442	4.27	SBm	0.061	13.46	8.08	13.06	0.40	300	78	48	Sculptor 3
HIPASS J2352-52	ESO149-G003	5.9	IBm	0.050	15.05	7.72	(14.73)	(0.32)	180	80	148	Sculptor 0
HIPASS J2357-32	NGC 7793	3.91	Sd	0.070	9.72	9.50	8.71	1.01	840	55	98	Sculptor 2

Notes: — Col. (3): Tully-Fisher (TF), Hubble (H_0), and membership (mem) distances are here given to one decimal accuracy, while TRGB and cepheid distances are given to two decimal points. ¹The optical properties listed are for ESO252-IG001 NED01.

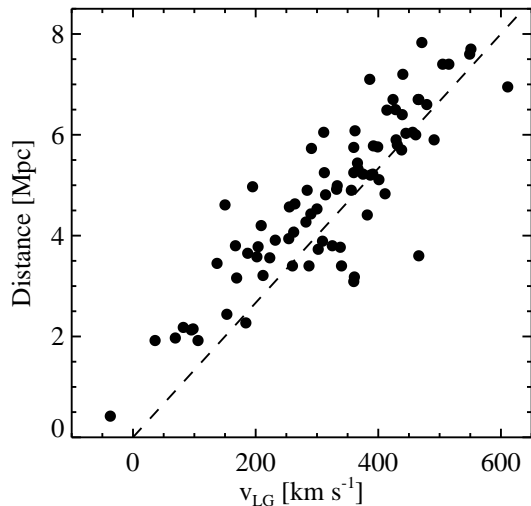


Figure 2. Distance versus Local Group velocity v_{LG} for all LVHIS galaxies as listed in Tables 2 and 4, respectively. The dashed line corresponds to $D = v_{\text{LG}} / H_0$, where H_0 is the Hubble constant (here $75 \text{ km s}^{-1} \text{ Mpc}^{-1}$).

(1982); Col. (13) galaxy subgroup and number of close neighbours (within $300'$ and $v_{\text{sys}} < 800 \text{ km s}^{-1}$). When magnitudes are not available in the Cousins filters (Lauberts & Valentijn 1989), we use SuperCosmos B_J and R magnitudes from Doyle et al. (2005) for AM0605–34, HIPASS J1337–29, ESO174-G?001, ESO222-G010 and ESO223-G009, and HST F606W/814W magnitudes for HIPASS J1247–77, CEN06, HIPASS J1348–37, and HIPASS J1351–47; these are less reliable due to calibration issues and are given in brackets.

For most of our sample, we use distance estimates from HST observations of the tip of the red giant branch (TRGB), which typically have uncertainties of 10%. Occasionally we use distances determined from the luminosity of cepheids, surface brightness fluctuations (SBF), the Tully-Fisher (TF) relation or based on group membership. For details see the descriptions of individual galaxies in Section 5.

Histograms of LVHIS galaxy properties are shown in Fig. 3, highlighting the wide ranges of, e.g., stellar colours, stellar masses (M_*) and H I mass to light ratios (M_{HI} / L_B). We note that Table 2 provides absolute B -band magnitudes and optical diameters (D_{opt} ; see Col. 10 in Table 2) for most of the galaxies with $M_{\text{HI}} > 10^7 M_{\odot}$ and R -band magnitudes for most of galaxies with $M_{\text{HI}} > 10^8 M_{\odot}$.

In Table 3 we give an (incomplete) overview of complementary datasets available for LVHIS galaxies. For example, Kirby et al. (2008a,b) and Young et al. (2014) obtained deep AAT H -band images of LVHIS dwarf galaxies to better understand their stellar populations. $H\alpha$ surveys of LV galaxies were carried out by — among others — Larsen & Richtler (1999), Rossa & Dettmar (2003), Karachentsev et al. (2005), Kaisin & Karachentsev (2006), Meurer et al. (2006), Kaisin et al. (2007), Bouchard et al. (2009), and Côté et al. (2009).

2.2 LVHIS — HIPASS Galaxy Properties

HIPASS covers two thirds of the sky (up to $\text{DEC} = +25^\circ$) and has an r.m.s. noise of $\sim 13 \text{ mJy beam}^{-1}$ per 13.2 km s^{-1} channel width. The HIPASS velocity resolution is 18 km s^{-1} . For details of the observations, calibration and imaging techniques see Barnes et al. (2001). A typical 3σ H I flux (F_{HI}) detection limit for galaxies with a velocity width of 50 km s^{-1} is 2 Jy km s^{-1} , and the respective H I column density limit is $N_{\text{HI}} \sim 10^{18} \text{ cm}^{-2}$ (for H I gas filling the $15.5'$ gridded beam). Efforts are currently under way to create an improved, significantly deeper version of the survey (HIPASS 2); for details and first results see Calabretta et al. (2014) and Westmeier et al. (2017). While most of the galaxies selected here are listed in the HIPASS Bright Galaxy Catalog (BGC; Koribalski et al. 2004) and/or in the southern HIPASS catalog (HICAT; Meyer et al. 2004), a few of the fainter LV galaxies missed out either because of the velocity cutoff used for HICAT ($v_{\text{GSR}} > 300 \text{ km s}^{-1}$; to avoid inclusion of HVCs and Galactic H I emission) or confusion with neighbouring large galaxies. The HIPASS properties of LVHIS galaxies are useful for comparison with our integrated ATCA H I spectra, in particular to estimate the amount of diffuse H I emission filtered out by the interferometer.

Table 4 gives the HIPASS properties of the LVHIS galaxies; the columns are as follows: Col. (1+2) HIPASS and optical galaxy name; Col. (3) the Local Group velocity, v_{LG} , as calculated in Koribalski et al. (2004); Col. (4+5) the H I flux density, F_{HI} , and its uncertainty, eF_{HI} ; Col. (6) logarithm of the H I mass, M_{HI} , as calculated from F_{HI} , as listed here, using the distance D given in Table 2; Col. (7) H I systemic velocity in the optical, heliocentric velocity frame, v_{hel} ; Cols. (8+9) H I velocity widths determined at 50% and 20% of the H I peak flux; Col. (10) HIPASS catalog from which the data were extracted: B99 = Banks et al. (1999), HIDEEP = Minchin et al. (2003), BGC = Koribalski et al. (2004), and HICAT = Meyer et al. (2004); and Col. (11) notes on the HIPASS sources: e = extended, c = confused, r = baseline ripple.

3 OBSERVATIONS AND DATA REDUCTION

Using the Australia Telescope Compact Array (ATCA) we obtained sensitive H I spectral line and 20-cm radio continuum data for a complete sample of 82 gas-rich galaxies in the Local Volume. Each LVHIS galaxy was typically observed for a full synthesis (12 hrs) in three different ATCA configurations, providing good sensitivity to both small- and large-scale structures. The three ATCA configurations combined provide 45 antenna baselines with lengths ranging from 30 m to 6 km and a total on-source integration time of typically ~ 30 hrs per target galaxy.

The observations, which are summarised in Table 5, were carried out with the original ATCA correlator using two intermediate frequency (IF) bands. The first band (IF 1) was typically centred on 1418 MHz with a bandwidth of 8 MHz, divided into 512 channels. This covers an H I velocity range from about -200 km s^{-1} to $+1200 \text{ km s}^{-1}$ with a velocity resolution of 4 km s^{-1} . The ATCA primary beam

Table 3. Multi-wavelength coverage for LVHIS galaxies

HIPASS Name	Galaxy Name	NIR	H α	Other	Other H I surveys
HIPASS J0008–34	ESO349-G031	H-band (K08)	K07, B09		
	ESO294-G010	H-band (K08)	B09	ANGST	
HIPASS J0015–32	ESO410-G005	H-band (Y14)	B09-N	ANGST	
HIPASS J0015–39	NGC 55		F96	ANGST, 11HUGS	
HIPASS J0047–20	NGC 247		LR99	ANGST, 11HUGS	
HIPASS J0047–25	NGC 253		(SINGG)	ANGST, 11HUGS	
HIPASS J0054–37	NGC 300		LR99	ANGST, 11HUGS	
HIPASS J0135–41	NGC 625	H-band (K08)	SINGG	11HUGS	
HIPASS J0145–43	ESO245-G005	H-band (K08)	SINGG	11HUGS	
HIPASS J0150–44	ESO245-G007				
HIPASS J0237–61	ESO115-G021	H-band (K08)		11HUGS	
HIPASS J0256–54	ESO154-G023	H-band (K08)	SINGG	11HUGS	
HIPASS J0258–49	ESO199-G007	H-band (Y14)			
HIPASS J0317–66	NGC 1313	H-band (K08)	(SINGG)	11HUGS	
HIPASS J0320–52	NGC 1311	H-band (K08)	SINGG	11HUGS	
HIPASS J0321–66	AM0319–662	H-band (K08)			
HIPASS J0333–50	IC 1959	H-band (K08)	SINGG	11HUGS	
HIPASS J0454–53	NGC 1705	H-band (K08)	SINGG	11HUGS, SINGS	
HIPASS J0457–42	ESO252-G001		SINGG		
HIPASS J0605–33	ESO364-G7029	H-band (K08)			
HIPASS J0607–34	AM0605–341	H-band (Y14)			
HIPASS J0610–34	NGC 2188	H-band (Y14)	RD03		
HIPASS J0615–57	ESO121-G020	H-band (K08)			
HIPASS J0639–40	ESO308-G022	H-band (K08)			
HIPASS J0705–58	AM0704–582	H-band (K08)			
HIPASS J0731–68	ESO059-G001	H-band (K08)			
HIPASS J0926–76	NGC 2915	H-band (K08)		11HUGS, SINGS, KINGFISH	
HIPASS J1043–37	ESO376-G016				
HIPASS J1047–38	ESO318-G013	H-band (Y14)			
HIPASS J1057–48	ESO215-G7009				
HIPASS J1118–32	NGC 3621			11HUGS, SINGS, KINGFISH	THINGS
HIPASS J1131–31	new				
HIPASS J1132–32	new				
HIPASS J1137–39	ESO320-G014	H-band (Y14)			
HIPASS J1154–33	ESO379-G007	H-band (Y14)	B09		FIGGS
HIPASS J1204–35	ESO379-G024	H-band (Y14)			
HIPASS J1214–38	ESO321-G014	H-band (Y14)	B09	ANGST	FIGGS
HIPASS J1219–79	IC 3104				
HIPASS J1244–35	ESO381-G018				
HIPASS J1246–33	ESO381-G020		B09	11HUGS	
HIPASS J1247–77	new				
HIPASS J1305–40	CEN06	H-band (Y14)	C09		
HIPASS J1305–49	NGC 4945				
HIPASS J1310–46A	ESO269-G058	H-band (Y14)			
HIPASS J1321–31	new	H-band (Y14) – N	SINGG – N		FIGGS
HIPASS J1321–36	NGC 5102				
HIPASS J1324–30	AM1321–304	H-band (Y14)	B09		FIGGS
HIPASS J1324–42	NGC 5128				
HIPASS J1326–30A	IC 4247	H-band (Y14)		11HUGS	
HIPASS J1327–41	ESO324-G024	H-band (Y14)	C09	11HUGS	
HIPASS J1334–45	ESO270-G017				
HIPASS J1336–29	UGCA 365	H-band (Y14)	C09		FIGGS
HIPASS J1337–29	NGC 5236		SINGG	11HUGS	THINGS
HIPASS J1337–39	new	H-band (Y14) – M	G07		
HIPASS J1337–42	NGC 5237	H-band (Y14)	C09		
HIPASS J1337–28	ESO444-G084	H-band (Y14)	SINGG	11HUGS	
HIPASS J1339–31	NGC 5253	H-band (Y14)	SINGG	11HUGS	
HIPASS J1340–28	IC 4316	H-band (Y14)	C09		FIGGS
HIPASS J1341–29	NGC 5264	H-band (Y14)	C09	11HUGS	
HIPASS J1345–41	ESO325-G7011	H-band (Y14)	C09		
HIPASS J1348–37	new	H-band (Y14) – N			
HIPASS J1348–53	ESO174-G7001	H-band (K08) – N			
HIPASS J1349–36	ESO383-G087	H-band (Y14)	C09		
HIPASS J1351–47	new	H-band (Y14) – N			
HIPASS J1403–41	NGC 5408		C09	SINGS, KINGFISH	
HIPASS J1413–65	Circinus		E98		
HIPASS J1428–46	UKS1424–460	H-band (Y14) – N	K07, C09		FIGGS
HIPASS J1434–49	ESO222-G010	H-band (Y14)	K07, C09		
HIPASS J1441–62	new				
HIPASS J1443–44	ESO272-G025	H-band (Y14)	K07, C09		
HIPASS J1501–48	ESO223-G009	H-band (Y14)	C09		
HIPASS J1514–46	ESO274-G001	H-band (Y14)	RD03, C09		
HIPASS J1526–51	new				
HIPASS J1620–60	ESO137-G018		K07		
HIPASS J1747–64	IC 4662	H-band (K08)	K07	11HUGS	
HIPASS J2003–31	ESO461-G036	H-band (K08)			FIGGS
HIPASS J2052–69	IC 5052	H-band (K08)	SINGG, RD03, K07	11HUGS	
HIPASS J2202–51	IC 5152	H-band (K08)	K07	ANGST, 11HUGS	
HIPASS J2326–32	UGCA 438	H-band (K08)	K07	ANGST, 11HUGS	FIGGS
HIPASS J2343–31	UGCA 442	H-band (K08)	(SINGG)	11HUGS	
HIPASS J2352–52	ESO149-G003	H-band (Y14)	(SINGG), K07	11HUGS	
HIPASS J2357–32	NGC 7793	H-band (K08)	(SINGG), SINGS, LR99	11HUGS, SINGS, KINGFISH	THINGS

Notes: F96 = Ferguson et al. (1996), E98 = Elmouttie et al. (1998a), LR99 - Larsen & Richtler (1999), RD03 = Rossa & Dettmar (2003), K08 = Kirby et al. (2008b), Y14 = Young et al. (2014), G07 = Grossi et al. (2007), K07 = Kaisin et al. (2007), B09 = Bouchard et al. (2009), C09 = Côté et al. (2009). — Brackets indicate that the data have not yet been publicly released. N = not detected; M = marginal detection. — The named surveys are described in Table 2.

Table 4. HIPASS properties of the LVHIS galaxies

(1) HIPASS Name	(2) Galaxy Name	(3) $v_{\text{LG}}^{\text{HI}}$ [km s^{-1}]	(4) $F_{\text{HI}}^{\text{HI}}$ [Jy km s^{-1}]	(5) $e F_{\text{HI}}^{\text{HI}}$ [Jy km s^{-1}]	(6) $\log M_{\text{HI}}^{\text{HI}}$ [M_{\odot}]	(7) $v_{\text{hel}}^{\text{HI}}$ [km s^{-1}]	(8) w_{50}^{HI} [km s^{-1}]	(9) w_{20}^{HI} [km s^{-1}]	(10) HIPASS catalog	(11) notes
HIPASS J0008-34	ESO349-G031	212	5.8	1.6	7.15	221	30	79	BGC	
HIPASS J0015-32	ESO294-G010	(106)	—	—	—	—	—	—	—	(ATCA)
HIPASS J0015-39	ESO410-G005	(36)	—	—	—	—	—	—	—	(ATCA)
HIPASS J0015-39	NGC 55	95	1990.2	145.1	9.33	129	169	197	BGC	e
HIPASS J0047-20	NGC 247	187	608.2	42.1	9.28	156	198	224	BGC	e
HIPASS J0047-25	NGC 253	254	692.9	42.2	9.40	243	407	431	BGC	e
HIPASS J0054-37	NGC 300	98	1972.6	156.1	9.33	146	147	166	BGC	e
HIPASS J0135-41	NGC 625	309	30.9	3.6	8.04	396	75	99	BGC	
HIPASS J0145-43	ESO245-G005	290	81.0	9.1	8.57	391	60	85	BGC	
	ESO245-G007	(-37)	—	—	—	(-23)	—	—	—	(ATCA)
HIPASS J0237-61	ESO115-G021	333	97.6	8.2	8.76	515	121	145	BGC	
HIPASS J0256-54	ESO154-G023	399	139.2	11.6	9.01	574	122	143	BGC	
HIPASS J0258-49	ESO199-G007	479	2.1	1.5	7.33	631	55	74	HICAT	
HIPASS J0317-66	NGC 1313	262	462.7	32.6	9.26	470	168	196	BGC	e
HIPASS J0320-52	NGC 1311	387	14.6	3.2	7.97	568	80	105	BGC	
HIPASS J0321-66	AM0319-662	(532)	—	—	—	—	—	—	—	(ATCA)
HIPASS J0333-50	IC 1959	456	27.2	3.2	8.37	640	128	155	BGC	
HIPASS J0454-53	NGC 1705	401	15.4	2.6	7.98	632	108	165	BGC	
HIPASS J0457-42	ESO252-IG001	440	10.9	1.9	8.13	657	58	99	BGC	
HIPASS J0605-33	ESO364-G7029	549	17.6	2.5	8.38	786	75	94	BGC	
HIPASS J0607-34	AM0605-341	515	9.0	2.1	8.07	766	123	211	HICAT	
HIPASS J0610-34	NGC 2188	505	32.5	3.9	8.62	747	111	149	BGC	
HIPASS J0615-57	ESO121-G020	311	14.1	2.9	8.09	577	65	96	BGC	c
HIPASS J0639-40	ESO308-G022	551	3.8	1.5	7.73	822	52	74	HICAT	
HIPASS J0705-58	AM0704-582	284	34.8	4.4	8.29	564	68	84	BGC	
HIPASS J0731-68	ESO059-G001	255	17.7	2.5	7.94	530	82	104	BGC	
HIPASS J0926-76	NGC 2915	204	108.4	13.9	8.56	468	148	164	BGC	e
HIPASS J1043-37	ESO376-G016	386	10.3	1.9	8.09	668	33	53	BGC	
HIPASS J1047-38	ESO318-G013	428	8.6	3.0	7.93	711	42	71	BGC	
HIPASS J1057-48	ESO215-G7009	312	104.4	11.5	8.83	598	67	83	BGC	
HIPASS J1118-32	NGC 3621	466	884.3	56.2	9.97	730	271	293	BGC	e
HIPASS J1131-31	new	465	2.5	1.8	7.42	717	29	—	—	
HIPASS J1132-32	new	424	2.8	1.8	7.47	699	59	105	HICAT	uncertain
HIPASS J1137-39	ESO320-G014	362	2.5	1.4	7.34	654	40	61	HICAT	
HIPASS J1154-33	ESO379-G007	391	5.2	1.7	7.52	641	25	45	BGC	
HIPASS J1204-35	ESO379-G024	356	3.4	1.4	7.28	631	39	58	HICAT	
HIPASS J1214-38	ESO321-G014	361	6.4	1.6	7.18	610	30	49	BGC	
HIPASS J1219-79	IC 3104	184	10.3	2.5	7.10	429	40	63	BGC	
HIPASS J1244-35	ESO381-G018	367	3.3	1.3	7.34	625	40	62	HICAT	
HIPASS J1246-33	ESO381-G020	366	30.9	3.7	8.34	589	83	100	BGC	
HIPASS J1247-77	new	169	4.7	1.4	7.04	413	32	46	BGC	
HIPASS J1305-40	CEN06	392	5.1	1.9	7.60	617	33	46	BGC	
HIPASS J1305-49	NGC 4945	325	319.1	20.7	9.04	563	361	386	BGC	e
HIPASS J1310-46A	ESO269-G058	167	7.2	2.3	7.39	400	62	84	B99	
HIPASS J1321-31	new	375	5.9	1.6	7.58	571	31	47	BGC	
HIPASS J1321-36	NGC 5102	260	80.1	6.0	8.34	468	200	222	BGC	
HIPASS J1324-30	AM1321-304	264	3.9	2.5	7.30	500	34	66	B99	
HIPASS J1324-42	NGC 5128	338	91.8	13.2	8.48	556	477	542	BGC	er
HIPASS J1326-30A	IC 4247	195	3.4	0.8	7.30	420	33	49	B99, HIDEEP	
HIPASS J1327-41	ESO324-G024	302	47.5	5.5	8.19	516	81	107	BGC	
HIPASS J1334-45	ESO270-G017	611	199.4	15.1	9.36	828	141	158	BGC	
HIPASS J1336-29	UGCA 365	360	1.2	1.2	7.04	572	30	43	HICAT	
HIPASS J1337-29	NGC 5236	332	1630.3	95.8	9.97	513	259	287	BGC	ec
HIPASS J1337-39	new	287	6.6	1.8	7.56	492	37	53	BGC	
HIPASS J1337-42	NGC 5237	150	12.1	2.6	7.52	361	77	96	BGC	
HIPASS J1337-28	ESO444-G084	411	21.1	3.2	8.02	587	56	75	BGC	
HIPASS J1339-31A	NGC 5253	223	44.4	4.7	8.12	407	67	104	BGC	
HIPASS J1340-28	IC 4316	382	2.1	0.2	6.98	581	?	50	HIDEEP	
HIPASS J1341-29	NGC 5264	300	12.8	2.4	7.79	478	35	55	BGC	
HIPASS J1345-41	ESO325-G7011	340	26.6	3.7	7.86	545	59	75	BGC	
HIPASS J1348-37	new	360	2.5	1.5	7.29	581	39	60	HICAT	
HIPASS J1348-53	ESO174-G7001	466	55.1	5.9	8.23	688	71	103	BGC	
HIPASS J1349-36	ESO383-G087	137	27.7	4.2	7.89	326	33	52	BGC	
HIPASS J1351-47	new	291	3.5	1.3	7.43	530	39	59	HICAT	
HIPASS J1403-41	NGC 5408	314	61.5	6.7	8.53	506	62	112	BGC	
HIPASS J1413-65	Circinus	209	1450.5	97.9	9.78	434	242	284	BGC	e
HIPASS J1428-46	UKS1424-460	202	17.3	2.6	7.72	390	48	66	BGC	
HIPASS J1434-49	ESO222-G010	431	7.0	2.0	7.74	622	38	62	BGC	
HIPASS J1441-62	new	461	4.7	2.8	7.60	672	52	68	BGC	
HIPASS J1443-44	ESO272-G025	429	1.7	1.3	7.15	627	42	71	HICAT	
HIPASS J1501-48	ESO223-G009	414	101.3	11.3	9.00	588	61	89	BGC	
HIPASS J1514-46	ESO274-G001	360	120.2	10.3	8.43	522	167	181	BGC	
HIPASS J1526-51	new	438	6.0	2.6	7.66	605	39	60	BGC	
HIPASS J1620-60	ESO137-G018	439	37.4	4.9	8.56	605	139	155	BGC	
HIPASS J1747-64	IC 4662	153	130.0	12.0	8.26	302	86	133	BGC	
HIPASS J2003-31	ESO461-G036	471	7.5	1.8	8.04	427	72	105	HICAT	
HIPASS J2052-69	IC 5052	445	101.7	7.6	8.94	584	174	203	BGC	
HIPASS J2202-51	IC 5152	69	97.2	9.5	7.95	122	84	100	BGC	
HIPASS J2326-32	UGCA 438	(82)	—	—	—	—	—	—	—	(ATCA)
HIPASS J2343-31	UGCA 442	282	50.1	5.3	8.33	267	94	112	BGC	
HIPASS J2352-52	ESO149-G003	491	6.9	1.6	7.75	576	39	70	BGC	
HIPASS J2357-32	NGC 7793	232	278.5	20.4	9.00	227	172	191	BGC	e

Notes: Col. (10) HIPASS catalogs: B99 (Banks et al. 1999), HIDEEP (Minchin et al. 2003), BGC (Koribalski et al. 2004), HICAT (Meyer et al. 2004); Col. (11) e = extended, c = confused, r = severe baseline ripple.

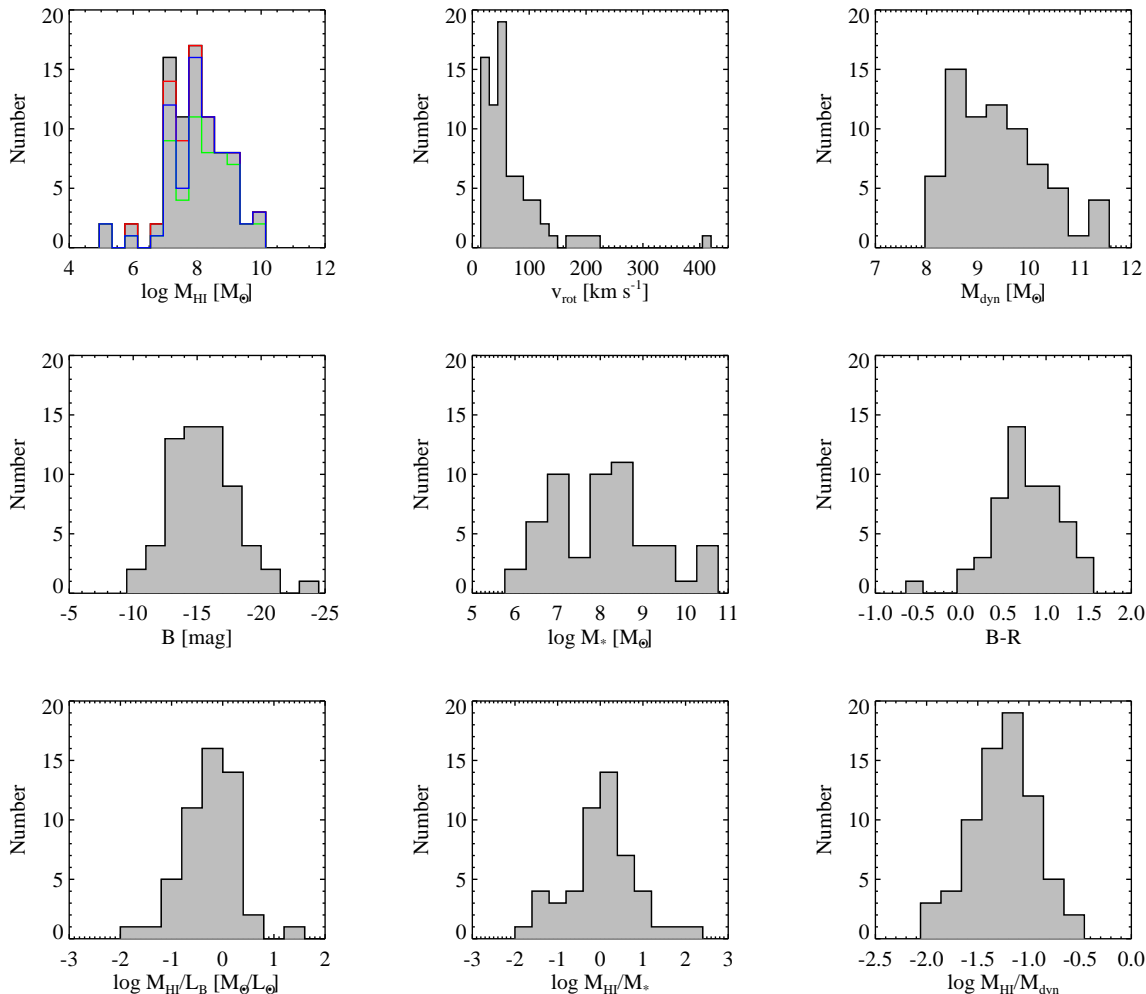


Figure 3. Histograms of LVHIS galaxy properties as given Tables 2, 6 and 8. The stellar mass, M_* , is estimated from the B -band magnitudes and $B - R$ colours based on the formula by Bell et al. (2003). The M_{HI} histogram (top left) shows all LVHIS galaxies (black), those with available B -band magnitudes (red), optical diameters (blue) and both B - and R -band magnitudes (green).

is 33.6 at 1418 MHz, i.e. the sensitivity of a single-pointing ATCA observation drops to 50% at a distance of 16.8 from the pointing centre. Large galaxies like NGC 55, NGC 247, NGC 300, M 83, NGC 3621 and Circinus were mosaicked to ensure that the extended HI emission of the outer disc was not missed. The second band (IF 2) was centred on 1384 MHz with a bandwidth of 128 MHz, divided into 32 channels to observe the 20-cm radio continuum emission. The results will be presented in a companion paper (Shao et al. 2017).

Data reduction was carried out with the MIRIAD software package (Sault, Teuben & Wright 1995) using standard procedures. The IF 1 data were split into a narrow band 20-cm radio continuum and an HI line data set using a first order fit to the line-free channels. For this paper the HI channel maps were made using ‘natural’ (na) weighting of the uv -data in the velocity range covered by the HI emission using steps of 4 km s^{-1} . We use the shortest 30 baselines of the combined data sets to study the large-scale HI emission in and around the selected galaxies. Together these provide good uv -coverage, angular resolution $\gtrsim 40''$ (ie., $\sim 1 \text{ kpc}$ at

$D = 5 \text{ Mpc}$) and sensitivity to structures up to $\sim 12'$. An on-source integration time of 30 hrs results in a theoretical r.m.s. sensitivity of $\sim 1.5 \text{ mJy beam}^{-1}$ per 4 km s^{-1} channel, which is reached in most of our data cubes.

In addition we made HI cubes with low velocity resolution (20 km s^{-1}), covering the whole observed velocity range. These cubes were then searched for extragalactic HI from companions and more distant galaxies (up to $\sim 1200 \text{ km s}^{-1}$) within the primary beam area. The rms of these cubes is typically $0.8 \text{ mJy beam}^{-1}$.

HI moment maps were obtained by applying a $\sim 3\sigma$ cut-off to the HI data cubes. No masking was applied here, but may in future be used to better study the outer HI edges and haloes of the LVHIS galaxies. Our 3σ HI column density (N_{HI}) sensitivity (for $\sigma = 1.5 \text{ mJy beam}^{-1}$) is $\sim 2.8 \times 10^{19} \text{ cm}^{-2}$ over 20 km s^{-1} for gas filling a $60''$ synthesized beam. All ATCA HI properties for LVHIS galaxies are obtained from primary-beam corrected cubes and moment maps.

The Table 5 columns are: Col. (1+2) HIPASS and optical galaxy name; Col. (3–5) ATCA configuration names. — Galaxies marked with a single (double) star in Col. (1) have

Table 5. ATCA H I observations of LVHIS galaxies

HIPASS Name	Galaxy Name	ATCA configurations		
HIPASS J0008-34	ESO349-G031	EW352	750B	1.5A
	ESO294-G010		750D	
HIPASS J0015-32	ESO410-G005	EW367	750B	1.5C
HIPASS J0015-39**	NGC 55	EW352/367	H I mosaic	
HIPASS J0047-20**	NGC 247	EW352/367	H I mosaic	
HIPASS J0047-25**	NGC 253	375/EW367	750A/B	1.5A/B/G
HIPASS J0054-37**	NGC 300	EW352/367	H I mosaic	
HIPASS J0135-41*	NGC 625	EW352	750D	1.5A
HIPASS J0145-43	ESO245-G005	EW352	750D	1.5C
HIPASS J0150-44	ESO245-G007	375/750D	H I mosaic	
HIPASS J0237-61*	ESO115-G021	EW352	750D	1.5C
HIPASS J0256-54*	ESO154-G023	EW367	750D	1.5C
HIPASS J0258-49	ESO199-G007	EW352	750B	1.5C
HIPASS J0317-66*	NGC 1313	375	750A/C	1.5C/D
HIPASS J0320-52	NGC 1311	EW352	750B	1.5C
HIPASS J0321-66	AM0319-662	EW367	750D	1.5C
HIPASS J0333-50	IC 1959	EW352	750B	1.5C
HIPASS J0454-53	NGC 1705	EW352	750D	1.5B
HIPASS J0457-42	ESO252-IG001	EW352	750D	1.5C
HIPASS J0605-33	ESO364-G?029	375	750C,e	1.5B
HIPASS J0607-34	AM0605-341	EW352	750D	1.5C
HIPASS J0610-34	NGC 2188	EW352	750D	1.5C
HIPASS J0615-57	ESO121-G020	EW352	750D	1.5B
HIPASS J0639-40	ESO308-G022	EW367	750B	1.5C
HIPASS J0705-58	AM0704-582	EW352	750C	1.5A
HIPASS J0731-68	ESO059-G001	EW352	750C	1.5B
HIPASS J0926-76	NGC 2915	375	750C	1.5D
HIPASS J1043-37	ESO376-G016	EW352	750D	1.5B
HIPASS J1047-38	ESO318-G013	EW352	750C	1.5B
HIPASS J1057-48	ESO215-G?009	EW352	750A	1.5C, 6A
HIPASS J1118-32**	NGC 3621	375	750A	1.5A
HIPASS J1131-31	new	EW352	750C	1.5B
HIPASS J1132-32	new	EW352	750C	1.5B
HIPASS J1137-39	ESO320-G014	EW352	750C	1.5B
HIPASS J1154-33	ESO379-G007	EW367	750A	1.5B
HIPASS J1204-35	ESO379-G024	EW352	750A	1.5B
HIPASS J1214-38	ESO321-G014	EW352	750A	1.5B
HIPASS J1219-79	IC 3104	EW367	750D	1.5B
HIPASS J1244-35	ESO381-G018	EW352	750A	1.5B
HIPASS J1246-33	ESO381-G020	EW352	750A	1.5B
HIPASS J1247-77	new	EW367	750D	1.5B
HIPASS J1305-40	CEN06	EW367	750D	1.5B
HIPASS J1305-49**	NGC 4945	EW367	750A	—
HIPASS J1310-46A	ESO269-G058	EW352	750A	1.5D
HIPASS J1321-31	new	EW367	750D	1.5D
HIPASS J1321-36*	NGC 5102	EW367	750B	1.5D
HIPASS J1324-30	AM1321-304	EW367	750A	1.5B
HIPASS J1324-42**	NGC 5128	—	750A	1.5A, 6A
HIPASS J1326-30A	IC 4247	EW367	750A	1.5B
HIPASS J1327-41	ESO324-G024	375	750D	1.5D
HIPASS J1334-45	ESO270-G017	EW367	750A	6A, 6C
HIPASS J1336-29	UGCA 365	EW367	750A	1.5A
HIPASS J1337-39	new	EW367	750D	1.5D
HIPASS J1337-42	NGC 5237	375	750D	1.5C,D
HIPASS J1337-28	ESO444-G084	375	750D	6D
HIPASS J1339-31*	NGC 5253	EW367	750A	1.5A
HIPASS J1340-28	IC 4316	EW367	750A	1.5B
HIPASS J1341-29	NGC 5264	375	750D	1.5A
HIPASS J1345-41	ESO325-G?011	EW367	750A	1.5B
HIPASS J1348-37	new	EW352	750A	1.5B
HIPASS J1348-53	ESO174-G?001	EW352	750B	1.5B
HIPASS J1349-36	ESO383-G087	375	750D	1.5A
HIPASS J1351-47	new	EW367	750B	1.5B
HIPASS J1403-41	NGC 5408	375	750D	1.5A
HIPASS J1413-65*	Circinus	375	H I mosaic	
HIPASS J1428-46	UKS1424-460	EW367	750A	1.5D
HIPASS J1434-49	ESO222-G010	EW367	750A	1.5D
HIPASS J1441-62	new	EW367	750A	1.5D
HIPASS J1443-44	ESO272-G025	EW352	750A	1.5D
HIPASS J1501-48	ESO223-G009	EW367	750A	1.5D
HIPASS J1514-46**	ESO274-G001	EW367	750A	1.5D
HIPASS J1526-51	new	EW367	750A	1.5D
HIPASS J1620-60	ESO137-G018	EW367	750A	1.5D
HIPASS J1747-64	IC 4662	EW367	750A	1.5D
HIPASS J2003-31	ESO461-G036	EW367	750B	1.5A
HIPASS J2052-69*	IC 5052	EW367	750B	1.5B
HIPASS J2202-51*	IC 5152	EW367	750A	1.5B
HIPASS J2326-32	UGCA 438	EW367	750A	1.5D
HIPASS J2343-31*	UGCA 442	EW367	750B	1.5C
HIPASS J2352-52	ESO149-G003	EW352	750B	1.5C
HIPASS J2357-32*	NGC 7793	EW352/367	H I mosaic	

Notes: Galaxies marked with a single (double) star in Col. (1) have optical diameters $> 5'$ ($10'$), and additional H I mosaics in the very compact ATCA H75 array (and in some cases the EW214 array) have been completed.

optical diameters $> 5'$ ($10'$), and additional H I mosaics in the very compact ATCA H75 array (and in some cases the EW214 array) have been completed.

4 RESULTS

Here we present the ATCA H I atlas of LVHIS galaxies, consisting of H I moment maps and position-velocity diagrams which are provided in the on-line Appendix. Colour figures are provided on our LVHIS webpages together with the opportunity to download FITS files of the ATCA H I data products (H I data cubes and moment maps). Most of the maps presented here were made with ‘natural’ weighting to maximise sensitivity to diffuse, extended H I emission in the outer discs of galaxies. The H I galaxy properties, as measured from the primary-beam corrected ATCA integrated H I intensity maps (mom0 maps), are listed in Table 6.

The Table 6 columns are: Col. (1+2) HIPASS and optical galaxy name; Col. (3) total H I flux density, F_{HI} ; Col. (4) total H I mass, $\log M_{\text{HI}}$; Cols. (5–7) H I radius, R_{HI} , inclination angle, i , and position angle, PA , as measured at $1 M_{\odot} \text{pc}^{-2}$, where $\cos(i)$ is the ratio of the fitted H I minor to major axes (see Wang et al. 2016); Col. (8) F_{HI}^* enclosed within that diameter; Col. (9) H I mass to optical light ratio, M_{HI}/L_B , calculated as $1.5 \times 10^{-7} F_{\text{HI}} 10^{0.4(m_B - A_B)}$ M_{\odot}/L_{\odot} , ie. independent of distance; and Col. (10) ratio of the D_{HI} to D_{opt} .

Correlations between these ATCA H I properties and between H I and optical properties are shown in Fig. 4. The M_{HI} versus B -band magnitudes and M_{HI} versus D_{HI} relations are consistent with the literature (e.g., Dénes et al. 2014, Wang et al. 2016). There is a weak anti-correlation between M_{HI}/L_B and $B - R$ colour, and a weak correlation between $D_{\text{HI}}/D_{\text{opt}}$ and M_{HI}/L_B . Both correlations show large scatter, which may be partly caused by the inhomogeneous optical dataset used in this study. Fig. 5 shows the measured HIPASS F_{HI} compared to the ATCA F_{HI} , listed in Tables 4 & 6, respectively, for all LVHIS galaxies.

Table 7 gives the ATCA H I centre positions for (a) galaxies newly detected in HIPASS, ie without a previously known optical or infrared counterpart, and (b) newly detected companions to the LVHIS sample galaxies. The accurate H I positions allow the secure identification of the stellar counterparts as shown in the ATCA H I moment maps. The Table 7 columns are: Col. (1) Galaxy name; Col. (2) notes; Col. (3–5) ATCA H I centre position, deconvolved major and minor axes diameters, and PA , as obtained from a Gaussian fit to the H I distribution (mom0). More accurate estimates will be obtained from the ATCA H I high resolution maps made with robust/uniform weighting (an example is given in Fig. 11).

The Table 8 columns are: Cols. (1+2) HIPASS and optical galaxy name; Col. (3) rotational velocity, calculated from the HIPASS 20% profile width (given in Table 4) corrected for instrumental broadening ($\sim 0.5 \times$ velocity resolution = 9 km s^{-1}), turbulence ($\sim 7 \text{ km s}^{-1}$) and the galaxy inclination angle (from Table 6): $v_{\text{rot}} = 0.5 (w_{20} - 16 \text{ km s}^{-1})/\sin(i)$; Col. (4) dynamical mass $M_{\text{dyn}} = 2.31 \times 10^5 v_{\text{rot}}^2 R_{\text{kpc}}$, where R_{kpc} is R_{HI} in kpc; and Col. (5)

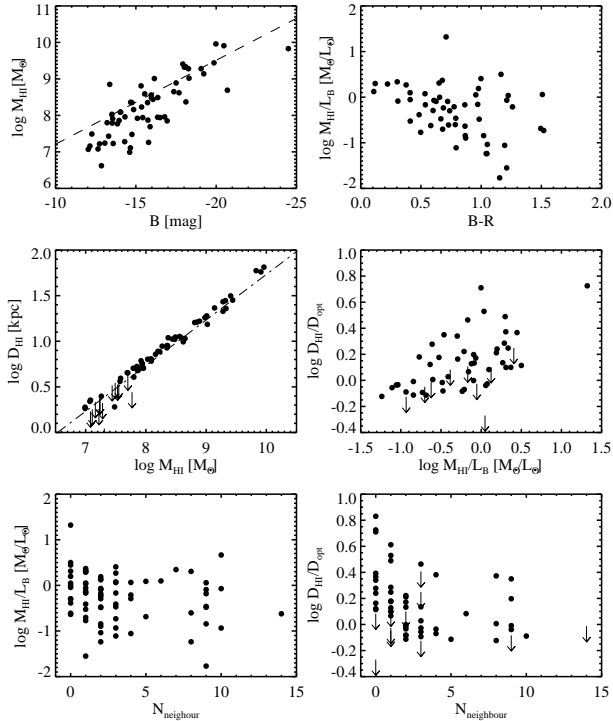
Table 6. ATCA H I properties of LVHIS galaxies

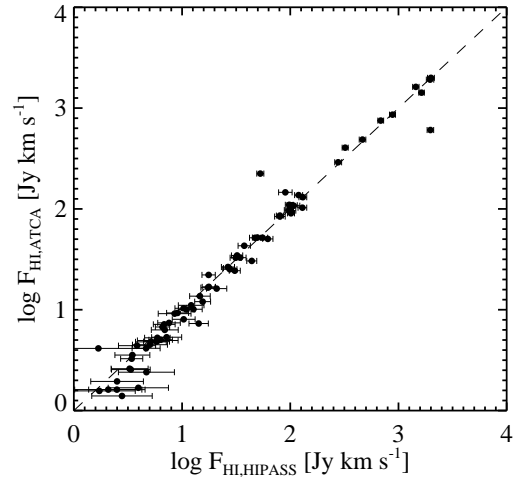
(1) HIPASS Name	(2) Galaxy Name	(3) F_{HI} [Jy km s ⁻¹]	(4) $\log M_{\text{HI}}$ [M _⊙]	(5) R_{HI} ["]	(6) i [deg]	(7) PA [deg]	(8) F_{HI}^* [Jy km s ⁻¹]	(9) $M_{\text{HI}} / L_{\text{B}}$ [M _⊙ /L _⊙]	(10) $D_{\text{HI}} / D_{\text{Opt}}$ ratio	(11) Figure No.	(12) notes
HIPASS J0008-34	ESO349-G031	4.8	7.07	70	38	32	3.5	1.2	0.94	A1	dSph/dIrr, (2)
	ESO294-G010	0.1	4.94	—	—	—	—	—	—	—	dSph/dIrr, (1)
HIPASS J0015-32	ESO410-G005	0.9	5.89	18	35	54	0.1	0.1	0.36	A2	dSph/dIrr, (2)
HIPASS J0015-39	NGC 55	2025.4	9.34	1106	69	103	1796.0	0.8	1.00	A3	W2013
HIPASS J0047-20	NGC 247	662.5	9.32	1544	73	173	661.2	0.9	1.72	A4	
HIPASS J0047-25	NGC 253	746.8	9.44	739	73	45	713.6	0.2	0.77	A5	H I absorption
HIPASS J0054-37	NGC 300	1758.3	9.28	1335	46	147	1486.1	0.8	1.48	A6	W2011
HIPASS J0135-41	NGC 625	24.6	7.94	150	64	106	17.5	0.1	0.77	A7	
HIPASS J0145-43	ESO245-G005	83.1	8.58	253	42	106	77.8	1.5	1.63	A8	
HIPASS J0150-44	ESO245-G007	2.3	4.98	—	—	—	—	0.1	—	Fig. 6	dSph/dIrr
HIPASS J0237-61	ESO115-G021	110.7	8.81	331	76	43	93.6	3.2	1.30	A9	
HIPASS J0256-54	ESO154-G023	130.3	9.01	339	73	29	110.5	2.3	1.26	A10	
HIPASS J0258-49	ESO199-G007	1.6	7.22	39	66	4	0.6	0.9	1.31	A11	(2)
HIPASS J0317-66	NGC 1313	491.3	9.28	540	51	14	479.4	0.3	1.50	A12	
HIPASS J0320-52	NGC 1311	13.6	7.94	112	73	40	9.7	0.4	1.07	A14	
HIPASS J0321-66	AM0319-662	0.3	6.05	—	—	—	—	0.3	—	A13	dSph/dIrr, (1)
HIPASS J0333-50	IC 1959	26.0	8.35	152	69	150	22.3	0.8	1.34	A15	
HIPASS J0454-53	NGC 1705	12.2	7.88	96	45	50	8.7	0.2	1.90	A16	
HIPASS J0457-42	ESO252-IG001	9.9	8.08	86	46	68	8.7	1.9	1.93	A17	
HIPASS J0605-33	ESO364-G7029	22.3	8.48	142	44	52	19.6	0.8	1.36	A18	
HIPASS J0607-34	AM0605-341	9.3	8.08	89	47	84	7.7	0.7	3.71	A19	
HIPASS J0610-34	NGC 2188	34.3	8.65	149	54	2	30.9	0.3	0.83	A20	
HIPASS J0615-57	ESO121-G020	7.3	7.80	69	32	56	7.0	2.2	1.77	A21	
HIPASS J0639-40	ESO308-G022	4.4	7.79	67	37	12	3.4	1.6	1.74	A22	
HIPASS J0705-58	AM0704-582	33.0	8.27	186	46	92	30.2	2.0	3.38	A23	
HIPASS J0731-68	ESO059-G001	16.9	7.92	137	48	143	14.0	0.5	2.19	A24	
HIPASS J0926-76	NGC 2915	108.7	8.56	308	56	102	50.7	1.0	5.13	A25	
HIPASS J1043-37	ESO376-G016	10.2	8.08	92	36	129	8.9	2.0	3.08	A26	
HIPASS J1047-38	ESO318-G013	9.1	7.96	—	—	—	—	1.1	—	A27	(1)
HIPASS J1057-48	ESO215-G7009	110.1	8.85	318	24	139	105.4	21.2	5.32	A28	
HIPASS J1118-32	NGC 3621	856.8	9.96	999	75	167	684.8	0.6	1.67	A29	
HIPASS J1131-31	new	1.1	7.07	—	—	—	—	—	—	A30	(1)
HIPASS J1132-32	new	1.4	7.17	—	—	—	—	0.9	—	A31	(1)
HIPASS J1137-39	ESO320-G014	2.0	7.24	49	35	86	1.3	0.4	1.51	A32	(2)
HIPASS J1154-33	ESO379-G007	4.8	7.49	75	32	90	3.7	2.5	1.94	A33	
HIPASS J1204-35	ESO379-G024	2.6	7.17	52	40	30	1.5	1.3	1.45	A34	(2)
HIPASS J1214-38	ESO321-G014	5.1	7.08	73	65	20	3.2	0.7	1.16	A35	
HIPASS J1219-79	IC 3104	8.1	6.99	83	38	39	7.0	0.1	0.93	A36	
HIPASS J1244-35	ESO381-G018	2.6	7.24	53	53	83	1.4	0.7	1.50	A37	(2)
HIPASS J1246-33	ESO381-G020	32.8	8.36	169	60	136	29.4	2.0	1.26	A38	
HIPASS J1247-77	new	4.2	6.99	61	48	55	3.4	0.5	—	A39	
HIPASS J1305-40	CEN06	4.5	7.55	69	57	81	2.4	1.2	—	A40	(2)
HIPASS J1305-49	NGC 4945	405.3	9.14	629	70	48	364.3	0.2	0.81	A41	H I absorption
HIPASS J1310-46A	ESO269-G058	5.4	7.26	67	48	69	4.3	0.1	0.75	A42	
HIPASS J1321-31	new	5.2	7.52	73	40	19	2.1	4.6	4.91	A43	dSph/dIrr, (2)
HIPASS J1321-36	NGC 5102	85.0	8.36	331	70	46	53.6	0.1	0.92	A44	
HIPASS J1324-30	AM1321-304	1.7	6.93	38	45	106	0.6	0.7	—	A45	(1)
HIPASS J1324-42	NGC 5128	(144)	(8.68)	(814)	—	—	—	(0.02)	—	—	H I absorption
HIPASS J1326-30	IC 4247	3.3	7.28	54	66	158	1.2	0.2	1.21	A46	(2)
HIPASS J1327-41	ESO324-G024	52.0	8.23	212	59	54	44.1	0.8	1.58	A47	
HIPASS J1334-45	ESO270-G017	224.7	9.41	466	79	108	199.4	1.1	0.91	A48	
HIPASS J1336-29	UGCA 365	2.9	7.27	—	—	—	—	0.6	—	A49	(1)
HIPASS J1337-29	NGC 5236	1428.5	9.91	1208	51	179	941.9	0.3	2.62	A50	
HIPASS J1337-39	new	6.7	7.57	77	45	8	5.7	2.2	3.89	A51	dSph/dIrr
HIPASS J1337-42	NGC 5237	11.0	7.48	57	59	26	2.0	0.2	1.02	A52	dSph/dIrr
HIPASS J1337-28	ESO444-G084	16.3	7.91	113	55	79	14.9	2.0	2.36	A53	
HIPASS J1339-31	NGC 5253	30.2	7.96	146	42	21	26.8	0.1	0.81	A54	
HIPASS J1340-28	IC 4316	2.6	7.08	53	35	52	1.4	0.3	1.12	A55	(2)
HIPASS J1341-29	NGC 5264	10.2	7.69	102	30	54	8.2	0.1	0.98	A56	
HIPASS J1345-41	ESO325-G7011	26.5	7.86	145	50	126	23.7	1.2	1.21	A57	
HIPASS J1348-37	new	1.6	7.10	—	—	—	—	1.2	—	A58	dSph/dIrr, (1)
HIPASS J1348-53	ESO174-G7001	52.3	8.20	222	45	160	41.6	0.9	2.47	A59	
HIPASS J1349-36	ESO383-G087	25.4	7.85	158	50	19	20.9	0.1	0.88	A60	
HIPASS J1351-47	new	3.5	7.43	67	50	19	2.3	1.4	—	A61	(2)
HIPASS J1403-41	NGC 5408	49.9	8.43	226	57	120	42.6	0.7	2.91	A62	
HIPASS J1413-65	Circinus	1624.5	9.83	1460	47	25	1318.0	0.9	6.96	A63	
HIPASS J1428-46	UKS1424-460	16.7	7.70	129	57	125	14.3	—	—	A64	
HIPASS J1434-49	ESO222-G010	6.3	7.70	85	60	8	4.3	0.3	2.87	A65	(2)
HIPASS J1441-62	new	2.4	7.31	42	58	111	0.7	—	—	A66	(2)
HIPASS J1443-44	ESO272-G025	1.6	7.12	42	49	62	0.8	0.1	1.00	A67	(2)
HIPASS J1501-48	ESO223-G009	97.0	8.98	288	42	165	72.8	0.5	2.41	A68	
HIPASS J1514-46	ESO274-G001	138.4	8.49	371	77	35	120.8	0.6	0.82	A69	
HIPASS J1526-51	new	5.0	7.58	71	34	137	2.5	—	—	A70	
HIPASS J1620-60	ESO137-G018	43.5	8.62	158	55	29	41.6	0.2	1.32	A71	
HIPASS J1747-64	IC 4662	103.5	8.16	304	35	79	86.5	1.1	3.38	A72	
HIPASS J2003-31	ESO461-G036	7.5	8.03	83	60	22	4.4	2.8	2.33	A73	
HIPASS J2052-69	IC 5052	90.0	8.89	284	71	121	69.5	0.5	1.46	A74	
HIPASS J2202-51	IC 5152	98.4	7.95	272	46	94	89.5	0.2	1.51	A75	
HIPASS J2326-32	UGCA 438	3.7	6.62	54	28	89	1.0	0.2	1.06	A76	(2)
HIPASS J2343-31	UGCA 442	52.2	8.35	204	67	43	47.2	1.9	1.37	A77	
HIPASS J2352-52	ESO149-G003	7.1	7.77	55	80	148	1.1	1.1	0.62	A78	(2)
HIPASS J2357-32	NGC 7793	292.6	9.02	991	55	98	290.1	0.4	1.21	A79	

Notes: (1) the H I distribution is unresolved; (2) the H I distribution is poorly resolved ($D_{\text{HI}} < 2 B_{\text{maj}}$), ie. D_{HI} and $D_{\text{HI}} / D_{\text{Opt}}$ are upper limits, and i and PA may differ significantly from the measured values; (3) F_{HI} is a lower limit due to significant H I absorption.

Table 7. ATCA HI properties for galaxies newly discovered in HIPASS and here

(1) Galaxy Name	(2) notes	(3) α, δ (J2000) [hms, dms]	(4) F_{HI} [Jy km s ⁻¹]	(5) HI dimensions (Gaussian fit)	(6) PA [degr]
HIPASS J1131–31	behind a star	11:31:34.6, –31:40:28.3	1.13	unresolved	
HIPASS J1132–32		11:33:10.6, –32:57:45.2	1.41	unresolved	
HIPASS J1247–77		12:47:32.4, –77:34:53.9	4.28	61'' × 37''	48
HIPASS J1321–31		13:21:09.4, –31:32:01.2	5.24	143'' × 111''	53
HIPASS J1337–39		13:37:25.0, –39:53:46.7	6.81	79'' × 50''	–12
HIPASS J1348–37		13:48:34.1, –37:58:08.0	1.54	49'' × 34''	–5
HIPASS J1351–47		13:51:21.2, –46:59:53.0	3.79	81'' × 51''	6
HIPASS J1441–62		14:41:42.2, –62:46:04.2	2.61	58'' × 29''	78
HIPASS J1526–51		15:26:22.4, –51:10:30.2	5.36	97'' × 70''	–53
ATCA J023658–611838	companion to ESO115-G021	02:36:58.8, –61:18:38.5	0.11	unresolved	
ATCA J025640–543537	background galaxy to ESO154-G023	02:56:40.3, –54:35:38.8	0.31	unresolved	
ATCA J045659–424758	HIPASS J0457–42 ¹	04:56:59.1, –42:47:58.3	9.96	84'' × 41''	75
ATCA J060511–332534	near ESO364-G?029	06:05:10.8, –33:25:34.4	0.99	69'' × 34''	20
ATCA J061608–574552	companion to ESO121-G020	06:16:08.9, –57:45:52.3	2.10	33'' × 27''	36
ATCA J124850–774930	companion to HIPASS J1247–77	12:48:50.3, –77:49:30.6	0.33	unresolved	

 Note: ¹ HI detected galaxy in ESO252-IG001 NED01

Figure 4. Correlations between optical and HI properties for the LVHIS sample. The dashed line in the top left panel shows the average relation from Dénes et al. (2014); the dashed line in the middle left panel shows the average relation from Wang et al. (2016). Arrows indicate the upper limits for the unresolved galaxies.

 the HI to dynamical mass ratio, $M_{\text{HI}}/M_{\text{dyn}}$.

Figure 5. Comparison of the HI flux densities of LVHIS galaxies as measured in HIPASS (Table 4) and with the ATCA in this study (Table 6).

4.1 HI diameter relations

Wang et al. (2016) compiled D_{HI} and M_{HI} estimates for a large sample of 561 nearby galaxies, incl. most of the LVHIS galaxies, and analyse the surprisingly tight $M_{\text{HI}}-D_{\text{HI}}$ relation. Fig. 4 (middle left panel) shows the relation for LVHIS galaxies, incl. upper limits for some unresolved LVHIS dwarf galaxies. A galaxy’s HI mass roughly scales as the square of its HI diameter: $M_{\text{HI}} \propto D_{\text{HI}}^2$ (see also Broeils 1992, Broeils & Rhee 1997). Wang et al. (2016) also determine and compare average HI radial profiles for some of the galaxy samples in their study. The tightness of the $M_{\text{HI}}-D_{\text{HI}}$ relation indicates a fundamental common mechanism in shaping the structure of HI discs for a wide range of galaxies.

We can use the $M_{\text{HI}}-D_{\text{HI}}$ relation to obtain an approximate estimate of a galaxy’s HI diameter based on its HI

Table 8. Derived properties of the LVHIS galaxies

(1) HIPASS Name	(2) Galaxy Name	(3) v_{rot} [km s^{-1}]	(4) $\log M_{\text{dyn}}$ [M_{\odot}]	(5) $\log M_{\text{HI}}/M_{\text{dyn}}$
HIPASS J0008-34	ESO349-G031	51	8.82	-1.75
	ESO294-G010	—	—	—
HIPASS J0015-32	ESO410-G005	—	—	—
HIPASS J0015-39	NGC 55	97	10.39	-1.06
HIPASS J0047-20	NGC 247	109	10.87	-1.56
HIPASS J0047-25	NGC 253	217	11.19	-1.75
HIPASS J0054-37	NGC 300	104	10.54	-1.26
HIPASS J0135-41	NGC 625	46	9.14	-1.20
HIPASS J0145-43	ESO245-G005	52	9.52	-0.94
HIPASS J0150-44	ESO245-G007	—	—	—
HIPASS J0237-61	ESO115-G021	66	9.91	-1.10
HIPASS J0256-54	ESO154-G023	66	9.98	-0.98
HIPASS J0258-49	ESO199-G007	32	8.46	-1.25
HIPASS J0317-66	NGC 1313	116	10.52	-1.24
HIPASS J0320-52	NGC 1311	47	9.15	-1.21
HIPASS J0321-66	AM0319-662	—	—	—
HIPASS J0333-50	IC 1959	74	9.76	-1.41
HIPASS J0454-53	NGC 1705	105	9.79	-1.91
HIPASS J0457-42	ESO252-IG001	58	9.36	-1.28
HIPASS J0605-33	ESO364-G7029	56	9.58	-1.10
HIPASS J0607-34	AM0605-341	133	10.12	-2.04
HIPASS J0610-34	NGC 2188	82	9.92	-1.28
HIPASS J0615-57	ESO121-G020	75	9.43	-1.63
HIPASS J0639-40	ESO308-G022	48	9.13	-1.34
HIPASS J0705-58	AM0704-582	47	9.36	-1.09
HIPASS J0731-68	ESO059-G001	59	9.39	-1.47
HIPASS J0926-76	NGC 2188	89	10.02	-1.45
HIPASS J1043-37	ESO376-G016	31	8.86	-0.78
HIPASS J1047-38	ESO318-G013	—	—	—
HIPASS J1057-48	ESO215-G7009	82	10.10	-1.25
HIPASS J1118-32	NGC 3621	143	11.19	-1.23
HIPASS J1131-31	new	—	—	—
HIPASS J1132-32	new	—	—	—
HIPASS J1137-39	ESO320-G014	39	8.71	-1.47
HIPASS J1154-33	ESO379-G007	27	8.52	-1.03
HIPASS J1204-35	ESO379-G024	33	8.48	-1.32
HIPASS J1214-38	ESO321-G014	18	7.94	-0.85
HIPASS J1219-79	IC 3104	38	8.49	-1.50
HIPASS J1244-35	ESO381-G018	29	8.42	-1.18
HIPASS J1246-33	ESO381-G020	48	9.38	-1.02
HIPASS J1247-77	new	20	7.94	-0.95
HIPASS J1305-40	CEN06	18	8.15	-0.61
HIPASS J1305-49	NGC 4945	197	11.02	-1.88
HIPASS J1310-46	ESO269-G058	46	8.78	-1.51
HIPASS J1321-31	new	24	8.39	-0.87
HIPASS J1321-36	NGC 5102	110	10.18	-1.82
HIPASS J1324-30	AM1321-304	35	8.39	-1.46
HIPASS J1324-42	NGC 5128	—	—	—
HIPASS J1326-30	IC 4247	18	7.99	-0.71
HIPASS J1327-41	ESO324-G024	53	9.40	-1.17
HIPASS J1334-45	ESO270-G017	72	10.28	-0.87
HIPASS J1336-29	UGCA 365	—	—	—
HIPASS J1337-29	NGC 5236	174	11.31	-1.40
HIPASS J1337-39	new	26	8.45	-0.89
HIPASS J1337-42	NGC 5237	47	8.67	-1.20
HIPASS J1337-28	ESO444-G084	36	8.88	-0.97
HIPASS J1339-31	NGC 5253	66	9.40	-1.45
HIPASS J1340-28	IC 4316	30	8.36	-1.29
HIPASS J1341-29	NGC 5264	39	8.90	-1.20
HIPASS J1345-41	ESO325-G7011	39	8.91	-1.05
HIPASS J1348-37	new	—	—	—
HIPASS J1348-53	ESO174-G7001	62	9.53	-1.33
HIPASS J1349-36	ESO383-G087	23	8.53	-0.68
HIPASS J1351-47	new	28	8.53	-1.10
HIPASS J1403-41	NGC 5408	57	9.60	-1.17
HIPASS J1413-65	Circinus	183	11.36	-1.53
HIPASS J1428-46	UKS1424-460	30	8.66	-0.96
HIPASS J1434-49	ESO222-G010	27	8.59	-0.89
HIPASS J1441-62	new	31	8.42	-1.11
HIPASS J1443-44	ESO272-G025	36	8.57	-1.45
HIPASS J1501-48	ESO223-G009	55	9.79	-0.81
HIPASS J1514-46	ESO274-G001	85	9.96	-1.47
HIPASS J1526-51	new	39	8.85	-1.26
HIPASS J1620-60	ESO137-G018	85	9.91	-1.29
HIPASS J1747-64	IC 4662	102	9.94	-1.77
HIPASS J2003-31	ESO461-G036	51	9.28	-1.25
HIPASS J2052-69	IC 5052	99	10.27	-1.39
HIPASS J2202-51	IC 5152	58	9.31	-1.36
HIPASS J2326-32	UGCA 438	—	—	—
HIPASS J2343-31	UGCA 442	52	9.42	-1.07
HIPASS J2352-52	ESO149-G003	27	8.44	-0.67
HIPASS J2357-32	NGC 7793	107	10.69	-1.67

mass alone. This is particularly useful for large single-dish HI surveys, like HIPASS, where the majority of galaxies are unresolved. We estimate that of the ~ 5000 catalogued HIPASS galaxies (Koribalski et al. 2004, Meyer et al. 2004, Wong et al. 2006) $\gtrsim 1000$ are larger than $4'$ (ie eight beams in WALLABY), suitable for a detailed HI kinematic analysis once observed in WALLABY (Koribalski 2012).

4.2 HI kinematic analysis

A common way of analyzing the HI kinematics of well-resolved disc galaxies is to fit tilted-ring models to the HI data, using either the data cube or a carefully derived velocity field (Rogstad et al. 1974, de Blok et al. 2008, Oh et al. 2011). Kamphuis et al. (2015) recently developed a code for automated kinematic modelling of disc galaxies that pipelines the *Tilted Ring Fitting Code* (TiRiFiC) by Józsa et al. (2007). The so-called “Fully Automated TiRiFiC” (FAT) is particularly useful for a kinematic modelling of warped galaxies like some of our LVHIS galaxies (e.g., HIPASS J1413-65). Ultimately, FAT aims to analyse the HI kinematics of well and marginally resolved galaxies from the upcoming SKA pathfinders’ large HI galaxy surveys like ASKAP WALLABY together with “2D Bayesian Automated Tilted ring fitter” (2DBAT; Oh et al. 2018) which is based on a Bayesian method for 2D tilted-ring analysis.

Kamphuis et al. (2015) and Wang et al. (2017) make use of FAT to derive tilted ring models and rotation curves for 26 and 10 LVHIS galaxies with large HI discs, respectively. An updated list of the derived HI properties for the successful fits is given in Table 9. The Kamphuis et al. (2015) sample was also analysed by Oh et al. (2018) using 2DBAT. The Table 9 columns are: Cols. (1+2) HIPASS and optical galaxy name; Col. (3) rotational velocity, v_{rot} , near the maximum fitted HI radius; Col. (4) radius of the fitted HI disc, R_{max} ; Cols. (5+6) range of fitted inclination and position angles over the fitted HI disc; Col. (7) dynamical mass $M_{\text{dyn}} = 2.31 \times 10^5 v_{\text{rot}}^2 R_{\text{max}}$; Col. (8) the $M_{\text{HI}}/M_{\text{dyn}}$ ratio; Col. (9) number of resolution elements across the HI disc major axis; and Col. (10) notes.

5 NOTES ON INDIVIDUAL GALAXIES

In the following we briefly introduce each of the LVHIS galaxies and discuss their stellar morphologies, HI properties and environment. We first discuss LVHIS galaxies in the Local Group (§ 5.1), followed by the well-known Sculptor Group (RA ~ 0 h; § 5.2) and Cen A Group (RA ~ 13 h; § 5.3), which host the majority of LVHIS galaxies (see the group associations in Table 2), followed by the remaining galaxies in RA order (§ 5.4).

5.1 The Local Group

A comprehensive overview of galaxies in and around the Local Group is provided by McConnachie (2012), who catalogs ~ 100 galaxies with reliable distance estimates of $D \lesssim 3$ Mpc. Of these 75 are Local Group members ($D < 1$ Mpc), mainly satellite galaxies around the Milky Way and Andromeda (M31). We note that the Milky Way sub-group contains only two gas-rich irregular galaxies, these are the Small and

Table 9. ATCA H I kinematic properties of LVHIS galaxies.

(1) HIPASS Name	(2) Galaxy Name	(3) v_{rot} [km s ⁻¹]	(4) R_{max} [kpc]	(5) i [degr]	(6) PA [degr]	(7) $\log M_{\text{dyn}}$ [M _⊙]	(8) $M_{\text{HI}}/M_{\text{dyn}}$	(9) No. of beams	(10) Notes
HIPASS J0008–34	ESO349-G031	19.3	2.0	42	298	8.24	0.066	9	C2000
HIPASS J0015–39	NGC 55	69.7	20.1	85–67	110–93	10.35	0.096	8+	warped, W2013
HIPASS J0047–25	NGC 253	200.0	17.2	77–80	229	11.20	0.017	8+	starburst
HIPASS J0054–37	NGC 300	82.7	20.8	40–50	290–332	10.52	0.058	8+	warped, W2011
HIPASS J0145–43	ESO245-G005	51	6.4	36	70–98	9.59	0.100	~12	warped, K2012
		47.7	6.7	54	88	9.55	0.110	~36	C2000
HIPASS J0237–61	ESO115-G021	63.0	10.4	90–80	~45	9.97	0.068	8+	
HIPASS J0256–54	ESO154-G023	63.6	15.7	79.7	218.3	10.17	0.070	8+	warped
HIPASS J0317–66	NGC 1313	220.0	10.3	20.0	~10	11.06	0.017	8+	
HIPASS J0320–52	NGC 1311	42.4	3.6	71.4	40.5	9.18	0.062	<8	
HIPASS J0333–50	IC 1959	65.9	5.3	78.8	149.0	9.73	0.042	<8	
HIPASS J0605–33	ESO364-G?029	40.0	4.4	70.5	60.0	9.21	0.186	?	
HIPASS J0607–34	AM0605–341	85	4.3	(50)	274	9.86	0.016	~5	K2012
HIPASS J0615–57	ESO121-G020	48.7	3.2	(40)	265	9.24	0.036	~7	K2012
HIPASS J0639–40	ESO308-G022	40	4.1	(40)	82	9.18	0.041	~5	K2012
HIPASS J0705–58	AM0704-582	38.5	6.1	53.6	275.9	9.32	0.092	8+	
		57	5.3	(35)	276	9.60	0.047	~9	K2012
HIPASS J0731–68	ESO059-G001	61.0	5.4	50.2	323.4	9.67	0.019	8+	
		61.8	4.4	45	329–319	9.59	0.021	~9	K2012
HIPASS J0926–76	NGC 2915	80.0	7.7	52.7	292.6	10.06	0.028	8+	E2011
HIPASS J1057–48	ESO215-G?009	93.0	9.3	18.5	119.7	10.27	0.040	?	$i < 20^\circ$, uncertain
		53.8	9.7	35	123–116	9.81	0.109	~9	K2012
HIPASS J1118–32	NGC 3621	130.0	39.0	65–77	345–362	11.18	0.060	8+	warped
HIPASS J1219–79	IC 3104	15.3	1.6	89.0	205.9	7.94	0.113	<8	
HIPASS J1246–33	ESO381-G020	46.7	5.3	55	295–314	9.43	0.086	~9	K2012
		50.5	5.8	57	311	9.53	0.068	25	C2000
HIPASS J1305–49	NGC 4945	173.6	16.7	82.8	44.2	11.07	0.010	8+	starburst
HIPASS J1321–36	NGC 5102	94.3	10.5	75.3	42.2	10.33	0.011	8+	warped
HIPASS J1324–42	NGC 5128	260.0	6.2	85–105	100–130	10.99	0.005	8+	warped, S2010
HIPASS J1337–28	ESO444-G084	63.1	4.2	32	104	9.59	0.021	11	C2000
HIPASS J1337–29	NGC 5236	150.0	54.9	37.0	227–180	11.46	0.028	8+	warped
HIPASS J1337–42	NGC 5237	75.2	4.9	33.8	50.2	9.81	0.005	8+	dSph/dIrr
HIPASS J1345–41	ESO325-G?011	46.0	3.1	42	302	9.18	0.048	~9	K2012
		43.1	3.4	52	310	9.16	0.050	10	C2000
HIPASS J1348–53	ESO174-G?001	97.3	4.5	22.7	218.4	9.99	0.016	8	
		66	6.6	40	233–202	9.82	0.024	~13	warped, K2012
HIPASS J1413–65	Circinus	161.4	47.2	62.2	199.6	11.46	0.023	8+	warped
HIPASS J1428–46	UKS1424–460	22.0	3.2	74.6	122.8	8.55	0.140	<8	
HIPASS J1501–48	ESO223-G009	85.6	15.3	20.3	256.1	10.41	0.037	8+	warped
HIPASS J1620–60	ESO137-G018	71.2	8.6	71.5	29.2	10.00	0.041	8+	
		80.1	5.6	50	33–28	9.92	0.050	~8	K2012
HIPASS J2003–31	ESO461-G036	51.0	6.8	65	330–350	9.61	0.026	8+	warped, K2011
HIPASS J2052–69	IC 5052	90.0	16.1	~70	140–125	10.48	0.026	8+	warped
HIPASS J2202–51	IC 5152	58.0	3.6	66–45	275–294	9.45	0.032	8+	warped
		59.5	4.0	49	271–198	9.51	0.027	~20	warped, K2012
HIPASS J2343–31	UGCA 442	57.8	6.2	64	228	9.68	0.046	10	warped, C2000
HIPASS J2357–32	NGC 7793	105.0	9.1	48	290–320	10.37	0.045	8+	warped

References: C2000 (Côté et al. 2000), E2011 (Elson et al. 2011b), K2011 (Kreckel et al. 2011), K2012 (Kirby et al. 2012), O2017 (Oh et al. 2018), S2010 (Struve et al. 2010), W2011 (Westmeier et al. 2011), W2013 (Westmeier et al. 2013).

Large Magellanic Clouds, and at least 25 dSphs. The M 31 sub-group is only slightly more diverse. In the outer reaches, McConnachie’s sample overlaps with nearby galaxy groups, such as the Sculptor Group. For recent studies of the H I content of Milky Way satellites see Westmeier et al. (2015). Our nearest neighbours, the Magellanic Clouds, have already been studied using large-scale Parkes and ATCA H I mosaic observations. Stanimirovic et al. (1999) obtain an H I mass

of $M_{\text{HI}} = 4.2 \times 10^8 M_{\odot}$ and $D_{\text{HI}} = 10.4$ kpc for the Small Magellanic Cloud (SMC), while Staveley-Smith et al. (2003) derive $M_{\text{HI}} = 4.8 \times 10^8 M_{\odot}$ and $D_{\text{HI}} = 18.6$ kpc for the Large Magellanic Cloud (LMC) (assuming a distance of 50 kpc).

ESO245-G007 (HIPASS J0150–44), also known as the Phoenix Dwarf Galaxy, is a member of the Local Group ($D_{\text{TRGB}} = 420 \pm 10$ kpc). Its distance has been well con-

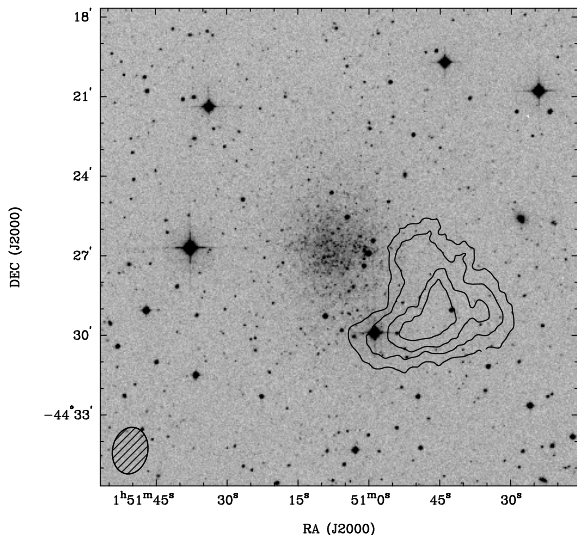


Figure 6. H I distribution (contours) of the galaxy ESO245-G007 (HIPASS J0150-44; $D_{\text{TRGB}} = 0.42$ Mpc), also known as the Phoenix Dwarf, overlaid on to a DSS2 R -band image. Contour levels are 0.1, 0.2, 0.3, and 0.4 $\text{Jy beam}^{-1} \text{ km s}^{-1}$. The angular resolution is $106''.2 \times 79''.6$ (216 pc \times 162 pc).

strained by several authors (e.g., Young et al. 2007). Our ATCA H I mosaic of ESO245-G007 is shown in Fig. 6, revealing an extended H I cloud embracing the stellar core to the south-west. We detect H I emission from about -40 to -8 km s^{-1} , no clear velocity gradient is seen. The H I emission associated with the Phoenix galaxy is also clearly detected in the re-calibrated HIPASS data. Phoenix is likely a transitional dwarf galaxy as previously suggested by Young & Lo (1997), St-Germain et al. (1999) and Young et al. (2007) who carry out detailed studies of its H I emission. Martín-Delgado et al. (1999) investigate the stellar content of the Phoenix Dwarf Galaxy and find a predominantly old population oriented north-south and a more compact, young population aligned east-west; the latter shows an asymmetry in its distribution with more blue stars in the south-western part of the galaxy. Later stellar velocity measurements of $-13 \pm 9 \text{ km s}^{-1}$ (Gallart et al. 2001, Irwin & Tolstoy 2002) confirmed that the H I cloud is indeed associated with the galaxy. Young et al. (2007) use deep VLA H I data of Phoenix to investigate mechanisms which may transform gas-rich irregulars into gas-poor dwarf spheroidal galaxies. As the H I cloud is associated with the most recent star formation in Phoenix, they suggest that the gas expulsion may have been caused by winds from supernovae. Using our ATCA maps we measure an H I flux density of $F_{\text{HI}} = 2.3 \text{ Jy km s}^{-1}$, corresponding to an H I mass of $M_{\text{HI}} \sim 10^5 M_{\odot}$. For comparison, St-Germain et al. (1999) measure $F_{\text{HI}} = 4.0 \text{ Jy km s}^{-1}$ with the ATCA, while Young et al. (2007) measure $F_{\text{HI}} = 2.95 \pm 0.10 \text{ Jy km s}^{-1}$ with the VLA (single pointing).

5.2 The Sculptor Group

Galaxies in the Sculptor Group, many of which have been observed with the ATCA as part of the LVHIS project,

are among the closest to the Local Group. They span a considerable range in heliocentric radial velocity (~ 30 to 600 km s^{-1}). Accurate distance measurements are available for the majority of group members (see Jerjen et al. 1998; Karachentsev et al. 2000, 2003; Tully et al. 2006; Gieren et al. 2008, Dalcanton et al. 2009). The large distance spread (~ 2 to 5 Mpc) suggests that the Sculptor Group is not a gravitationally bound group like the Centaurus A group, but a loosely bound filament of several distinct subgroups which are introduced below. The Sculptor Group has over 20 known members; subgroups are identified around NGC 55/NGC 300 ($D \sim 2$ Mpc), NGC 247/NGC 253 ($D \sim 4$ Mpc), NGC 7793, NGC 625, and NGC 45 (see Fig. 7). A deep Parkes multibeam H I survey of the northern Sculptor Group and the more extended Sculptor filament is presented by Westmeier et al. (2017).

5.2.1 NGC 55 / NGC 300 subgroup

The large galaxies NGC 55 and NGC 300, together with the dwarf galaxies ESO294-G010, ESO410-G005, UGCA 438 and IC 5152 (all detected in H I) form a small subgroup at the near side of the Sculptor Group at a distance of ~ 2 Mpc.

NGC 55 (HIPASS J0015-39) is a Magellanic barred spiral galaxy, viewed nearly edge-on, with a stellar diameter of at least half a degree, while **NGC 300 (HIPASS J0054-37)** is an equally large, late-type spiral galaxy located $\sim 8^{\circ}$ (300 kpc) from NGC 55. Both galaxies and their large-scale surroundings were recently mosaicked in H I with the ATCA by Westmeier et al. (2011, 2013) who used 32 pointings covering an area of $\sim 2^{\circ} \times 2^{\circ}$ to reveal much larger gas envelopes than previously known. They also found disturbed outer disc gas in both galaxies as well as high-velocity clouds (HVCs) surrounding NGC 55. We refer to Westmeier et al. for a detailed analysis and literature overview of both Sculptor galaxies.

The ATCA H I distribution of the edge-on spiral **NGC 55** is quite asymmetric, with the neutral gas more extended towards the east (receding side) and north (see Fig. 7). Contours in the west and south are much more compressed suggesting the influence of ram pressure stripping. The twisting of the H I velocity contours hints at a mild warp of the outer disc (Westmeier et al. 2013). Star formation is prominent in the disc, possibly responsible for extraplanar H II regions (Tüllmann et al. 2003).

The ATCA H I distribution of **NGC 300** is huge, extending well beyond previous measurements (see Fig. 7). The outer H I disc is strongly warped, exhibiting a significant twist of the position angle from east-west to nearly north-south. The wide-field H I mapping with a compact array was crucial to discover the extent of the outer disc, which contains nearly 50% of the H I mass. Westmeier et al. (2011) carry out a detailed analysis of the gas kinematics and dark matter distribution, finding a slightly decreasing rotation curve ($v_{\text{max}} \sim 100 \text{ km s}^{-1}$) that extends to a radius of ~ 20 kpc. Significant asymmetries in NGC 300's outer disc hint at the possibility of ram-pressure stripping of gas by the intra-group medium. We measure $F_{\text{HI}} = 1758.3 \text{ Jy km s}^{-1}$, $\sim 10\%$ lower than Parkes H I measurements (Koribalski et al. 2004,

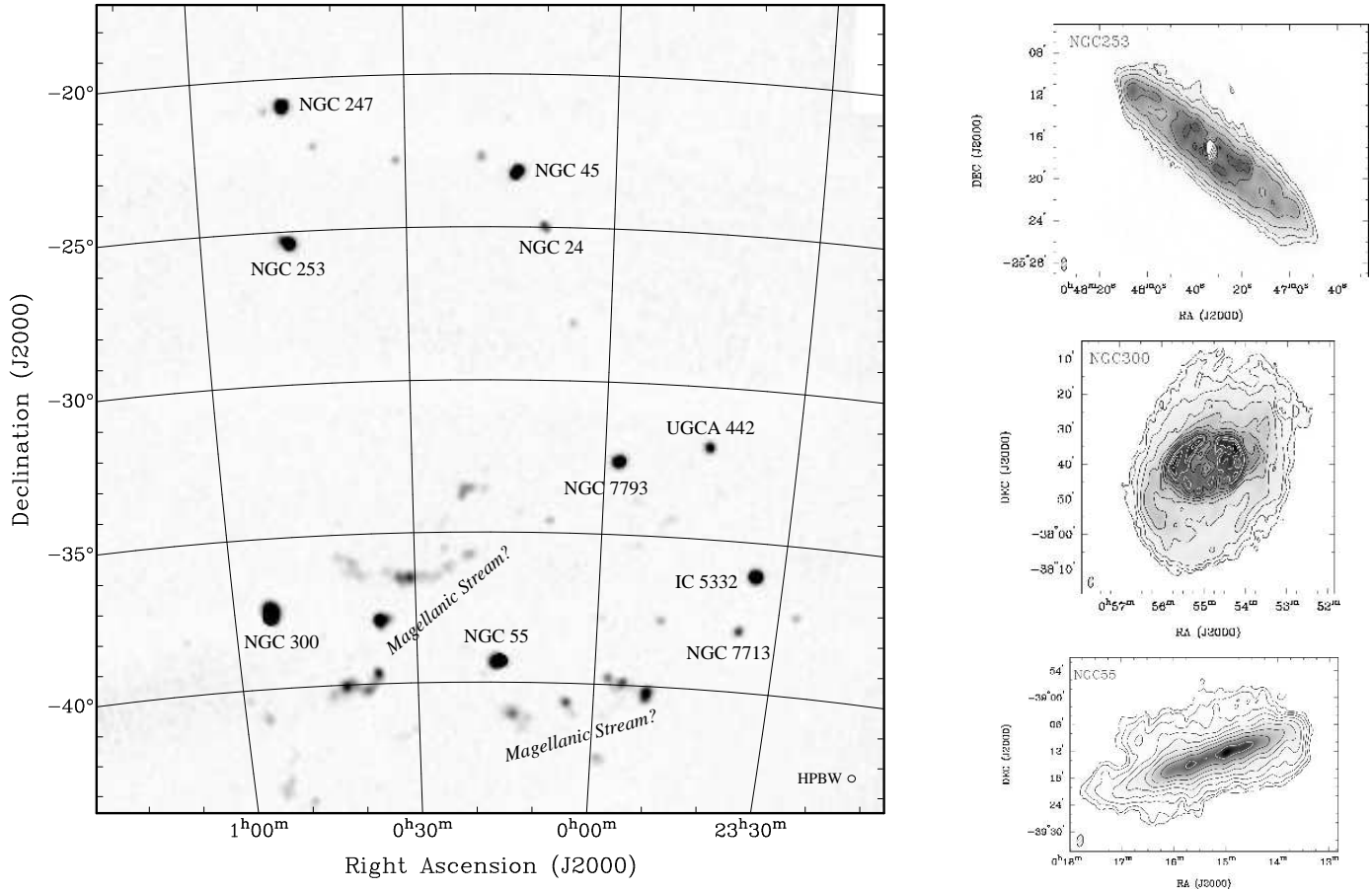


Figure 7. Sculptor Group galaxies. — **Left:** HIPASS peak flux density map of the central Sculptor Group, marked with the names of the brightest galaxies (see also Westmeier et al. 2017). Extended H I emission in the southern half of the map is associated with the Magellanic Stream. The gridded Parkes beam of $15'.5$ is displayed in the lower right corner. — **Right:** ATCA H I distributions of NGC 253 (top), NGC 300 (middle), and NGC 55 (bottom); H I contour levels as given in the Appendix.

Westmeier et al. 2017).

Of the four dwarf galaxies in this subgroup, three are detected in HIPASS and one, ESO294-G010, shows a marginal ATCA H I detection. Because of their low velocities, the H I emission of the nearby Sculptor galaxies in some cases overlaps with that of Galactic HVCs and H I gas in the Magellanic Stream.

ESO294-G010 is a dwarf galaxy at $D_{\text{TRGB}} = 1.92 \pm 0.10$ Mpc (Karachentsev et al. 2002). Optical images show a rather smooth stellar body typical of dwarf spheroidal galaxies, whereas GALEX *UV* images clearly reveal a clumpy inner structure. Some signs of star formation are present (Jerjen et al. 1998, Karachentsev et al. 2002). ATCA H I data show a weak source around ~ 106 km s $^{-1}$, slightly offset from its optical position as already indicated by Bouchard et al. (2005). It remains unclear if the detected H I emission belongs to the dwarf galaxy. The optical velocity of 117 ± 5 km s $^{-1}$ (Jerjen et al. 1998) is also slightly offset. We measure $F_{\text{HI}} = 0.1$ Jy km s $^{-1}$ and derive $M_{\text{HI}} = 9 \times 10^4 M_{\odot}$. ESO294-G010 appears to be similar to dwarf galaxies of mixed type like Phoenix, LGS 3 and KK 3.

galaxy at $D_{\text{TRGB}} = 1.92 \pm 0.19$ Mpc (Karachentsev et al. 2000). Its stellar morphology resembles that of a dwarf elliptical, while our H I detections at $v_{\text{hel}} = 20 - 52$ km s $^{-1}$, both with the Parkes telescope and the ATCA, suggest that it is most likely a transition-type dwarf galaxy. No H I emission was detected with the ATCA at velocities around $+160$ km s $^{-1}$ where Bouchard et al. (2005) report a detection using the Parkes telescope. Using our ATCA H I data we determine a center position of $\alpha, \delta(\text{J2000}) = 00:15:30.9, -32:10:52$, an H I diameter of $1'.5 \times 1'.0$ (840 pc \times 560 pc), $PA = 320^\circ$, a systemic velocity of $v_{\text{sys}} = 36 \pm 2$ km s $^{-1}$ ($v_{\text{LG}} = 53$ km s $^{-1}$) and a 50% (20%) velocity width of 22.8 km s $^{-1}$ (31.3 km s $^{-1}$). Furthermore, we measure $F_{\text{HI}} = 0.93$ Jy km s $^{-1}$, corresponding to an H I mass of $8 \times 10^5 M_{\odot}$. We calculate a mass-to-light ratio (M_{HI}/L_B) = $0.22 M_{\odot}/L_{\odot}$. The ATCA H I velocity field shows a gradient perpendicular to the stellar disc, similar to that discussed for ESO349-G031. High resolution ATCA H I images indicate the H I emission is offset from the optical centre, located on both sides of the minor axis. It is unclear if the gas is rotating or being accreted/ejected. If the observed velocity gradient is due to rotation ($v_{\text{rot}} = 15$ km s $^{-1}$) we calculate $M_{\text{dyn}} = 2 \times 10^7 M_{\odot}$.

ESO410-G005 (HIPASS J0015-32) is a dwarf

IC 5152 (HIPASS J2202-51) is a dwarf irregular

galaxy at a TRGB distance of 1.97 Mpc (Tully et al. 2006). Its ATCA H I distribution extends well beyond the bright stellar disc (see Fig. 8). We measure $F_{\text{HI}} = 98.6 \text{ Jy km s}^{-1}$, in agreement with HIPASS (Koribalski et al. 2004), and derive $M_{\text{HI}} = 9.0 \times 10^7 M_{\odot}$. The H I velocity field, which shows a twisting PA , was analysed by van Eymeren et al. (2009c) who determine the rotation curve up to a radius of 4 kpc. A comprehensive multi-wavelength description of IC 5152 is given by Kirby et al. (2012), who also carry out some kinematic modelling. Using 3D FAT Wang et al. (2017) obtain an H I rotation curve indicating $v_{\text{rot}} = 58 \text{ km s}^{-1}$ at $R_{\text{max}} = 3.6 \text{ kpc}$ (see Table 9) and $M_{\text{dyn}} = 2.8 \times 10^9 M_{\odot}$. HST images of IC 5152 reveal several blue star complexes and dust patches. Our 20-cm ATCA radio continuum images show two bright star forming regions, coincident with the MIPS $24\mu\text{m}$ emission peaks (Shao et al. 2017). $\text{H}\alpha$ emission is detected in and between those two regions (Meurer et al. 2006).

UGCA 438 (HIPASS J2326–32) is a dwarf irregular galaxy at a TRGB distances of $2.18 \pm 0.09 \text{ Mpc}$ (Dalcanton et al. 2009). The results of stellar photometry, made difficult by a bright foreground star, are presented by Lee & Byun (1999). Kaisin et al. (2007) spot a single $\text{H}\alpha$ emission region, while the GALEX UV emission is clearly extended. Buyle et al. (2006) report CO non-detections for both UGCA 438 and IC 5152 and show preliminary ATCA H I intensity maps. Here we show — for comparison with ESO410-G005 — high-resolution ($30''$) ATCA H I distributions of both galaxies overlaid on to DSS2 B -band optical images (see Fig. 8). The H I gas associated with UGCA 438 is mostly found outside the stellar disc, with H I peaks to the north and south plus a minor peak to the east. The gas distribution is highly peculiar and gives the appearance of a fragmented H I ring; the H I velocity field shows no clear signs of rotation. H I emission is detected in the velocity range from ~ 46 to 80 km s^{-1} . Using our ATCA H I data we measure $F_{\text{HI}} = 3.7 \text{ Jy km s}^{-1}$ which corresponds to an H I mass of only $4.1 \times 10^6 M_{\odot}$. We note that in HIPASS the galaxy UGCA 438 is confused with Galactic H I emission.

5.2.2 NGC 247 / NGC 253 subgroup

The large spiral galaxies NGC 247 and NGC 253, together with the dwarf galaxies ESO540-G030, ESO540-G031 and ESO540-G032 form another small association ($D \sim 4 \text{ Mpc}$) within the Sculptor Group.

NGC 247 (HIPASS J0047–20) is a late-type spiral galaxy at a cepheid distance of $D = 3.65 \pm 0.17 \text{ Mpc}$ (Madore et al. 2009). This value agrees with its TRGB distance estimate by Karachentsev et al. (2006). Our ATCA H I moment maps show a mildly warped, regularly rotating disc extending about a factor two beyond the stellar disc. We measure $F_{\text{HI}} = 662.5 \text{ Jy km s}^{-1}$, about 10% higher than the HIPASS value (Koribalski et al. 2004). High-resolution, single-pointing VLA H I maps were obtained by Carignan & Puche (1990b) and Ott et al. (2012), who measure $F_{\text{HI}} = 528 \pm 18 \text{ Jy km s}^{-1}$ and $382.6 \text{ Jy km s}^{-1}$ (VLA-ANGST project), respectively. Both are missing substantial amounts of H I gas due to the lack of very short baselines and limited field-of-view. NGC 247’s closest neighbour is the dIrr galaxy

ESO540-G031 (HIPASS J0049–20; UGCA 015).

NGC 253 (HIPASS J0047–25) is a well-known starburst spiral galaxy and the brightest member of the Sculptor Group. It is oriented close to edge-on with an optical extent of $32' \times 8'$ (see Table 2) and $\sim 50' \times 30'$ at $\sim 28 \text{ mag arcsec}^{-2}$ (Malin & Hadley 1997). We have adopted a TRGB distance of $3.94 \pm 0.37 \text{ Mpc}$ (Karachentsev et al. 2003). Our ATCA data show bright H I emission extending barely beyond the stellar disc and H I absorption (visible as the central hole) against the prominent starburst region. The mean H I velocity field highlights the fast rotating disc ($v_{\text{rot}} = 213 \text{ km s}^{-1}$, see Table 8) with only minor deviations from regular rotation in its outskirts. The brightest H I emission is detected in the barred region of NGC 253.

Previous ATCA H I observations of NGC 253 were presented by Koribalski, Whiteoak & Houghton (1995) and Boomsma et al. (2005). Lucero et al. (2015) use the Karoo Array Telescope (KAT-7) to map the extended H I structure of NGC 253 at low resolution ($\sim 3'.5$) down to column densities of $N_{\text{HI}} = 1.3 \times 10^{19} \text{ cm}^{-2}$. They measure $F_{\text{HI}} = 728 \pm 36 \text{ Jy km s}^{-1}$, in agreement with the HIPASS F_{HI} of $692.9 \pm 42.2 \text{ Jy km s}^{-1}$ (Koribalski et al. 2004). Both are lower limits due to significant H I absorption against the bright star-forming inner region of NGC 253, which covers the same velocity range as the H I emission (Koribalski, Whiteoak & Houghton 1995). Using our ATCA H I maps we measure $F_{\text{HI}} = 746.8 \text{ Jy km s}^{-1}$ and derive $M_{\text{HI}} = 2.7 \times 10^9 M_{\odot}$. Using 3D FAT Wang et al. (2017) obtained an H I rotation curve indicating $v_{\text{rot}} = 200 \text{ km s}^{-1}$ at $R_{\text{max}} = 17.2 \text{ kpc}$ (see Table 9) and $M_{\text{dyn}} = 1.6 \times 10^{11} M_{\odot}$.

In the following we briefly discuss three faint dwarf galaxies (ESO540-G030, ESO540-G031, and ESO540-G032) near NGC 247; these are not part of the LVHIS galaxy atlas presented here. Karachentsev et al. (2003) obtained TRGB distances of $3.40 \pm 0.34 \text{ Mpc}$ (ESO540-G030), $3.34 \pm 0.24 \text{ Mpc}$ (ESO540-G031), and $3.42 \pm 0.27 \text{ Mpc}$ (ESO540-G032), suggesting that this dwarf grouping lies slightly in front of the spiral galaxy NGC 247.

ESO540-G030 is a low surface brightness dwarf galaxy. Jerjen et al. (1998, 2000) measured an integrated magnitude of $B_{\text{T}} = 16.37 \text{ mag}$ and an SBF distance of $3.19 \pm 0.13 \text{ Mpc}$. In addition to a large number of red stars, Karachentsev et al. (2003) also detect a number of blue stars in the central region of ESO540-G030, suggesting that it is a transition dSph/dIrr type galaxy. Deep Parkes and ATCA H I observations were presented by Bouchard et al. (2005), resulting in a tentative detection. They derive a total H I mass of $8.9 \pm 1.9 \times 10^5 M_{\odot}$ and note a positional offset between the H I gas and the stellar component.

ESO540-G031 (HIPASS J0049–20) is a dwarf irregular galaxy at a TRGB distance of $3.34 \pm 0.24 \text{ Mpc}$ (Karachentsev et al. 2003), located only $40'$ east of NGC 247. The HIPASS BGC gives $F_{\text{HI}} = 3.9 \pm 1.5 \text{ Jy km s}^{-1}$ and $v_{\text{sys}} = 294 \text{ km s}^{-1}$ (Koribalski et al. 2004). H I maps of ESO540-G031 (UGCA 015, DDO6) obtained with the GMRT (Bergum et al. 2008) and the VLA (Ott et al. 2012) show $F_{\text{HI}} = 2.6 \pm 0.3$ and 1.2 Jy km s^{-1} , respectively. Using our low-resolution ATCA H I mosaic of NGC 247 and surroundings

we measure $F_{\text{HI}} \approx 3.2 \text{ Jy km s}^{-1}$ for ESO540-G031 and derive $M_{\text{HI}} = 8.2 \times 10^6 M_{\odot}$ (see also Warren et al. 2007). The HI emission of ESO540-G031 is offset towards the south-western side of the stellar body. Its relatively bright GALEX UV emission suggests significant star formation ($\text{SFR} = 1.4 \times 10^{-3} M_{\odot} \text{ yr}^{-1}$; Ott et al. 2012).

ESO540-G032 is another transition-type dwarf galaxy. Parkes and ATCA HI data by Bouchard et al. (2005) suggest a centre velocity of 228 km s^{-1} . The detection was later confirmed by Da Costa et al. (2008) who also obtain new HST-ACS optical data, deriving a TRGB distance of $3.7 \pm 0.2 \text{ Mpc}$ and $M_{\text{HI}} = 9.1 \times 10^5 M_{\odot}$. Their ATCA image shows an HI source with a faint eastern extension.

5.2.3 NGC 7793 subgroup

NGC 7793 (HIPASS J2357–32) is a bright spiral galaxy in the Sculptor group at a TRGB distance of $3.91 \pm 0.41 \text{ Mpc}$ (Karachentsev et al. 2003). We use the low-resolution ATCA 16-pointing mosaic data of NGC 7793 and its surroundings to obtain HI maps of NGC 7793. The ATCA HI distribution extends beyond the previously published single-pointing VLA maps (Carignan & Puche 1990a; Walter et al. 2008). We measure $D_{\text{HI}} = 16'.5$ (see Table 6) and $F_{\text{HI}} = 292.6 \text{ Jy km s}^{-1}$, in agreement with the HIPASS BGC F_{HI} of $278.5 \pm 20.4 \text{ Jy km s}^{-1}$ (Koribalski et al. 2004). For comparison, Walter et al. (2008) measure $F_{\text{HI}} = 246 \text{ Jy km s}^{-1}$ with the VLA, missing HI gas mainly in the extended outer disc. Our mean HI velocity field shows that the position angle of NGC 7793's outer disc ($PA = 300^\circ$) is much larger than that of its stellar disc ($PA = 278^\circ$), suggesting a significant warp. This is also supported by the closed velocity contours. Carignan & Puche (1990a) also notice the PA change. They determine the rotation curve out to a radius of $7'.5$ (see also de Blok et al. 2008). Significant uncertainties remain about the inclination angle change in the outer disc, affecting the shape of the rotation curve. Combining the ATCA and VLA HI data would be of significant benefit for studying the outer disc gas distribution and kinematics (see also Radburn-Smith et al. 2012, 2014). NGC 7793 has two dwarf companions, ESO349-G031 and UGCA 442, located at projected distances of $\sim 3^\circ$.

ESO349-G031 (HIPASS J0008–34), best known as the Sculptor Dwarf Irregular Galaxy (SDIG), has an extremely low stellar luminosity and is most likely a transition-type dwarf galaxy (Côté et al. 2000). For a comprehensive study of its stellar properties and star formation history see Heisler et al. (1997) and Lianou & Cole (2013), respectively. Karachentsev et al. (2006) determined a TRGB distance of $3.21 \pm 0.26 \text{ Mpc}$. Its nearest neighbour is the spiral galaxy NGC 7793 (see Fig. 7), which lies at a projected distance of $\sim 3^\circ$ ($\sim 200 \text{ kpc}$). Our ATCA data show a resolved HI source with a clear velocity gradient. We measure $F_{\text{HI}} = 4.8 \text{ Jy km s}^{-1}$ and derive $M_{\text{HI}} = 1.2 \times 10^7 M_{\odot}$; our fitted HI position agrees with the optical centre. Using higher resolution VLA HI maps Côté et al. (2000) find the HI kinematical major axis (118°) — also seen in our ATCA HI maps — perpendicular to the optical position angle (30.3°), suggesting that the gas is rotating about the optical minor axis. This would make SDIG another dwarf transitional galaxy.

Similar misalignments are seen in Sextans A (Skillman et al. 1988), NGC 5253 (Kobulnicky & Skillman 1995; López-Sánchez et al. 2008, 2012), and GR 8 (Carignan et al. 1990). H α images of SDIG show very faint regions of diffuse emission (Meurer et al. 2006; Kaisin et al. 2007) and two point sources (Bouchard et al. 2009). Higher resolution ATCA HI maps will provide more information on the morphology and peculiar kinematics of the cold gas.

UGCA 442 (HIPASS J2343–31) is a Magellanic barred spiral galaxy oriented close to edge-on. Karachentsev et al. (2003) give a TRGB distance of $4.27 \pm 0.52 \text{ Mpc}$. Its nearest neighbour is the bright spiral galaxy NGC 7793, just over 3° away (see Fig. 7). Using our ATCA HI data we find an extended, regular rotating HI disc apart from minor deviations towards the southern (receding) end (see also Côté et al. 2000). We measure $F_{\text{HI}} = 52.2 \text{ Jy km s}^{-1}$, in agreement with HIPASS (Koribalski et al. 2004), and derive $M_{\text{HI}} = 2.2 \times 10^8 M_{\odot}$. H α imaging of UGCA 442 revealed five HII regions within the stellar disc, which are discussed by Miller (1996), Lee et al. (2003), and Meurer et al. (2006).

5.2.4 NGC 625 subgroup

NGC 625 (HIPASS J0054–37) is a Magellanic barred spiral galaxy at a distance of $D_{\text{TRGB}} = 3.89 \pm 0.22 \text{ Mpc}$ (Cannon et al. 2003). Its nearest neighbour is the dwarf irregular galaxy ESO245-G005 (HIPASS J0145–43) at a projected distance of $170'.3$. Our ATCA data show HI emission extending well beyond the stellar disc, including a peculiar HI feature on the western side, and a complex velocity field. The latter shows two HI components, likely a rotating disc ($PA \sim 90^\circ$) along the major axis and an equally prominent kinematic feature along the minor axis. Côté et al. (2000) find that NGC 625's dominant HI velocity gradient is along the minor axis and speculate whether a recent merger or accretion event could have led to the peculiar kinematics of the HI disc. Using higher resolution observations, Cannon et al. (2004) show that the velocity gradient is due to outflowing HI gas. NGC 625 is also classified as a 'blue amorphous galaxy' (Marlowe, Meurer & Heckman 1999), suggesting a recent burst of star formation.

ESO245-G005 (HIPASS J0145–43) is a Magellanic barred irregular galaxy at a TRGB distance of $4.43 \pm 0.45 \text{ Mpc}$ (Karachentsev et al. 2003). It is located $\sim 3^\circ$ (200 kpc) at a distance of 4 Mpc from the spiral galaxy NGC 625 in the outskirts of the Sculptor Group. Our ATCA HI data show a large, somewhat warped HI disc extending well beyond the star-forming stellar body. The HI emission is brightest near three prominent star-forming regions shown in the multi-wavelength image by Wang et al. (2017); we observe an HI depression towards the galaxy center. Côté et al. (2000) use ATCA HI maps to carry out a tilted-ring analysis; they find the HI kinematical axis of ESO245-G005 to depart from the optical major axis. For a detailed discussion of the HI kinematics see Kirby et al. (2012). We measure $F_{\text{HI}} = 83.2 \text{ Jy km s}^{-1}$, in agreement with HIPASS (Koribalski et al. 2004). SINGG H α (Meurer et al. 2006) and GALEX UV (Dale et al. 2009; Wong et al. 2016) images allow a detailed study of the galaxy's local star formation properties with

respect to the H I gas density.

ESO149-G003 (HIPASS J2352–52) is a Magellanic barred irregular galaxy at a distance of $D_{\text{TF}} = 5.9$ Mpc. It is seen close to edge-on and has a remarkable low-surface brightness (LSB) extension, possibly due to accretion of a dwarf companion. ESO149-G003 is relatively isolated and lies in the southern outskirts of the Sculptor Group. Ryan-Weber et al. (2004) detect filamentary H α emission in its bright stellar disc. Furthermore they find an isolated H II region ~ 1.5 to the west, which might be associated with ESO149-G003. Close inspection of the optical images shows some flaring of the outer LSB component and potentially a very small companion (PGC 441599) to the south-east. The latter lies within the H I envelope. Our ATCA H I moment maps show a slight asymmetry of ESO149-G003's H I distribution, which is further emphasized by its unusual two-component velocity field. The peculiar H I emission towards the northern (receding) end of the galaxy, which shows a velocity gradient nearly 90° different from the rotating disc, is offset from the very faint stellar extension. We suggest that ESO149-G003 may have undergone a minor merger event, the debris of which are detected in the form of H I tidal tails and extended stellar streams. Wang et al. (2016) find the galaxy to lie offset from the $D_{\text{HI}}-M_{\text{HI}}$ relation, which is not surprising given the extended peculiar emission. We measure $F_{\text{HI}} = 7.2$ Jy km s $^{-1}$, in agreement with HIPASS (Koribalski et al. 2004), and derive an H I mass of $5.9 \times 10^7 M_\odot$.

5.2.5 NGC 45 subgroup

The NGC 45 subgroup consists of the galaxies NGC 24, NGC 45, NGC 59 (Fouqué et al. 1992), and possibly MCG-04-02-003 (all at $\delta \gtrsim -25^\circ$). It is located at a larger distance than the main Sculptor members, but is often considered part of the Sculptor group (see Fig. 7). These galaxies are briefly described below, but are not part of the LVHIS galaxy atlas presented here. See also Westmeier et al. (2017) for deep Parkes H I observations.

NGC 45 (HIPASS J0014–23) is a low surface brightness spiral galaxy with a TRGB distance measurement of 6.6 ± 0.2 Mpc (Jacobs et al. 2009). Its H I disc ($M_{\text{HI}} = 2.0 \times 10^9 M_\odot$) was studied in detail with the VLA by Chemin et al. (2006) who derive a total mass of $3.7 \times 10^{10} M_\odot$ within a radius of 16.7 kpc from rotation curve analysis. GALEX UV images were presented by Lee et al. (2011).

NGC 24 (HIPASS J0009–24) is a nearly edge-on spiral galaxy with a TRGB distance measurement of 7.7 Mpc. It was studied in H I with the VLA by Chemin et al. (2006) who find a rather regular rotating disc and determine $M_{\text{HI}} = 7.5 \times 10^8 M_\odot$ and $M_{\text{dyn}} = 2.8 \times 10^{10} M_\odot$ within a radius of 10.5 kpc.

NGC 59 is a small, elliptical galaxy of type dS0. Karachentsev et al. (2003) list an SBF distance of 5.3 Mpc. It is detected in HIPASS at $v_{\text{hel}} = 364$ km s $^{-1}$, but was too faint for inclusion in either the HIPASS BGC (Koribalski et al. 2004) or HICAT (Meyer et al. 2004). We measure a HIPASS F_{HI} of 2.6 Jy km s $^{-1}$ and derived $M_{\text{HI}} = 1.7 \times 10^7 M_\odot$. Westmeier et al. (2017) measure $F_{\text{HI}} = 2.3$ Jy km s $^{-1}$ in

much deeper Parkes H I data. Beaulieu et al. (2006) obtain low-resolution ATCA H I data and determine $M_{\text{HI}} = 1.5 \times 10^7 M_\odot$. They show a barely resolved H I source centred on the stellar body and derive $M_{\text{HI}}/L_B = 0.07 M_\odot L_\odot$, similar to typical dIrr galaxies. We suggest that NGC 59 is likely a dwarf transitional galaxy.

MCG-04-02-003 (HIPASS J0019–22) appears to be a blue compact dwarf galaxy with an LSB outer disc (radius $\sim 110''$) at a Hubble distance of 9.5 Mpc (Warren et al. 2006, 2007). Warren et al. obtained deep optical images and low-resolution ATCA H I data; they measure $F_{\text{HI}} = 16.2$ Jy km s $^{-1}$, in agreement with the HIPASS BGC (Koribalski et al. 2004), and obtain $M_{\text{HI}} = 3.4 \times 10^8 M_\odot$ and $M_{\text{HI}}/L_B = 3.0 \pm 0.3 M_\odot/L_\odot$. The H I distribution is very extended, reaching well beyond the faint stellar disc. GALEX UV images show star formation in the galaxy core as well as a ring-like structure ($\sim 5' \times 2'$) encompassing the faint stellar disc. Higher resolution H I observations are needed to study the structure and kinematics of this galaxy in greater detail.

5.3 The Cen A Group

The nearby Cen A Group consists of two spatially separated sub-groups, one around the spiral galaxy M 83 (NGC 5236) and the other around the giant elliptical galaxy Centaurus A (NGC 5128). Karachentsev et al. (2007) estimate mean group distances of 4.8 and 3.8 Mpc, respectively, as well as virial masses of ~ 0.82 and $8.1 \times 10^{12} M_\odot$. The M 83 sub-group is significantly smaller, a factor 10 less massive and more compact than the Cen A sub-group. Their velocity dispersions differ by a factor two (61 km s $^{-1}$ for the M 83 and 136 km s $^{-1}$ for the Cen A sub-group). The gas-rich neighbours of the Cen A galaxy, as measured by the LVHIS project, are nicely visualised in Johnson et al. (2015; their Fig. 1). The Cen A Group covers ~ 1000 sq deg on the sky and has at least 60 confirmed members, of these the majority are dwarf irregular galaxies. Woodley (2006) estimate a total mass of $9.2 \times 10^{12} M_\odot$ for the Cen A group.

5.3.1 The M 83 subgroup

The M 83 subgroup consists of at least 10 galaxies. Of these six gas-rich dwarf galaxies are in the immediate vicinity of M 83 (see Fig. 10). Thim et al. (2003) and Jacobs et al. (2009) discuss the group and determine a group distance of 4.5 ± 0.2 Mpc. Some of the closest neighbours to M 83 are the dIrr galaxies UGCA 365 (= ESO444-G078), NGC 5264 (= DDO 242), IC 4316, ESO444-G084, IC 4247, AM1321–304, and the peculiar starburst galaxy NGC 5253. Within the $\sim 10\%$ uncertainty of their independent distances it appears that either NGC 5264, which lies 59.8 (78 kpc) east of M 83, or UGCA 365, located 38.4 (50 kpc) north of M 83, are closest to M 83. Recently, Müller et al. (2015) imaged an area of 60 sq deg around the M 83 subgroup, detecting 16 new dwarf galaxy candidates, which may be group members.

M 83 (HIPASS J1337–29) is a grand-design spiral galaxy with an unusually large H I envelope. It is located in the Cen A Group and forms the centre of a subgroup

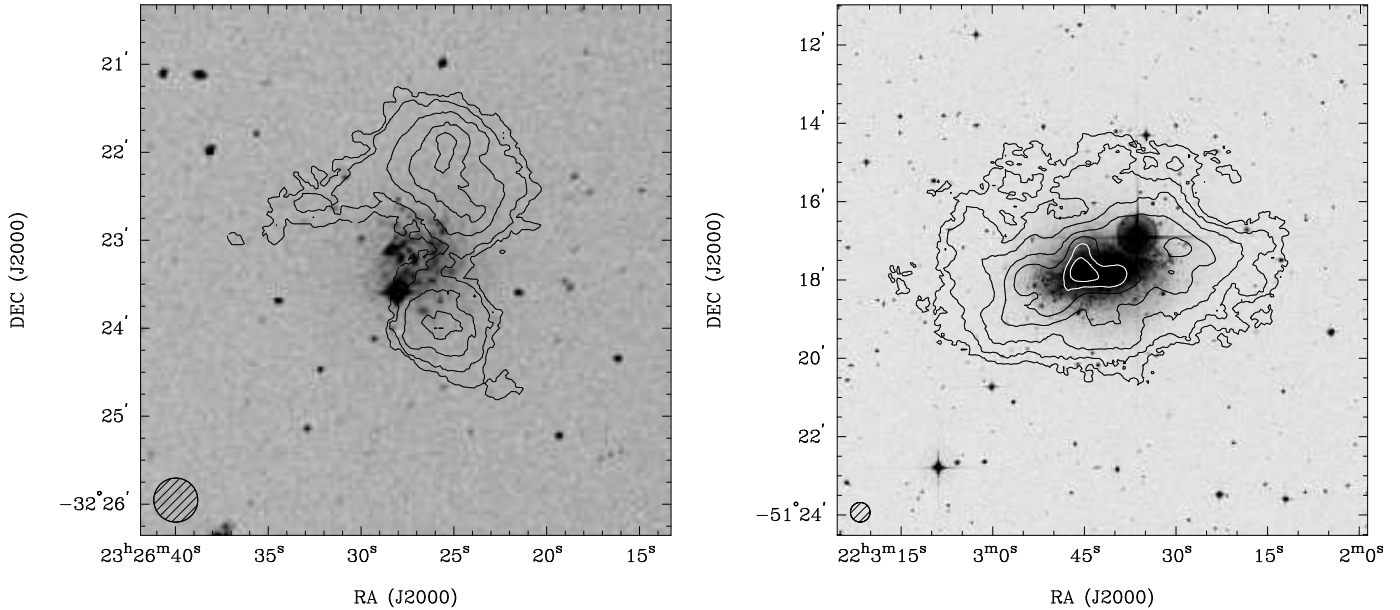


Figure 8. High-resolution ATCA H I column density maps of the Sculptor Group dIrr galaxies UGCA 438 (left) and IC 5152 (right). Contour levels are 0.05, 0.1, 0.2, 0.3, and 0.4 $\text{Jy beam}^{-1} \text{ km s}^{-1}$ (for UGCA 438) and 0.1, 0.2, 0.4, 0.8, 1.2, 1.6 and 2.0 $\text{Jy beam}^{-1} \text{ km s}^{-1}$ (for IC 5152). The synthesized beam ($30''$) is displayed in the bottom left corner.

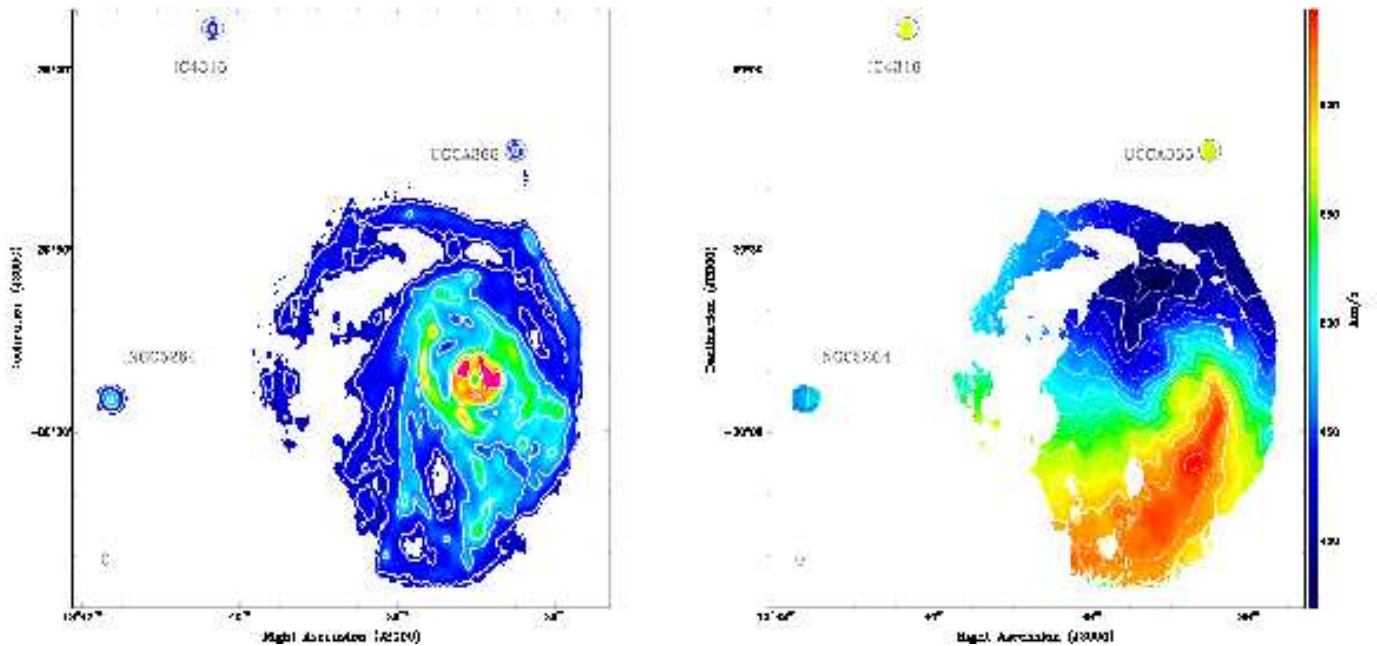


Figure 9. ATCA H I distribution (left) and mean H I velocity field (right) of the giant spiral galaxy M 83 (HIPASS J1337-29) and its dwarf companions NGC 5264, IC 4316 and UGCA 365. The contour levels are 0.4, 1.5, 3, 5 and 7 $\text{Jy beam}^{-1} \text{ km s}^{-1}$ (mom0) and 380 to 640 km s^{-1} in steps of 20 km s^{-1} (mom1). The angular resolution is $113''.1 \times 64''.1$.

consisting of ~ 10 known galaxies. A large range of distance estimates exist for M 83, the majority of which agree to within 10%. We adopt the TRGB distance estimate of 4.92 ± 0.10 Mpc by Jacobs et al. (2009). For comparison, Thim et al. (2003) estimate 4.5 ± 0.3 Mpc from ground-based cepheid measurements, while Herrmann et al. (2008) obtain 4.85 ± 0.12 Mpc from the planetary nebula luminosity function. We calculate a Hubble distance of 4.4 Mpc from

M 83's Local Group velocity of $v_{LG} = 332 \text{ km s}^{-1}$ (Koribalski et al. 2004), assuming $H_0 = 75 \text{ km s}^{-1} \text{ Mpc}^{-1}$. We note that Karachentsev et al. (2002) also estimate a TRGB distance (4.68 ± 0.46 Mpc) for the stellar stream located $18'.5$ north of M 83, likely an accreted dSph galaxy. This stream was discovered by Malin & Hadley (1997).

Our ATCA H I mosaic of M 83 and its dwarf companions NGC 5264, IC 4316 and UGCA 365, is shown in Fig. 9.

The integrated H I flux density of M83 as measured with the ATCA in the maximum entropy moment map is $F_{\text{HI}} = 1384 \text{ Jy km s}^{-1}$ compared to $1440 \text{ Jy km s}^{-1}$ in the CLEANed map, both are $\sim 10\%$ lower than the measured single-dish H I flux density. Walter et al. (2008) recover only a quarter of the total H I flux density (361 Jy km s^{-1}), due to their single pointing VLA observations and low sensitivity to extended, diffuse H I emission. The H I distribution of M83, as mapped with the ATCA, is most remarkable (Koribalski 2015, 2017; Jarrett et al. 2013). It extends well beyond the GALEX *XUV* disc (Thilker et al. 2007), referred to as a giant 2X-H I disc by Koribalski (2017). No longer does this grand-design spiral look regular and undisturbed. Our ATCA H I maps show outer disc streamers, irregular enhancements, an asymmetric tidal arm, diffuse emission, and a thoroughly twisted velocity field, much in contrast to its regular appearance in short-exposure optical images. M83's H I distribution is enormous, several times larger than its stellar disc. It is also a rather massive galaxy, mildly interacting with the neighbouring dwarf galaxies. The effect of this interaction on the dwarfs can of course be rather devastating. It is indeed quite likely that M83 has accreted dwarf galaxies in the past. While the H I distribution of M83 has previously been studied, we show the first detailed study of the large-scale emission in M83 and its surroundings.

Huchtmeier & Bohnenstengel (1981) measured an integrated H I flux density of about $1632 \text{ Jy km s}^{-1}$ which agrees well with the HIPASS estimate of $1630 \pm 96 \text{ Jy km s}^{-1}$ for M83 by Koribalski et al. (2004). At a distance of 4.92 Mpc this corresponds to an H I mass of $M_{\text{HI}} = 9.3 (\pm 0.5) \times 10^9 M_{\odot}$. They also derived a total H I extent of $76'$ (EW) $\times 95'$ (NS) for M83 at a column density of $N_{\text{HI}} = 6 \times 10^{18} \text{ atoms cm}^{-2}$. For comparison we show the deep Parkes multi-beam H I data of M83 and its surroundings in Fig. 10. Note that the gridded Parkes beam is $15.5'$, and $1 \text{ Jy beam km s}^{-1}$ corresponds to $\sim 1.4 \times 10^{18} \text{ atoms cm}^{-2}$. We measure a very similar H I extent of roughly $80' \times 88' (\pm 4')$, i.e. roughly 100 kpc. The H I distribution is clearly asymmetric as already noted by Huchtmeier & Bohnenstengel, the reason for which becomes immediately obvious in our high-resolution ATCA H I images (see Fig. 9). The latter reveal an extended arm emerging from the western part of M83 and curving 180° around to the east. The overall impression of M83 in neutral hydrogen is that of a distorted one-armed spiral, indicating that it may have interacted or merged with another, smaller galaxy. While the velocity field in this extended arm appears to follow the general pattern of rotation, the gas distribution shows numerous irregularities, clumps and bifurcations. The $20'$ long ridge in the northwest ends in a noticeable H I clump and marks a kink in the outer arm. The H I velocity field of M83 highlights the warped nature of the disc. Using 3D FAT Kamphuis et al. (2015) obtained an H I rotation curve indicating $v_{\text{rot}} = 157.0 \text{ km s}^{-1}$ at $R_{\text{max}} = 50.0 \text{ kpc}$ (for $i = 40.3^\circ$ and $PA = 226.9^\circ$; see Table 9) and $M_{\text{dyn}} = 2.8 \times 10^{11} M_{\odot}$.

The eastern-most H I emission of M83 which forms part of its peculiar, outer arm lies at $\alpha, \delta(\text{J2000}) = 13:39:40, -29:51:45$ ($v_{\text{hel}} = 536 \text{ km s}^{-1}$), i.e. $\sim 34.5'$ (45 kpc) away from the centre of M83. We note that the dwarf irregular galaxy NGC 5264 (HIPASS J1341–29; $v_{\text{sys}} = 478 \text{ km s}^{-1}$) lies at a projected distance of only $25.5'$ (33 kpc) from the eastern H I edge of M83. Given that the independently measured dis-

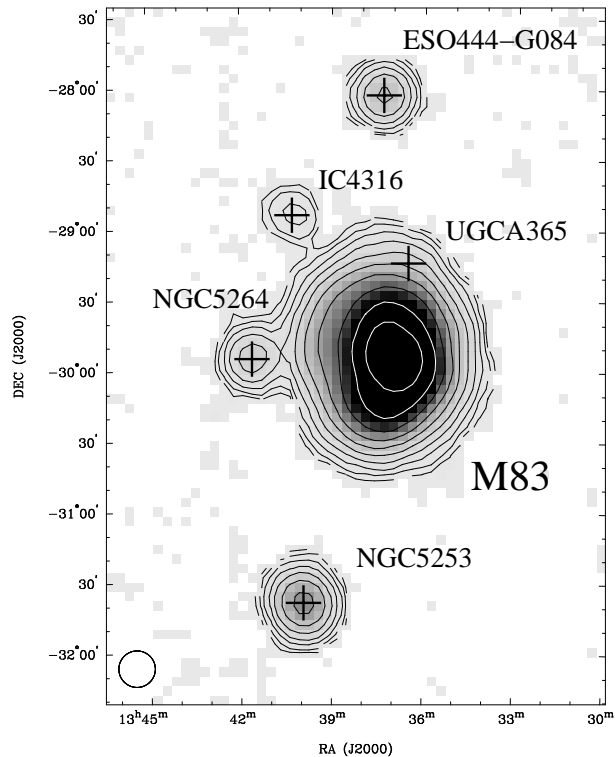


Figure 10. H I distribution of the M83 group as obtained from the re-calibrated deep Parkes H I multibeam survey (HIDEEP). The contour levels are 0.5, 1, 2, 4, 8, 16, 32, 64, 128 and 256 $\text{Jy beam}^{-1} \text{ km s}^{-1}$ (the first contour corresponds to an H I column density of $\sim 7 \times 10^{17} \text{ atoms cm}^{-2}$). The gridded Parkes beam of $15.5'$ is indicated at the bottom left.

tances to M83 and NGC 5264 are very similar (see Table 2) both galaxies are likely to be interacting.

UGCA 365 (HIPASS J1336–29) is a dwarf irregular galaxy located $38.4'$ from the spiral galaxy M83, just north of its extended H I envelope. Its TRGB distance is $5.25 \pm 0.43 \text{ Mpc}$ (Karachentsev et al. 2007), similar to that of M83 within the given uncertainty. UGCA 365 has an optical size of $1.2' \times 0.5'$ ($PA = 31^\circ$) and a *B*-band magnitude of 15.43 mag. Our low-resolution ATCA H I data of UGCA 365 show an unresolved source; at higher resolution a velocity pattern along the optical major axis is detected. We measure $F_{\text{HI}} = 2.9 \text{ Jy km s}^{-1}$ and derive $M_{\text{HI}} = 1.9 \times 10^7 M_{\odot}$. Both the stellar and the gas distribution show some extent to the south-east along the galaxy minor axis, possibly due to the tidal interaction with M83. Using an inclination-corrected ($i = 66^\circ$) rotational velocity of 50 km s^{-1} we calculate a total dynamical mass of $\sim 1.2 \times 10^9 M_{\odot}$ for UGCA 365. The tidal limit at the position of UGCA 365, $38.4'$ (50 kpc) from the centre of M83, is $\sim 5 \text{ kpc}$. Begum et al. (2008) observed UGCA 365 as part of the FIGGS project. They measure an H I diameter of $0.9'$ ($\sim 1.7 \times$ the optical diameter) and an H I flux density of $F_{\text{HI}} = 2.3 \pm 0.2 \text{ Jy km s}^{-1}$. Their H I map hints at an extension towards the north-west.

ESO444-G084 (HIPASS J1337–28) is a dwarf irregular galaxy located at a distance of $D_{\text{TRGB}} = 4.61 \pm 0.46 \text{ Mpc}$ (Karachentsev et al. 2002). Its closest neighbours

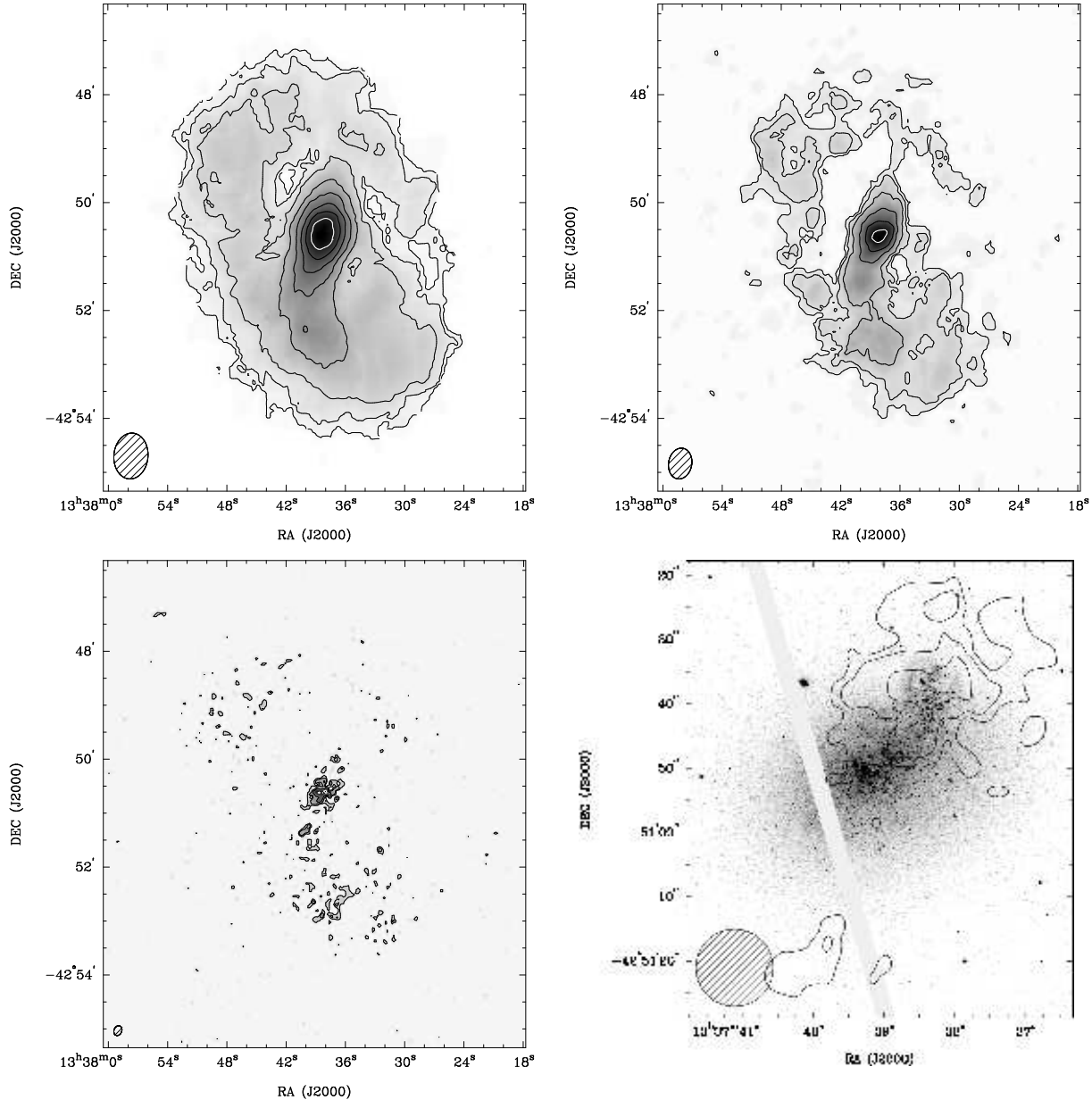


Figure 11. HI moment maps of the dwarf galaxy NGC 5237 (HIPASS J1337–42) at different weightings of the ATCA uv -data. The resulting synthesized beam is displayed in the bottom left corner of each panel and given in brackets here. **Top:** natural weighting (left: beam = $51''.1 \times 37''.9$; contour levels = 0.05, 0.1, 0.2, 0.4, 0.6, 0.8, 1.0 and $1.2 \text{ Jy beam}^{-1} \text{ km s}^{-1}$) and robust $r = 0$ weighting (right: beam = $34''.5 \times 25''.8$; contours = 0.05, 0.1, 0.2, 0.4, 0.6, and $0.8 \text{ Jy beam}^{-1} \text{ km s}^{-1}$) excluding the longest baselines. **Bottom:** robust weighting including the longest baselines (left: beam = $11''.2 \times 8''.6$; contours = 0.025, 0.05, 0.1, and $0.2 \text{ Jy beam}^{-1} \text{ km s}^{-1}$) with a zoom-in to the central area overlaid on to an HST F606-band image (right: beam = $12''$; contours = 0.05, 0.1, and $0.2 \text{ Jy beam}^{-1} \text{ km s}^{-1}$), showing the high density HI emission associated with a young star-forming region to the north-west of the galaxy’s stellar core. The measured HI flux densities decrease with increasing resolution (10.9 , 7.5 and 2 Jy km s^{-1} from top left to bottom left) due to extended HI emission being filtered by the interferometer.

are IC 4316 ($64''.2$), UGCA 365 ($72''.2$), M 83 ($109''.3$) and NGC 5264 ($125''.4$), all members of the M 83 group. ESO444-G084 is located 147 kpc north of the massive spiral galaxy M 83. Our ATCA HI moment maps reveal a symmetric disc, at least twice as large as the stellar B_{25} extent, with a significant ($\sim 35^\circ$) warp of the outer parts (see also Côté et al. 2000). We measure $F_{\text{HI}} = 16.5 \text{ Jy km s}^{-1}$, lower than the HIPASS F_{HI} of $21.1 \pm 3.2 \text{ Jy km s}^{-1}$ (Koribalski et al. 2004), and derive $M_{\text{HI}} = 8.3 \times 10^7 M_\odot$. We calculate an HI

mass to light ratio of $M_{\text{HI}}/L_B = 2.1$, well above the typical value for dwarf irregular galaxies (Roberts & Haynes 1994; see also Warren et al. 2004). Côté et al. (2000) obtain an HI rotation curve which reaches $v_{\text{rot}} = 63.1 \text{ km s}^{-1}$ at a radius of 3.2 kpc. Côté et al. (2009) estimate an SFR of $0.8 \times 10^{-3} M_\odot \text{ yr}^{-1}$.

NGC 5253 (HIPASS J1339–31) is a peculiar starburst galaxy at a distance of $D_{\text{TRGB}} = 3.56 \text{ Mpc}$ (Mould &

Sakai 2008), located $\sim 2^\circ$ south of M 83 ($D_{\text{TRGB}} = 4.92$ Mpc) but significantly closer. For a detailed, multi-wavelength study see López-Sánchez et al. (2012). NGC 5253 is one of the closest known BCD galaxies; its outer optical isophotes resemble that of a dwarf elliptical galaxy but the core is dominated by a young starburst and it contains a large amount of gas. Fig. 10 shows a very deep Parkes H I map of the M 83 group, using re-calibrated data from the HIDEEP survey (Koribalski 2006, Minchin et al. 2003); no diffuse H I gas is detected between NGC 5253 and M 83 down to $N_{\text{HI}} = 10^{18}$ atoms cm^{-2} for gas filling the beam. Furthermore, the large separation between NGC 5253 and M 83 (at least 1 Mpc based on their independent distances), suggests that no recent tidal interactions occurred between the two galaxies. The H I dynamics of NGC 5253 was studied by Kobulnicky & Skillman (1995) using very short (45 min.) VLA observations. They found that most of the H I gas appears to rotate around the major axis of the stellar distribution. We note that the integrated H I flux density measured with the VLA ($F_{\text{HI}} = 24$ Jy km s^{-1}) is only 54% of that detected by HIPASS (see Table 2). Kobulnicky & Skillman (2008) explore if gas inflow, outflow or galaxy interactions are the cause of NGC 5253’s unusual H I gas dynamics. Using ATCA H I data from the LVHIS project López-Sánchez et al. (2008, 2012) further investigate NGC 5253 and conclude that NGC 5253 experienced infall of a low-metallicity H I cloud along the minor axis, triggering the powerful starburst. NGC 5253 is one of several dwarf starburst galaxies with highly unusual H I kinematics, including NGC 625 (Cannon et al. 2004), M 82 (Yun, Ho & Lo 1993), and IC 10 (Huchtmeier 1979; Wilcots & Miller 1998; Manthey & Oosterloo 2008). The latter two, M 82 and IC 10, show H I streamers most likely due to galaxy interactions.

IC 4316 (HIPASS J1340–28) is a dwarf irregular galaxy at a distance of $D_{\text{TRGB}} = 4.41 \pm 0.44$ Mpc (Karachentsev et al. 2002), located $72.5'$ north-east of M 83 (see Fig. 10). The large (mostly red) low surface brightness stellar body resembles that of an early-type galaxy while optical and GALEX *UV* images of the inner region are typical of dIrr galaxies. Our ATCA H I data show a marginally resolved source with just a hint of gas motions along the N–S axis, well offset from the stellar major axis (see also López-Sánchez et al. 2012). We measure $F_{\text{HI}} = 2.6$ Jy km s^{-1} , somewhat more than in HIDEEP (Minchin et al. 2003), and derive $M_{\text{HI}} = 1.2 \times 10^7 M_\odot$. Begum et al. (2008) show a barely resolved GMRT H I intensity map of IC 4316.

NGC 5264 (HIPASS J1341–29) is a Magellanic irregular galaxy of type IB(s)m), located very close to the eastern tidal arm of M 83 (see Figs. 9 and 10). Our ATCA H I maps reveal an extended, slowly rotating, possibly warped disc. The independent distance estimates for NGC 5264 ($D_{\text{TRGB}} = 4.53 \pm 0.45$ Mpc, Karachentsev et al. 2002) and M 83 ($D_{\text{TRGB}} = 4.92 \pm 0.10$ Mpc) suggest they may be physically close and are likely tidally interacting. Their respective Local Group velocities are 300 km s^{-1} (NGC 5264) and 332 km s^{-1} (M 83); see Table 6. NGC 5264 lies $\sim 1^\circ$ from the centres of M 83 (HIPASS 1337–29) and IC 4316 (HIPASS J1340–28). Our ATCA H I maps show a well-resolved H I distribution and rather peculiar velocity field. We measure $F_{\text{HI}} = 10.3$ Jy km s^{-1} , in agreement with HIPASS and HIDEEP

(Koribalski et al. 2004, Minchin et al. 2003), and derive $M_{\text{HI}} = 5.0 \times 10^7 M_\odot$. Very short VLA observations by Simpson & Gottesman (2000) show H I emission in an asymmetric ring-like distribution or central depression; they detect only $\sim 40\%$ of the total H I flux. López-Sánchez et al. (2012) study the nearby starburst dwarf galaxy NGC 5253, south of M 83, and provide a comparison with its dwarf neighbours, incl. NGC 5264. For a separation of 80 kpc between NGC 5264 and M 83 the tidal radius at the position of NGC 5264 is ~ 7 kpc, similar to the size of the ATCA H I distribution. GALEX *UV* and H α emission is detected in NGC 5264, which is dominated by two bright H II regions; $\text{SFR} \sim 0.02 M_\odot \text{ yr}^{-1}$ (Lee et al. 2009). ATCA 20-cm radio continuum emission is detected (Shao et al. 2017).

AM1321–304 (HIPASS J1324–30) is a Magellanic dwarf irregular (dIm) galaxy at a distance of $D_{\text{TRGB}} = 4.63$ Mpc (Karachentsev et al. 2002). Its nearest large neighbour is the spiral galaxy M 83 at a projected distance of $173.7'$. Our ATCA H I maps reveal a marginally resolved source without a distinct velocity gradient. We measure $F_{\text{HI}} = 1.7$ Jy km s^{-1} , in agreement with Begum et al. (2008) who observed AM1321–304 as part of the FIGGS project. The HIPASS F_{HI} of 3.9 ± 2.5 Jy km s^{-1} is higher but with a large uncertainty (Banks et al. 1999). Begum et al. (2008) measure an H I diameter of $1.4'$ (\sim the optical diameter).

IC 4247 (HIPASS J1326–30A) is a dwarf irregular galaxy in the M 83 sub-group with $D_{\text{TRGB}} = 4.97 \pm 0.49$ Mpc (Karachentsev et al. 2007). Its systemic velocity is 420 km s^{-1} (Banks et al. 1999; Minchin et al. 2003). IC 4247’s nearest neighbours are AM 1321–304 ($45.8'$), HIPASS J1321–31 ($100.5'$), KKs 54 ($113.2'$) and M 83 ($136.6'$); projected distances are given in brackets. Our low-resolution ATCA H I data show a marginally resolved source with a velocity gradient along the major axis. Higher resolution ATCA H I images reveal a tear-drop shaped gas distribution, hinting at tidal interactions. We measure $F_{\text{HI}} = 3.3$ Jy km s^{-1} , in agreement with HIDEEP (Minchin et al. 2003), and derive an H I mass of $1.9 \times 10^7 M_\odot$. Lee et al. (2007) measure the properties of two H II regions in IC 4247. There are luminous AGB stars, helium-burning stars and some early type stars detected in this galaxy, indicating ongoing star formation. A detailed analysis of its star formation history shows the galaxy was constantly forming stars during its lifetime (Crnojević et al. 2011).

5.3.2 The Cen A subgroup

The Cen A subgroup is dominated by the giant elliptical galaxy NGC 5128 (Cen A), an active radio galaxy which lies $\sim 13.3^\circ$ (~ 1 Mpc) south of M 83. Fig. 14 shows the 20-cm radio continuum emission of Cen A as mapped by the Parkes 64-m telescope (Calabretta et al. 2014), overlaid with HIPASS contours and galaxy labels. Cen A’s giant radio lobes extend over 10° in the north-south direction. New radio and optical images of Cen A are presented by McKinley et al. (2018) who investigate its jets, outflows, and filaments. LVHIS galaxies in the vicinity of Cen A are visualised in Johnson et al. (2015; their Fig. 1) using our ATCA H I maps colour-coded by distance. A multitude of gas-poor

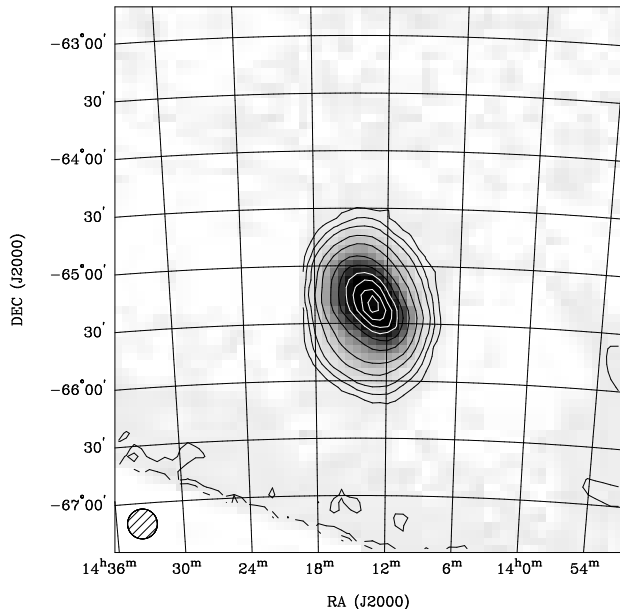


Figure 12. Low-resolution HI distribution of the Circinus galaxy and surroundings as obtained from the deep Parkes HI multi-beam survey of the Zone of Avoidance (Jurazsek et al. 2000, Staveley-Smith et al. 2016). The contour levels are $7 \times (0.4, 1, 2, 5, 10, 20, 30, 40, 50, 60 \text{ and } 66)$ $\text{Jy beam}^{-1} \text{ km s}^{-1}$, where $7 \text{ Jy beam}^{-1} \text{ km s}^{-1}$ corresponds to an HI column density of 10^{19} cm^{-2} . The levels were chosen to match those by Freeman et al. (1977; their Fig. 6) above their detection limit of $N_{\text{HI}} = 5 \times 10^{19} \text{ cm}^{-2}$; our detection limit is a factor ~ 10 lower. The gridded beam of $15'5$ is shown in the bottom left corner.

dwarf galaxies are also known in the vicinity of Cen A.

Recent deep imaging of NGC 5128 (Cen A) by Crnojević et al. (2016) using Megacam on the Magellan telescope reveals new stellar streams, shells, and faint dwarf galaxies in its vicinity. For the nine dwarf galaxies with distance estimates, they give upper limits of $M_{\text{HI}} \sim 5 \times 10^6 M_{\odot}$ from HIPASS.

Grossi et al. (2007) present an in-depth study of three unusual dwarf galaxies in the Cen A Group: HIPASS J1321–31, HIPASS J1337–39 and HIDEEP J1337–3320. They obtain deep HST WFPC2 images through the F555W and F814W filters ($\sim 5000 \text{ s}$ each), R -band and $H\alpha$ images with the WIYN 3.5-m telescope as well as ATCA HI moment maps. Only HIPASS J1337–39 is detected in $H\alpha$. They also note that HIPASS J1328–30 is a distant LSB galaxy with $v_{\text{hel}} \sim 8100 \text{ km s}^{-1}$ which lies in the line-of-sight to a Galactic HVC. Crnojević et al. (2012) study five dIrr galaxies in the Cen A Group: CEN06, ESO269-G058, AM1318–444, HIPASS J1348–37 and ESO384-G016. They analyse archival HST ACS data in the F606W and F814W filters to study the stellar populations, metallicities and stellar masses. Neither AM1318–44 nor ESO384-G016 were detected in HIPASS and therefore not selected as part of the LVHIS sample. AM1318–444 (KK 196) has a distance of $D_{\text{TRGB}} = 3.98 \pm 0.29 \text{ Mpc}$ (Karachentsev et al. 2007), located at $\alpha, \delta(\text{J2000}) = 13:21:47.1, -45:03:48.0$. It appears to be in or near the southern radio lobe of Cen A. Lee et al. (2007) detect $H\alpha$ emission and derive a stellar mass of about $2.7 \times 10^7 M_{\odot}$. Using HIPASS we determine an upper

limit of $F_{\text{HI}} = 5 \text{ Jy km s}^{-1}$, assuming $v_{\text{hel}} = 741 \text{ km s}^{-1}$ and a velocity width of 100 km s^{-1} . The r.m.s. noise in the area is increased due to the bright radio emission from Cen A’s southern lobe.

ESO376-G016 (HIPASS J1043–37) is a dwarf irregular galaxy at a distance of $D_{\text{TF}} = 7.1 \text{ Mpc}$. Its nearest neighbour is ESO318-G013 (HIPASS J1047–38; $v_{\text{hel}} = 716 \text{ km s}^{-1}$) about 2° away. Our ATCA data show a regularly rotating HI disc extending well beyond the stellar body. We measure $F_{\text{HI}} = 10.2 \text{ Jy km s}^{-1}$, in agreement with HIPASS (Koribalski et al. 2004), and derive $M_{\text{HI}} = 1.2 \times 10^8 M_{\odot}$.

ESO318-G013 (HIPASS J1047–38) is a small, edge-on spiral galaxy at a distance of $D_{\text{TF}} = 6.5 \text{ Mpc}$. Its nearest neighbour is ESO376-G016 (HIPASS J1043–37; $v_{\text{hel}} = 668 \text{ km s}^{-1}$) about 2° away. Our ATCA data show a well-resolved, but somewhat lopsided HI disc extending well beyond the stellar body. While its rotation appears regular, the gas distribution shows some peculiar features. A faint HI tail on the western (receding) side may hint at tidal interactions. We measure $F_{\text{HI}} = 9.1 \text{ Jy km s}^{-1}$, in agreement with HIPASS (Koribalski et al. 2004), and derive $M_{\text{HI}} = 9.1 \times 10^7 M_{\odot}$.

ESO215-G?009 (HIPASS J1057–48) is a highly obscured ($b = 10.5^\circ$) dwarf irregular galaxy at a TRGB distance of $5.25 \pm 0.41 \text{ Mpc}$ (Karachentsev et al. 2007). It appears to be rather isolated with a low current star formation rate. Its nearest known neighbour is likely the small spiral galaxy ESO318-G013 (HIPASS J1047–38) nearly 10° away. Warren, Jerjen & Koribalski (2004) determine an HI mass to light ratio of $M_{\text{HI}} / L_{\text{B}} = 22 \pm 4 M_{\odot} / L_{\odot}$, the highest recorded for a galaxy in the literature. Our ATCA data show the HI disc of ESO215-G?009 to extend over six times the Holmberg radius of the stellar disc. We measure $F_{\text{HI}} = 110.1 \text{ Jy km s}^{-1}$, in agreement with HIPASS (Koribalski et al. 2004), and derive $M_{\text{HI}} = 7.1 \times 10^8 M_{\odot}$. Warren et al. (2004) note that its azimuthally averaged surface density remains below the critical gas surface density at all radii. While its rotation pattern is very regular, the galaxy’s near circular shape (suggesting a near face-on orientation if the gas rotates in circular orbits) is somewhat in contrast to the measured rotation amplitude. Using 3D FAT Kamphuis et al. (2015) obtain an HI rotation curve indicating $v_{\text{rot}} = 93.0 \text{ km s}^{-1}$ at $R_{\text{max}} = 9.3 \text{ kpc}$ (for $i = 18:5$ and $PA = 119:7$; see Table 9) and $M_{\text{dyn}} = 1.9 \times 10^{10} M_{\odot}$. See also previous HI kinematics analysis by Warren et al. (2004) and Kirby et al. (2012).

ESO320-G014 (HIPASS J1137–39) is a dwarf irregular galaxy at a distance of $D_{\text{TRGB}} = 6.08 \pm 0.65 \text{ Mpc}$ (Karachentsev et al. 2007), located in the outskirts of the Cen A group. Its closest known companion is the dwarf galaxy HIPASS J1132–32, and its most massive companions are NGC 3621 (HIPASS J1118–32) and Cen A (HIPASS J1324–42). Our ATCA data show a barely resolved HI source centred on the fuzzy stellar body; a faint GALEX UV source is also detected. Deep infrared photometry was obtained by Young et al. (2014). A weak gradient is seen in the HI velocity field, but higher resolution is needed for fur-

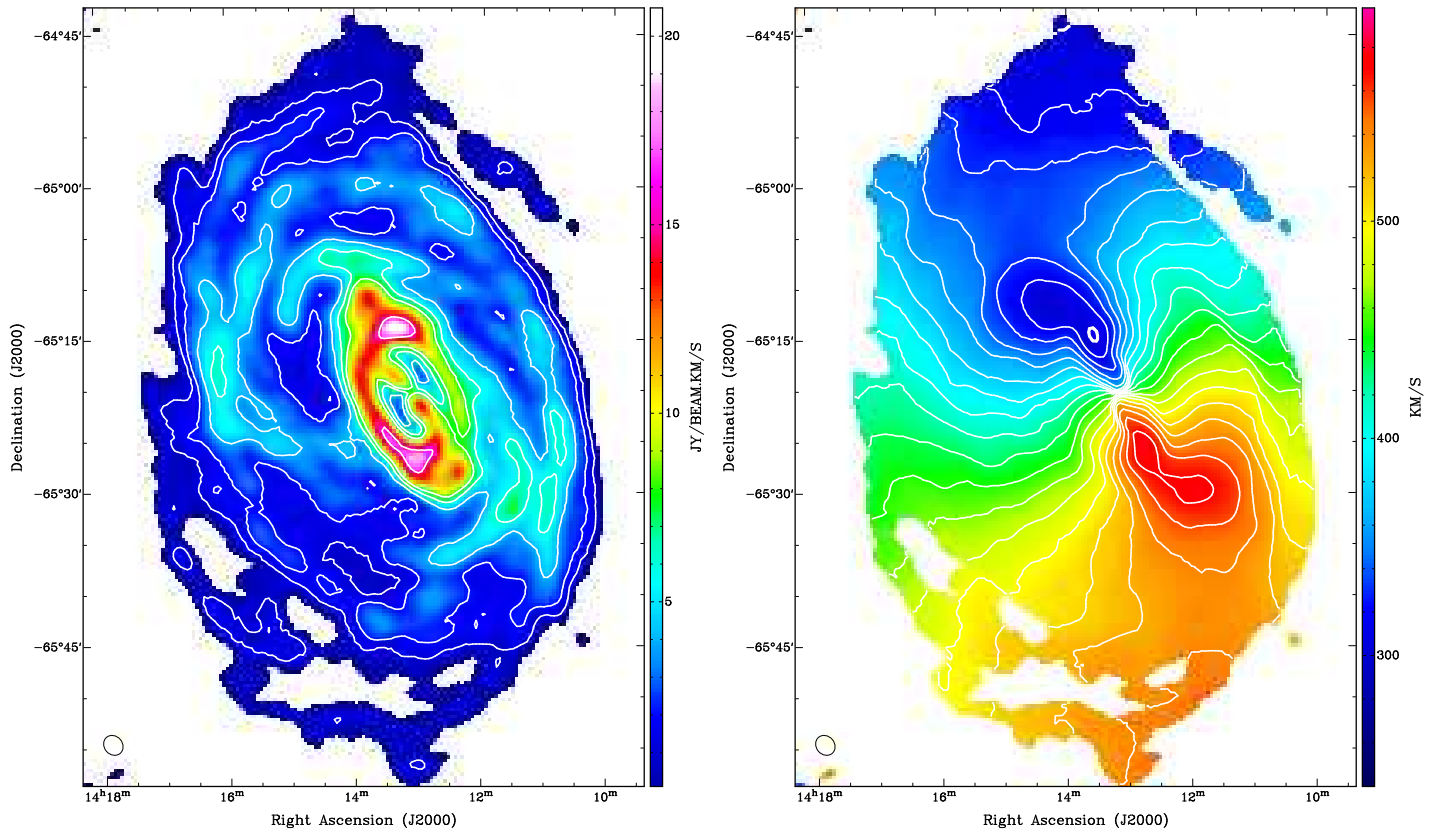


Figure 13. ATCA HI distribution (left) and mean velocity field (right) of the giant Circinus Galaxy (HIPASS J1413–65, $D_{\text{TF}} = 4.2$ Mpc) from 12-pointing ATCA mosaic observations. The contour levels are 1, 2, 4, 8, and 16 $\text{Jy beam}^{-1} \text{ km s}^{-1}$ (mom0) and 300 to 570 km s^{-1} in steps of 15 km s^{-1} (mom1). The angular resolution is $124'' \times 107''$.

ther analysis of the gas kinematics. We measure $F_{\text{HI}} = 2.0$ Jy km s^{-1} , in agreement with HIPASS (Meyer et al. 2004), and derive $M_{\text{HI}} = 1.7 \times 10^7 M_{\odot}$.

ESO379-G007 (HIPASS J1154–33) is a dwarf irregular galaxy at a distance of $D_{\text{TRGB}} = 5.22 \pm 0.52$ Mpc (Karachentsev et al. 2002), located in the outskirts of the Cen A group. The stellar core appears to be embedded in a low-surface brightness disc, which is somewhat extended to the east. Its nearest neighbour is likely ESO379-G024 (181'6 away), discussed below. Our ATCA data show the HI distribution and velocity field to be somewhat asymmetric, with the eastern side more diffuse and extended than the western side. We measure $F_{\text{HI}} = 4.8$ Jy km s^{-1} and derive $M_{\text{HI}} = 3.1 \times 10^7 M_{\odot}$. Begum et al. (2008) observed ESO379-G007 as part of the FIGGS project. They measure an HI diameter of 3'6 and an HI flux density of $F_{\text{HI}} = 5.0 \pm 0.5$ Jy km s^{-1} , in agreement with our HIPASS and ATCA measurements. Bouchard et al. (2009) find just one H II region, located $\sim 10''$ west of the optical centre. The galaxy shape and kinematics suggest that ram pressure or tidal forces may play a role and could possibly be responsible for the offset star-forming region.

ESO379-G024 (HIPASS J1204–35) is a dwarf irregular galaxy at a Hubble distance of 4.9 Mpc, also located in the outskirts of the Cen A group. Using HIPASS we mea-

sure $v_{\text{sys}} = 631$ km s^{-1} and obtain $v_{\text{LG}} = 356$ km s^{-1} . The 6dF optical velocity for ESO379-G024 is 652 ± 55 km s^{-1} . Its nearest neighbour is likely the galaxy ESO379-G007 (HIPASS J1154–33), $\sim 3^{\circ}$ away. The ATCA HI distribution of ESO379-G024 is noticeably lopsided, with more HI gas on the south-western side. The HI velocity field is somewhat irregular, suggesting a mixture of low rotation and peculiar velocities. We measure $F_{\text{HI}} = 2.6$ Jy km s^{-1} , within the uncertainties of the HIPASS F_{HI} , and derive $M_{\text{HI}} = 1.5 \times 10^7 M_{\odot}$.

ESO321-G014 (HIPASS J1214–38) is a dwarf irregular galaxy (type IABm) at $D_{\text{TRGB}} = 3.18 \pm 0.23$ Mpc (Dalcanton et al. 2009), located in the outskirts of the Cen A group. Its nearest known neighbour, the galaxy ESO379-G024 (discussed above), lies 3° away. Using our ATCA HI data we measure $F_{\text{HI}} = 5.1$ Jy km s^{-1} , more than three times the HI emission detected by Begum et al. (2008) with the GMRT. The HIPASS F_{HI} value of 6.4 ± 1.6 Jy km s^{-1} (Koribalski et al. 2004) agrees within the uncertainties. We derive an HI mass of $1.2 \times 10^7 M_{\odot}$. We find the HI distribution to be quite symmetric apart from small deviations of the velocity field towards the northern end. The stellar distribution has a peculiar arrow shape (very prominent in GALEX UV images) with star formation most prominent in the southern part. Bouchard et al. (2009) present an H α im-

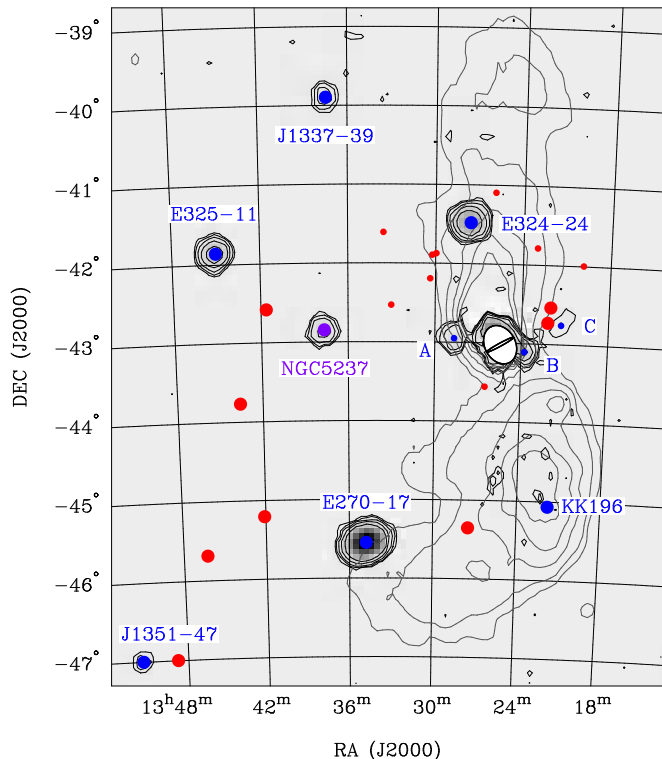


Figure 14. Galaxies in the vicinity of the radio galaxy Centaurus A. Three newly discovered HI sources near Cen A are labelled A, B, and C. Black contours ($1, 2, 4, 8,$ and $16 \text{ Jy beam}^{-1} \text{ km s}^{-1}$) and greyscales show the HI distribution from HIPASS, while grey contours show the 20-cm radio continuum emission from CHIPASS (Calabretta et al. 2014). All known group members in the displayed area are marked: dIrr galaxies (blue circles; named), dSph galaxies (red circles), and the dwarf transitional galaxy NGC 5237 (purple circle; named). The gridded HIPASS beam is $15''.5$.

age, indicating weak emission along the galaxy minor axis.

ESO381-G018 (HIPASS J1244-35) is a dwarf irregular galaxy in the Cen A group, located at a TRGB distance of $5.32 \pm 0.51 \text{ Mpc}$ (Karachentsev et al. 2007). Its nearest neighbour is ESO381-G020 (HIPASS J1246-33), just over 2° away. Our ATCA HI maps show a barely resolved source with a regular rotating disc. We measure $F_{\text{HI}} = 2.6 \text{ Jy km s}^{-1}$, in agreement with HIPASS (Meyer et al. 2004), and derive an HI mass of $1.7 \times 10^7 M_\odot$. A detailed study of its star formation history suggests there were two recent star formation bursts (Crnojević et al. 2011).

ESO381-G020 (HIPASS J1246-33) is a dwarf irregular galaxy in the Cen A group, located at a TRGB distance of $5.44 \pm 0.37 \text{ Mpc}$ (Karachentsev et al. 2007). Its outer stellar disc has a slightly triangular shape, appearing much wider in the SE than the NW. Our ATCA HI data reveal a well-resolved, regular rotating disc, ~ 10 times more massive than that of its nearest neighbour ESO381-G018 (HIPASS J1244-35). The mean HI velocity field indicates a mild warp of the outer HI disc (Côté et al. 2000, Kirby et al. 2012). We measure $F_{\text{HI}} = 32.8 \text{ Jy km s}^{-1}$, in agreement with HIPASS (Koribalski et al. 2004), and derive $2.3 \times 10^8 M_\odot$. In contrast to its neighbour, ESO381-G020 is clearly detected

in H α , indicating ongoing star formation (Lee et al. 2007, Bouchard et al. 2009, Côté et al. 2009) at a rate of $\sim 3\text{--}6 \times 10^{-3} M_\odot \text{ yr}^{-1}$; see also Crnojević et al. (2011).

NGC 4945 (HIPASS J1305-49) is a well-known starburst spiral galaxy (type SBcd) in the Cen A group. It is oriented close to edge-on, highly obscured in the optical and located at a distance of $D_{\text{TRGB}} = 3.80 \text{ Mpc}$ (Mould & Sakai 2008). Its nearest neighbours are ESO269-G058 ($157''.1$), ESO269-G7066 ($285''.1$; $v_{\text{hel}} = 784 \text{ km s}^{-1}$) and NGC 5206 ($290''.2$); projected distances are given in brackets. About $7'$ north-west of the centre of NGC 4945 lies a faint galaxy, sometimes known as CEN05, but identified to be a distant spiral galaxy by Bouchard et al. (2004). Early ATCA HI maps of NGC 4945 were published by Ott et al. (2001). They also map the extended 20-cm radio continuum emission of NGC 4945 and estimate a flux density of $4.2 \pm 0.1 \text{ Jy}$ over the central source. Consequently, HI absorption dominates in the galaxy core, extending over $\pm 200 \text{ km s}^{-1}$ with respect to the systemic velocity. This is similar to the velocity range of the main HI emission. Here we present HI results from new ATCA mosaic observations in the EW367 and 750A arrays. The overall impression is that of a large, symmetric, regularly rotating HI disc, which does not extend much beyond the bright stellar disc. Using 3D FAT Kamphuis et al. (2015) obtain an HI rotation curve indicating $v_{\text{rot}} = 173.6 \text{ km s}^{-1}$ at $R_{\text{max}} = 16.7 \text{ kpc}$ (for $i = 82^\circ.8$ and $PA = 44^\circ.2$; see Table 9) and $M_{\text{dyn}} = 1.2 \times 10^{11} M_\odot$. NGC 4945 has the highest rotational velocity in our sample. A peculiar HI feature is seen towards the south, possibly extraplanar gas lagging behind. Combining all the available ATCA HI data will allow a much more detailed analysis. Using our low-resolution ATCA mosaic we measure $F_{\text{HI}} = 405.3 \text{ Jy km s}^{-1}$ and derive $M_{\text{HI}} = 1.4 \times 10^9 M_\odot$. This is $\sim 20\%$ higher than the HIPASS F_{HI} , which is significantly affected by HI absorption (Koribalski et al. 2004).

Bouchard et al. (2007) obtained HI observations for 18 dwarf galaxies in the Cen A Group. They detect five galaxies (ESO269-G037, CEN06, UGCA 365, ESO384-G016 and ESO272-G025) with the ATCA and quote upper limits for the remaining galaxies. For the dE galaxy ESO269-G7066 (KK 190; $D_{\text{TRGB}} = 3.82 \pm 0.26 \text{ Mpc}$; Karachentsev et al. 2007), which was observed with the 64-m Parkes telescope for over 10 h, Bouchard et al. (2007) give an upper limit of $F_{\text{HI}} = 0.026 \text{ Jy km s}^{-1}$. This corresponds to an M_{HI} limit of $\sim 9 \times 10^4 M_\odot$. In the vicinity is also the dwarf galaxy ESO269-G037 (type dSph or dIrr). Using ATCA HI observation Bouchard et al. (2007) find $v_{\text{hel}} = 744 \text{ km s}^{-1}$ and $F_{\text{HI}} = 0.14 \pm 0.02 \text{ Jy km s}^{-1}$. The latter corresponds to an HI mass of only $4 \times 10^5 M_\odot$ for $D_{\text{TRGB}} = 3.48 \pm 0.35 \text{ Mpc}$ (Karachentsev et al. 2002).

CEN06 (HIPASS J1305-40) is a dwarf galaxy, also known as KK 182, at a distance of $D_{\text{TRGB}} = 5.78 \pm 0.42 \text{ Mpc}$ (Karachentsev et al. 2007). It is located behind M83 and Cen A, separated by ~ 1 and 2 Mpc , respectively. CEN06's nearest neighbour is likely NGC 5011C, located more than $3''.5$ away ($v_{\text{hel}} = 647 \text{ km s}^{-1}$, Saviane & Jerjen 2007). Our ATCA HI maps show the emission centred on the optical galaxy and a north-south velocity gradient. We measure $F_{\text{HI}} = 4.5 \text{ Jy km s}^{-1}$, in agreement with HIPASS (Koribalski et

al. 2004), and derive an H I mass of $3.5 \times 10^7 M_{\odot}$. CEN06 was detected in H α by Côté et al. (2009), and Crnojević et al. (2012) derive a stellar mass close to $10^6 M_{\odot}$.

ESO269-G058 (HIPASS J1310–46A) is a peculiar I0-type dwarf galaxy at a distance of $D_{\text{TRGB}} = 3.80 \pm 0.29$ Mpc (Karachentsev et al. 2007). It was first catalogued in H I by Banks et al. (1999), who established it as a member of the Cen A Group. Using our ATCA H I data we measure a systemic velocity of 400 km s^{-1} and $F_{\text{HI}} = 5.4 \text{ Jy km s}^{-1}$, slightly lower than the HIPASS F_{HI} (Koribalski et al. 2004), and derive $M_{\text{HI}} = 1.8 \times 10^7 M_{\odot}$. ESO269-G058 exhibits a regular H I velocity, but we note that its H I emission barely extends beyond the optical body. Its nearest neighbour is probably NGC 4945, over $2^{\circ}5$ away. H α emission was detected by Phillips et al. (1986), and Crnojević et al. (2012) derive a stellar mass of $\sim 9 \times 10^8 M_{\odot}$. The enhanced star formation observed in ESO269-G058 may have been triggered by tidal interactions ~ 1 Gyr in the past (Davidge 2007).

HIPASS J1321–31 (KK 195) is an unusual dwarf galaxy at a distance of $D_{\text{TRGB}} = 5.22 \pm 0.30$ Mpc (Pritzel et al. 2003). Its stellar body (diameter $\sim 70''$) is very faint and diffuse; no H α emission was detected (Banks et al. 1999, Meurer et al. 2006, Grossi et al. 2007). Using our ATCA H I data we determine a center position of $\alpha, \delta(\text{J2000}) = 13:21:09.4, -31:32:01.2$, just east of the stellar body. Faint GALEX UV emission is also detected. The ATCA H I distribution is resolved and shows an east-west velocity gradient. Grossi et al. (2007) detect only the bright H I component, which is located to the south-east of the optical centre, while we find further H I emission to the west. We measure $F_{\text{HI}} = 5.2 \text{ Jy km s}^{-1}$, in agreement with HIPASS (Koribalski et al. 2004), and derive $M_{\text{HI}} = 3.3 \times 10^7 M_{\odot}$. HIPASS J1321–31 has a high $M_{\text{HI}}/L_{\text{B}}$ ratio of 4.6. Begum et al. (2008) observed HIPASS J1321–31 as part of the FIGGS project. They measure an H I diameter of 5 arcmin and an H I flux density of $F_{\text{HI}} = 4.8 \pm 0.5 \text{ Jy km s}^{-1}$, slightly lower than our HIPASS and ATCA measurements.

NGC 5102 (HIPASS J1321–36) is a large lenticular galaxy of type SA0 at a distance of $D_{\text{TRGB}} = 3.40 \pm 0.39$ Mpc (Karachentsev et al. 2002) located in the outskirts of the Cen A group. Its nearest neighbours are HIPASS J1337–39 ($267^{\circ}5$), HIPASS J1305–40 ($287^{\circ}2$), and ESO324-G024 ($298^{\circ}4$); projected distances are given in brackets. Our ATCA H I moment maps reveal a large, somewhat asymmetric H I disc with a central H I depression that coincides with the bright stellar body. Most of the galaxy’s H I emission resides in a ring-like structure of 3.5 radius, also seen by van Woerden et al. (1993), surrounded by much fainter emission in the outskirts. A prominent H I extension to the south-west resembles a tidal arm, suggesting ongoing gas accretion. NGC 5102’s H I velocity field highlights the lopsided and mildly warped nature of the disc. We measure $F_{\text{HI}} = 85.4 \text{ Jy km s}^{-1}$, within the uncertainties of the HIPASS F_{HI} (Koribalski et al. 2004), resulting in $M_{\text{HI}} = 2.3 \times 10^8 M_{\odot}$. Using the VLA CnD-array van Woerden et al. (1993) only detect the H I emission within the inner disc/ring of NGC 5102 and measure $F_{\text{HI}} = 50 \text{ Jy km s}^{-1}$. Using 3D FAT Kamphuis et al. (2015) obtain an H I rotation curve indicating $v_{\text{rot}} = 94.3 \text{ km s}^{-1}$ at $R_{\text{max}} = 10.5$ kpc (for $i = 75^{\circ}3$ and $PA =$

$42^{\circ}2$; see Table 9) and $M_{\text{dyn}} = 2 \times 10^{10} M_{\odot}$. Based on a stellar population study Davidge (2008) find NGC 5102 to be a post-starburst galaxy. Mitzkus et al. (2016) provide an excellent literature overview and analyse the stellar population and kinematics in the central region of NGC 5102 via MUSE data, suggesting two counter-rotating stellar discs. Faint radio continuum emission is detected in the galaxy core ($1.7 \pm 0.5 \text{ mJy}$).

NGC 5128 (HIPASS J1324–42; Cen A) is a nearby radio galaxy ($D_{\text{TRGB}} = 3.77 \pm 0.38$ Mpc; Rejkuba 2004) with two giant lobes spanning ~ 8 degrees on the sky (ie., ~ 0.5 Mpc). It is the dominant elliptical galaxy in the Cen A/M83 galaxy group, which is known to contain ~ 100 members. The bright and extended 20-cm radio continuum emission provides some technical challenges for accurate H I measurements which are further complicated by the presence of both H I emission and absorption over a wide velocity range (see Koribalski et al. 2004). In Fig. 14 we show the radio lobes of Cen A as well as the locations of gas-rich or gas-poor group members.

Cen A’s optical appearance is that of a giant elliptical surrounded by a prominent band of highly opaque dust, which matches the H I disc detected with the ATCA. Struve et al. (2010) measure $F_{\text{HI}} = 144 \text{ Jy km s}^{-1}$, somewhat more than obtained by van Gorkom et al. (1990), and derive $M_{\text{HI}} = 4.9 \times 10^8 M_{\odot}$. For a comparison with Parkes F_{HI} measurements see the discussion in Koribalski et al. (2004; their Section 3.6). Struve et al. (2010) obtain an H I extent of $814''$ or 15 kpc and find a regular rotating, highly warped disc. Further H I emission is detected in the outer disc, somewhat aligned with the faint optical shells of Cen A and likely the result of gas accretion in a recent merger event. Schiminovich et al. (1994) also find H I emission associated with the diffuse shells of NGC 5128 and measure $F_{\text{HI}} = 208 \text{ Jy km s}^{-1}$. Parkes H I spectra obtained by Gardner & Whiteoak (1976) shows emission from ~ 250 to 850 km s^{-1} . Using HIPASS we estimate an H I mass of at least $6 \times 10^8 M_{\odot}$.

Furthermore, we detect H I emission east and west of Cen A (sources A, B and C in Fig. 14) without stellar counterparts. These could either be very faint dwarf galaxies near Cen A or another set of H I shells. Their $\alpha, \delta(\text{J2000})$ positions and H I properties are as follows. Source A: $13:28:39.9, -42:56:56.5$ ($\sim 349 - 507 \text{ km s}^{-1}$, 35.4 east of Cen A, $F_{\text{HI}} = 7.9 \pm 1.1 \text{ Jy km s}^{-1}$; slightly elongated N–S); source B: $13:23:46.2, -43:06:19.9$ ($\sim 257 - 414 \text{ km s}^{-1}$, 19.2 west of Cen A, unresolved in HIPASS), and source C: $13:21:16.9, -42:45:24.1$ ($\sim 507 - 534 \text{ km s}^{-1}$, 48.5 east of Cen A, elongated NW–SE in HIPASS. GALEX UV images do not reveal any counterparts).

ESO324-G024 (HIPASS J1327–41) is a Magellanic irregular galaxy located near or within the northern radio lobe of Cen A (Johnson et al. 2015). Its TRGB distance of 3.73 ± 0.43 Mpc (Karachentsev et al. 2002; Jacobs et al. 2009) places it $\gtrsim 100$ kpc from the centre of Cen A, making it the closest dIrr companion. Numerous dSph galaxies (eg., KKs 55, AM1318–444, KK 197) are possibly located even closer to Cen A than ESO324-G024 (see Fig. 15). Our ATCA data show a tadpole-shaped H I distribution, the head of which agrees with the stellar body. The H I tail points in a north-east direction and shows a disturbed velocity field.

Côté et al. (2009) detect just a few H II regions, mostly outside the bright stellar disc. For a detailed analysis of ESO324-G024's H I morphology, kinematics, star formation and polarisation properties see Johnson et al. (2015).

ESO270-G017 (HIPASS J1334–45), also known as the Fourcade-Figueroa galaxy, is a highly obscured edge-on spiral. Karachentsev et al. (2013) assigned a distance of $D_{\text{mem}} = 3.6$ Mpc based on the assumption that it is a member of the Cen A subgroup. Here we adopt the TRGB distance of 6.95 ± 0.16 Mpc derived by Jacobs et al. (2009), in agreement with the Hubble distance obtained from ESO270-G017's Local Group velocity ($v_{\text{LG}} = 611 \text{ km s}^{-1}$). Our ATCA H I maps reveal a well-resolved disc with a mostly regular rotation pattern (see also Koribalski 2008). Some peculiar motions are discernible on the western (approaching) side, which also shows a higher velocity dispersion. The observed H I extent of ESO270-G017 is only slightly larger than the stellar disc detected in deep optical images by David Malin. Mild asymmetries in the stellar disc (typical for SBm type galaxies) match those in the H I distribution. We measure $F_{\text{HI}} = 224.7 \text{ Jy km s}^{-1}$, $\sim 10\%$ higher than the HIPASS F_{HI} (Koribalski et al. 2004), and derive $M_{\text{HI}} = 2.6 \times 10^9 M_{\odot}$.

NGC 5237 (HIPASS J1337–42) appears to be a dwarf transitional galaxy, located in the Cen A group at a distance of $D_{\text{TRGB}} = 3.40 \pm 0.23$ Mpc (Karachentsev et al. 2007). Its nearest neighbours are the dSph galaxy Kks 57 ($D_{\text{TRGB}} = 3.93 \pm 0.28$), the IBm galaxy ESO325-G?011 (HIPASS J1345–41) and the giant elliptical Cen A, separated by $46'.7$, $100'.7$ and $134'.3$ (~ 133 kpc), respectively. Our ATCA H I moment maps reveal a large H I disc, extending well beyond the bright stellar body, and a slightly warped velocity field. In Fig. 11 we show the NGC 5237 H I distribution at different angular resolutions, revealing areas of high-density H I emission within the extended H I disc. Interestingly, we find the densest H I peak to coincide with a young star-forming region, well-resolved in HST images from the Hubble Legacy Archive. While the overall stellar population resembles that of a dwarf elliptical galaxy, the single H II region to the north-west and offset H I emission suggest that NGC 5237 is a dwarf transitional galaxy. Its vicinity to Cen A makes it likely that tidal interactions / harassment are responsible for the observed peculiarities. Fig. 11 also highlights the difference in position angles between the outer and inner H I distribution, which are both significantly offset from the stellar distribution. Thomson (1992) presents numerical simulations of galaxy interactions in the Cen A group and discusses the likely impact on NGC 5237 and the edge-on galaxy ESO270-G017, also known the Fourcade-Figueroa shred. Using our low-resolution ATCA H I maps we measure $F_{\text{HI}} = 10.9 \text{ Jy km s}^{-1}$, comparable to the HIPASS F_{HI} of $12.1 \pm 2.6 \text{ Jy km s}^{-1}$ (Koribalski et al. 2004), and derive $M_{\text{HI}} = 3 \times 10^7 M_{\odot}$. Using 3D FAT Kamphuis et al. (2015) obtain an H I rotation curve indicating $v_{\text{rot}} = 75.2 \text{ km s}^{-1}$ at $R_{\text{max}} = 4.9$ kpc (for $i = 33^\circ.8$ and $PA = 50^\circ.2$; see Table 9) and $M_{\text{dyn}} = 6.5 \times 10^9 M_{\odot}$. Côté et al. (2009) detect H α emission from the bright H II region and derive $\text{SFR} = 4.6 \times 10^{-3} M_{\odot} \text{ yr}^{-1}$. Radio continuum emission from that region is detected in our ATCA 20-cm data (see Shao et al. 2017).

HIPASS J1337–39 appears to be an old dwarf galaxy at a distance of $D_{\text{TRGB}} = 4.83 \pm 0.20$ Mpc (Grossi et al. 2007). It is located in the outskirts of the Cen A group, $\sim 4^\circ$ from NGC 5128. Its closest known neighbour is ESO325-G?011, $\sim 2^\circ.5$ to the south. HIPASS J1337–39's near spherical stellar distribution (diameter $\sim 40''$) resembles that of dSph galaxies, while the ongoing star formation activity, as revealed by the detected H α emission (Grossi et al. 2007), is more typical of dIrr galaxies. Our low-resolution ATCA H I moment maps show a symmetric, regularly rotating disc aligned NE to SW. Its centre position is $\alpha, \delta(J2000) = 13^{\text{h}} 37^{\text{m}} 25^{\text{s}}$, $-39^\circ 53' 46''.7$ (see Table 8), in agreement with the optical centre. In contrast, at high resolution the H I distribution is elongated in the direction perpendicular to the main rotation axis and the velocity field and dispersion becomes noticeably more irregular. The ATCA H I moment maps shown by Grossi et al. (2007), at a resolution of $31'' \times 24''$, reveal a NW extension with a distinct velocity field (possibly an accreted H I gas cloud or companion that triggered the recent SF). The overall impression is that of a dwarf transitional galaxy. We find $F_{\text{HI}} = 6.9 \text{ Jy km s}^{-1}$, comparable to Grossi's $F_{\text{HI}} = 7.2 \text{ Jy km s}^{-1}$ and in agreement with the HIPASS F_{HI} of $6.6 \pm 1.8 \text{ Jy km s}^{-1}$ (Koribalski et al. 2004), and derive $M_{\text{HI}} = 3.8 \times 10^7 M_{\odot}$. HIPASS J1337–39 somewhat resembles the Sagittarius dwarf irregular galaxy (SagDIG; HIPASS J1929–17; $D = 1.16$ Mpc) which is located in the outskirts of the Local Group (Hunter et al. 2012; Begum et al. 2006; Higgs et al. 2016).

HIDEEP J1337–3320 is a small, low luminosity dwarf galaxy, located at a projected distance of $\sim 3.5^\circ$ ($\lesssim 300$ kpc) from M 83. Grossi et al. (2007) derive a distance of $D_{\text{TRGB}} = 4.4 \pm 0.2$ Mpc. They suggest it is a transition type dwarf galaxy, similar to LGS3, Phoenix and DDO 210 (the Aquarius dwarf galaxy), based on its very smooth and regular optical morphology (diameter $\sim 30''$) and H I gas content ($M_{\text{HI}} = 5.1 \times 10^6 M_{\odot}$; $M_{\text{HI}}/L_{\text{B}} = 1.4$). This galaxy is currently not part of the LVHIS galaxy atlas. For a detailed discussion and ATCA H I maps see Grossi et al. (2007).

ESO325-G?011 (HIPASS J1345–41) is a Magellanic barred irregular galaxy at a distance of $D_{\text{TRGB}} = 3.40 \pm 0.39$ Mpc (Karachentsev et al. 2002). Its nearest neighbour appears to be NGC 5237 at a projected distance of $100'.7$, while the giant elliptical Cen A is nearly 4° away. Our ATCA H I maps show a well-resolved, rather regular rotating disc. ESO325-G?011's H I flux density and velocity dispersion are somewhat higher at the north-western (receding) side, which also shows minor asymmetries in the velocity field. The stellar brightness is also significantly higher on the H I-bright side. Using tilted-ring modelling Kirby et al. (2012), who provide a detailed description of ESO325-G?011, find $v_{\text{rot}} = 46 \text{ km s}^{-1}$ (for $PA = 302^\circ$, $i = 42^\circ$) at $R_{\text{max}} = 3.1$ kpc, similar to Côté et al. (2000). We measure $F_{\text{HI}} = 26.4 \text{ Jy km s}^{-1}$, in agreement with HIPASS (Koribalski et al. 2004). Côté et al. (2009) identify eight H II regions across the stellar disc and derive $\text{SFR} = 2.5 \times 10^{-3} M_{\odot} \text{ yr}^{-1}$.

ESO174-G?001 (HIPASS J1348–53) is very low surface brightness galaxy at a distance of $D_{\text{TF}} = 3.6$ Mpc. This is much lower than the Hubble distance of 6.2 Mpc derived from the HIPASS v_{LG} of 466 km s^{-1} (Koribalski et

al. 2004). ESO174-G?001 — not be confused with the more distant spiral galaxy ESO174-G001 — appears to be rather isolated with the nearest neighbours being NGC 5206, a gas-poor lenticular galaxy, and NGC 4945 (HIPASS J1305–49), a gas-rich starburst galaxy, both more than 5° away. ESO174-G?001’s stellar disc is highly obscured by foreground stars due to its low Galactic latitude of $8^\circ.6$. The galaxy was not detected in deep *H*-band observations by Kirby et al. (2008b). Our ATCA H I moment maps show a very extended H I disc, ~ 3 times larger than the stellar disc, and a clear rotation pattern (see also Koribalski 2015, 2017). We find the kinematic major axis of ESO174-G?001 ($PA = 218^\circ$) differs significantly from the morphological major axis ($PA \sim 165^\circ$) both of the stellar and the inner H I disc. Kirby et al. (2012) discuss these misalignments and employ tilted-ring fitting to show that the position angle decreases with radius from 233° to 202° . Their rotation curve, which appears to flatten reaching $R_{\max} = 360''$ (6.3 kpc), shows $v_{\text{rot}} = 66 \text{ km s}^{-1}$ for $i = 40^\circ$. Using 3D FAT Kamphuis et al. (2015) obtain a much higher rotational velocity ($v_{\text{rot}} = 97.3 \text{ km s}^{-1}$) assuming $i = 22^\circ.7$ and $PA = 218^\circ.4$ (see Table 9). Neither model fits the observed kinematics well. Similar misalignments are found in NGC 625 (Côte  t et al. 2000; Cannon et al. 2004), IC 4662 (van Eymeren et al. 2010) and GR8 (Begum & Chengalur 2003), who discuss infall/outflow, polar rings and minor mergers. The X-shaped H I distribution in the inner region of ESO174-G?001 provides further clues as to the nature of its peculiar gas kinematics. Using our ATCA H I data we measure $F_{\text{HI}} = 52.6 \text{ Jy km s}^{-1}$, in agreement with the HIPASS F_{HI} (Koribalski et al. 2004), and derive $M_{\text{HI}} = 1.6 \times 10^8 M_\odot$. A 20-cm radio continuum source ($\sim 7 \text{ mJy}$) is detected just offset from the galaxy centre (Shao et al. 2017).

HIPASS J1348–37 is a dwarf irregular galaxy at $\alpha, \delta(\text{J2000}) = 13:48:34.1, -37:58:08.0$ (see Table 7) as measured using our ATCA H I data. It was discovered by Banks et al. (1999) in a detailed HIPASS study of the Cen A Group. Its distance of $D_{\text{TRGB}} = 5.75 \pm 0.66 \text{ Mpc}$ (Karachentsev et al. 2007) places it beyond M 83 and more than 2 Mpc from Cen A. Its nearest neighbours are the dwarf galaxies ESO383-G087 (HIPASS J1349–36), ESO384-G016, ESO325-G?011 (HIPASS J1345–41) and NGC 5408 (HIPASS J1403–41). Crnojevi   et al. (2012) suggest that HIPASS J1348–37 may be a transition-type dwarf galaxy, given its absence of recent star formation. They derive a stellar mass of $\sim 2 (\pm 1) \times 10^7 M_\odot$. Our ATCA H I data show a barely resolved source, centred on the faint optical body. There is a hint of a north-south velocity gradient. We measure $F_{\text{HI}} = 1.6 \text{ Jy km s}^{-1}$, in agreement with HIPASS (Meyer et al. 2004), and derive an H I mass of at least $1.2 \times 10^7 M_\odot$.

ESO383-G087 (HIPASS J1349–36) is a barred Magellanic dwarf galaxy at a TRGB distance of $3.45 \pm 0.27 \text{ Mpc}$ (Karachentsev et al. 2007), located roughly between M 83 and Cen A. Its nearest neighbours are the dwarf galaxies ESO384-G016 (see Bouchard et al. 2009, Crnojevi   et al. 2012) and HIPASS J1348–37, at projected distances of $103'.9$ and $114'.8$, respectively, while the more massive S0 galaxy NGC 5102 (HIPASS J1321–36) is $5^\circ.5$ away. Our ATCA data show an extended, but highly asymmetric H I distribution of ESO383-G087 and an unusual H I velocity field. The latter

is similar to the H I velocity dispersion map and shows no clear sign of rotation (Koribalski 2007), which is likely due to the galaxy’s face-on orientation. This interpretation is supported by the narrow velocity widths of the integrated H I profile. The very faint spheroidal halo seen in co-added optical images by Kemp & Meaburn (1994) is similar in size to the detected ATCA H I envelope. The somewhat asymmetric H I extensions to the north and south are likely spiral arms. We measure $F_{\text{HI}} = 25.4 \text{ Jy km s}^{-1}$, in agreement with HIPASS (Koribalski et al. 2004), and derive $M_{\text{HI}} = 7.1 \times 10^7 M_\odot$. Only a partial GALEX *UV* image is currently available.

ESO384-G016 is a lenticular or transition-type dwarf galaxy, located at $\alpha, \delta(\text{J2000}) = 13:57:01.6, -35:20:02.0$ and $D_{\text{TRGB}} = 4.53 \pm 0.31 \text{ Mpc}$ (Karachentsev et al. 2007). It is not detected in HIPASS. Beaulieu et al. (2006) report $v_{\text{hel}} = 504 \text{ km s}^{-1}$ and $F_{\text{HI}} = 1.3 \text{ Jy km s}^{-1}$, ie. $M_{\text{HI}} = 6.5 \times 10^6 M_\odot$. They show a marginally resolved ATCA H I distribution and suggest the galaxy may be experiencing ram pressure stripping from its passage through the intragroup medium. Jerjen et al. (2000) measure a stellar velocity of $561 \pm 32 \text{ km s}^{-1}$. ESO384-G016 is detected in H α by Bouchard et al. (2009), is clearly visible in GALEX *UV* images and looks like blue compact galaxy in optical images.

HIPASS J1351–47 is a dwarf irregular galaxy at $\alpha, \delta(\text{J2000}) = 13:51:21.2, -46:59:53.0$ (see Table 7) as measured using our ATCA H I data. It was discovered by Banks et al. (1999) who measured $v_{\text{sys}} = 530 \text{ km s}^{-1}$. Its distance of $D_{\text{TRGB}} = 5.73 \pm 0.73 \text{ Mpc}$ (Karachentsev et al. 2007) is similar to that of HIPASS J1348–37; both are located in the outskirts of the Cen A Group. Its nearest neighbours appear to be several dSph galaxies, for example LEDA 166179 (see Fig. 15). The low Local Group velocity ($v_{\text{LG}} = 291 \text{ km s}^{-1}$, Table 2) of HIPASS J1351–47 indicates an infall velocity of $\sim 140 \text{ km s}^{-1}$ towards the group. Our ATCA H I data show a marginally resolved source and hint at a kinematic *PA* of $\sim 45^\circ$. We measure $F_{\text{HI}} = 3.6 \text{ Jy km s}^{-1}$, in agreement with HIPASS (Meyer et al. 2004), and derive an H I mass of $2.8 \times 10^7 M_\odot$.

NGC 5408 (HIPASS J1403–41) is a barred Magellanic irregular galaxy (type IB(s)m) in the Cen A group, located at a distance of $4.81 \pm 0.48 \text{ Mpc}$ (Karachentsev et al. 2002). Its closest neighbours are ESO325-G?011 (HIPASS J1345–41), HIPASS J1348–37, and NGC 5237 (HIPASS J1337–42) at projected distances of $207'.7, 264'.5, \text{ and } 299'.1$, respectively. Our ATCA data show a well-resolved, fairly asymmetric H I distribution with a reasonably regular velocity field. The galaxy’s south-western side shows peculiar motions and relatively high velocity dispersion. The disturbed appearance, studied in detail by van Eymeren et al. (2010), could be due to gas outflows and/or accretion. The total H I extent of NGC 5408 is about $10'.0 \times 6'.3$ ($PA = 302^\circ$), four times larger than its optical size. Van Eymeren et al. (2010) also studied the distribution and kinematics of the ionized gas using H α images and spectra, revealing a diffuse filamentary structure similar to IC 4662. NGC 5408 is a well-studied galaxy, mainly because of its ultra-luminous X-ray source, possibly an intermediate mass black hole. Strong 20-cm radio continuum emission is associated with the bright

H II region detected by van Eymeren et al. (2010).

Circinus (HIPASS J1413–65) is a highly obscured, late-type spiral galaxy with a very large, warped H I disc (Freeman et al. 1977; Jones et al. 1999; Curran et al. 2008; For, Koribalski & Jarrett 2012). It is located behind the Galactic Plane (at $l, b = 311.3^\circ, -3.8^\circ$), which makes it difficult to study its optical properties and large-scale environment due to high stellar density and dust extinction ($A_B = 5.3$ mag, Schlafly & Finkbeiner 2011). For the same reason, the distance to Circinus is still rather uncertain. Based on a variety of methods, Freeman et al. (1977) derived an approximate distance of 4.2 ± 0.8 Mpc, which we adopt here. Karachentsev et al. (2007) estimated $D_{\text{TF}} = 2.82 \pm 0.28$ Mpc using 2MASS infrared magnitudes, while K13 give $D_{\text{TF}} = 4.2$ Mpc. Freeman et al. (1977) determine de Vaucouleurs and Holmberg optical diameters for the Circinus Galaxy of 11'.9 and 17'.2, respectively, after extinction correction (their Table 3) as well as $PA = 210^\circ$ and $i = 65^\circ$. They give $L_B = 7.2 \times 10^9 L_\odot$. Using our ATCA H I mosaic we find an enormous H I envelope for the Circinus Galaxy, extending over 60' (at the outermost H I contour), well beyond the optical Holmberg radius. We measure an $D_{\text{HI}} = 48'.7$ at $1 M_\odot \text{pc}^{-2}$. Its large H I extent was also noted in the H I surveys of the Zone of Avoidance (HIZOA, Juraszek et al. 2000, Staveley-Smith et al. 2016) and in HIPASS (Koribalski et al. 2004); see Fig. 13. The ATCA H I distribution and mean H I velocity field of the Circinus galaxy, obtained with a 12-pointing mosaic in the 375-m configuration, show its large-scale warped H I disc. For, Koribalski & Jarrett (2012) analyse high-resolution Spitzer mid-infrared images of the Circinus Galaxy and compare with Parkes and ATCA H I data. They derive star formation rates and analyse the local star formation conditions. The ionized gas in Circinus was studied by Elmouttie et al. (1998a) via Fabry-Perot H α imaging. No GALEX UV images are available yet. Circinus also hosts bipolar radio lobes extending perpendicular to the inner disc (Elmouttie et al. 1998b, Wilson et al. 2011). The large H I discs of Circinus and M 83 are typical for their M_{HI} (see Wang et al. 2016) and allow us to obtain accurate rotation curves out to radii of ~ 50 kpc. Using 3D FAT Kamphuis et al. (2015) obtain an H I rotation curve indicating $v_{\text{rot}} = 161.4 \text{ km s}^{-1}$ at $R_{\text{max}} = 47.2$ kpc (for $i = 62^\circ.2$ and $PA = 199^\circ.6$; see Table 9) and $M_{\text{dyn}} = 2.9 \times 10^{11} M_\odot$.

ESO222-G010 (HIPASS J1434–49) is a dwarf irregular galaxy at low Galactic latitude, located in the outskirts of the Cen A group. Its systemic velocity of $v_{\text{hel}} = 622 \pm 5 \text{ km s}^{-1}$ (Koribalski et al. 2004) and $v_{\text{LG}} = 431 \text{ km s}^{-1}$ suggest a Hubble distance of 5.8 Mpc. No TRGB distance is currently available. Our ATCA H I data show a resolved distribution and a regular velocity field ($PA \sim 20^\circ$), aligned with the faint stellar body. Higher resolution maps are needed to study its H I morphology and velocity field in detail. We measure $F_{\text{HI}} = 6.1 \text{ Jy km s}^{-1}$, in agreement with HIPASS (Koribalski et al. 2004), and derive $M_{\text{HI}} = 4.8 \times 10^7 M_\odot$. Bright H α emission detected by Kaisin et al. (2007) agrees with the centre of the ATCA H I distribution presented here.

HIPASS J1441–62 is a dwarf irregular galaxy at $\alpha, \delta(\text{J2000}) = 14:41:42.2, -62:46:04.2$ (see Table 7) as mea-

sured from our ATCA H I data. The galaxy is located at low Galactic latitude ($l, b = 315^\circ.2, -2^\circ.55, A_B = 4.9$). Its systemic velocity of $v_{\text{hel}} = 672 \pm 8 \text{ km s}^{-1}$ (Koribalski et al. 2004) and $v_{\text{LG}} = 461 \text{ km s}^{-1}$ suggest an approximate Hubble distance of 6.0 Mpc. No stellar counterpart is identified. Its nearest known neighbour is the Circinus galaxy, $\sim 4^\circ$ away. Our ATCA data show a resolved H I distribution and a regular velocity field ($PA \sim 260^\circ$). We measure $F_{\text{HI}} = 2.4 \text{ Jy km s}^{-1}$, within the uncertainty of the HIPASS F_{HI} (Koribalski et al. 2004), and derive $M_{\text{HI}} = 2.0 \times 10^7 M_\odot$.

ESO223-G009 (HIPASS J1501–48) is a Magellanic irregular galaxy at a TRGB distance of 6.49 ± 0.51 Mpc (Karachentsev et al. 2007). Due to its low Galactic latitude ($b = 9^\circ.2$) it is obscured by dust and foreground stars. While the *B*-band Galactic extinction in this direction is moderate ($A_B = 0.94$), the density of Galactic foreground stars is quite high, making it difficult to estimate the galaxy's optical dimensions and orientation. No optical velocity has yet been measured. Using HST ACS images we find that the main stellar body of ESO223-G009 is best described by an ellipse of size $160'' \times 130''$ ($5 \text{ kpc} \times 4 \text{ kpc}$), $PA = 135^\circ$, centered at $\alpha, \delta(\text{J2000}) = 15:01:08, -48:17:30$. ESO223-G009 appears to be a relatively isolated galaxy, with only one known neighbour, the late-type spiral ESO274-G001 (HIPASS 1514–46 at $D = 3.1$ Mpc, i.e. in the foreground), within 3° . It may form a loose association with the dwarf irregular galaxies ESO222-G010, ESO272-G025 and HIPASS J1526–51 (at projected distances of 266', 282', and 300', respectively), about 2 Mpc behind the Cen A Group. Our ATCA H I maps of ESO223-G009 reveal a large, nearly circular gas distribution and a very peculiar velocity field (see Koribalski 2010). We measure $F_{\text{HI}} = 97.0 \text{ Jy km s}^{-1}$, in agreement with HIPASS (Koribalski et al. 2004), and derived $M_{\text{HI}} = 9.6 \times 10^8 M_\odot$. The highly twisted and warped H I velocity field is indicative of a face-on warp where the gaseous disc wobbles in and out of the plane. Using 3D FAT Kamphuis et al. (2015) obtain an H I rotation curve indicating $v_{\text{rot}} = 85.6 \text{ km s}^{-1}$ at $R_{\text{max}} = 15.3$ kpc (for $i = 20^\circ.3$ and $PA = 256^\circ.1$; see Table 9) and $M_{\text{dyn}} = 2.6 \times 10^{10} M_\odot$. ESO223-G009 shows similarities to the spiral galaxies NGC 628 (Kamphuis & Briggs 1992), NGC 3642 (Verdes-Montenegro et al. 2002), IC 10 (Manthey & Oosterloo 2008) and the lenticular galaxy ESO381-G047 (Donovan et al. 2009). The common feature of these rather different galaxies is their warped, nearly face-on H I discs.

ESO274-G001 (HIPASS J1514–46) is a late-type spiral galaxy in the outskirts of the Cen A group, located at a distance of $D_{\text{TRGB}} = 3.09 \pm 0.23$ Mpc (Karachentsev et al. 2007). Its Local Group velocity of 360 km s^{-1} suggests peculiar motions of $\sim 130 \text{ km s}^{-1}$ towards the Cen A group. Its nearest known neighbours are ESO223-G009 (HIPASS J1501–48) and HIPASS J1526–51 at projected distances of 160' and 287', respectively. The edge-on stellar disc of ESO274-G001 is obscured by Galactic foreground dust and stars. Our ATCA data show an extended, regular rotating H I disc with signs of a minor warp in the outskirts (see also Koribalski 2008). We measure $F_{\text{HI}} = 138.4 \text{ Jy km s}^{-1}$, $\sim 10\%$ more than the published HIPASS F_{HI} (Koribalski et al. 2004), and derive $M_{\text{HI}} = 3.1 \times 10^8 M_\odot$. We measure H I dimensions of about $17' \times 4'$, corresponding to $15 \text{ kpc} \times$

3 kpc. Using high-resolution ($10''$) ATCA H I maps O'Brien et al. (2010) measure $F_{\text{HI}} = 152.6 \text{ Jy km s}^{-1}$, which seems rather high compared to our measurements. They derive a maximum rotational velocity of 89.4 km s^{-1} . TIRIFIC modeling shows that ESO274-G001 is slightly warped. The scale height obtained in the best-fit model is $\sim 250 \text{ pc}$. H α imaging by Rossa & Dettmar (2003) reveals prominent extraplanar ionised gas. Lee et al. (2007) and Côté et al. (2009) also obtain H α images and find most H II regions located in the southern (approaching) side of the galaxy; they derive an SFR of $1.5 \times 10^{-2} \text{ M}_{\odot} \text{ yr}^{-1}$. Our ATCA 20-cm radio continuum maps reveal extended emission in the disc as well as a bright nucleus.

UKS1424–460 (HIPASS J1428–46) is a Magellanic irregular galaxy (type IB(s)m) of low surface brightness, located close to a foreground star. Its location and TRGB distance of $3.58 \pm 0.33 \text{ Mpc}$ (Karachentsev et al. 2004) places it in the far outskirts of the Cen A group. Its nearest neighbours are ESO272-G025 (HIPASS J1443–44) and ESO222-G010 (HIPASS J1434–49) at projected distances of $188'$ and $200'$, respectively. Both are located well behind UKS1424–460. Our ATCA data show an extended, regularly rotating H I disc. We measure an H I flux density of $16.7 \text{ Jy km s}^{-1}$, in agreement with HIPASS (Koribalski et al. 2004), corresponding to an H I mass of $M_{\text{HI}} = 5.0 \times 10^7 \text{ M}_{\odot}$. Begum et al. (2008) observed UKS1424–460 as part of the FIGGS project. They measure an H I diameter of $6'.5$ ($\sim 2.7 \times$ the optical diameter) and an H I flux density of $F_{\text{HI}} = 17.4 \pm 1.7 \text{ Jy km s}^{-1}$, in agreement with our measurements. Using 3D FAT Kamphuis et al. (2015) obtain an H I rotation curve indicating $v_{\text{rot}} = 22.0 \text{ km s}^{-1}$ at $R_{\text{max}} = 3.2 \text{ kpc}$ (for $i = 74^{\circ}6$ and $PA = 122^{\circ}8$; see Table 9) and $M_{\text{dyn}} = 3.6 \times 10^8 \text{ M}_{\odot}$; note these values are highly uncertain. Optical magnitudes are hard to obtain due to significant foreground dust and stars. Kaisin et al. (2007) and Côté et al. (2009) show a marginal detection of H α emission on the north-western (approaching) side of the galaxy. They derive an SFR of $1.4 \times 10^{-4} \text{ M}_{\odot} \text{ yr}^{-1}$.

ESO272-G025 (HIPASS J1443–44) is a dwarf irregular galaxy located in the outskirts of the Cen A group at a Hubble distance of 5.9 Mpc . Its nearest neighbour is most likely the galaxy ESO223-G009 (HIPASS J1501–48). Our ATCA data show a barely resolved H I source centred on the bright and compact optical body; no rotation is discernible in our velocity field (see also Bouchard et al. 2007). Galactic cirrus filaments are visible in the optical image. We measure $F_{\text{HI}} = 1.6 \text{ Jy km s}^{-1}$, in agreement with HIPASS (Meyer et al. 2004), and derive $M_{\text{HI}} = 1.3 \times 10^7 \text{ M}_{\odot}$. Reduzzi & Rampazzo (1995) suggest ESO272-G025 has an extended low-surface brightness disc or is possibly a galaxy pair. ESO272-G025 shows clumpy and diffuse H α emission (Kaisin et al. 2007; Côté et al. 2009), with an estimated star formation rate of $1.5 \times 10^{-3} \text{ M}_{\odot} \text{ yr}^{-1}$.

5.4 Other Galaxies (in RA order)

ESO115-G021 (HIPASS J0237–61) is a Magellanic barred spiral galaxy at a distance of $D_{\text{TRGB}} = 4.99 \pm 0.10 \text{ Mpc}$ (Tully et al. 2006). Apart from its small H I companion noted below, ESO115-G021 has no known neighbours within 5° . Our ATCA maps show an extended, reg-

ular rotating, nearly edge-on H I disc with a diameter of $\sim 15'$, corresponding to 22 kpc . We measure $F_{\text{HI}} = 110.7 \text{ Jy km s}^{-1}$, $\sim 10\%$ higher than quoted in the HIPASS BGC using a point-source fit (Koribalski et al. 2004), and derive $M_{\text{HI}} = 6.5 \times 10^8 \text{ M}_{\odot}$. The H I velocity field of ESO115-G021 shows some peculiar motions: (1) a disturbance in the disc area closest to the companion, suggesting mild interactions, and asserting the close proximity of the two galaxies, and (2) a significant twist in the iso-velocity contours towards the south-western (approaching) end of the disc, indicating a warp. Using high-resolution ($9''$) ATCA H I maps O'Brien et al. (2010) measure a projected scale height of $26''.7$ (646 pc) with vertical H I structures extending to nearly 2 kpc . They measure a rotational velocity of 63 km s^{-1} . Furthermore, our deep ATCA H I observations reveal a dwarf companion, ATCA J023658–611838 at $\alpha, \delta(\text{J2000}) = 02:36:58.8, -61:18:38.5$, with a systemic velocity of 508 km s^{-1} at a projected distance of $6'$ (8.6 kpc) from ESO115-G021's centre ($v_{\text{sys}} = 515 \pm 2 \text{ km s}^{-1}$). The companion's H I flux density is $0.11 \text{ Jy km s}^{-1}$, corresponding to an H I mass of $6.5 \times 10^5 \text{ M}_{\odot}$ (assuming $D = 5 \text{ Mpc}$). A faint GALEX UV counterpart to the H I source is visible at $\alpha, \delta = 02^{\text{h}} 36^{\text{m}} 59.5^{\text{s}}, -61^{\circ} 18' 38''.7$; we measure FUV and NUV magnitudes of 21.02 and 21.17 , corrected for Galactic extinction ($\text{NUV-FUV} = 0.15$). The detected H I source is therefore not an HVC complex. For further discussions see Koribalski (2008) and O'Brien et al. (2010).

ESO154-G023 (HIPASS J0256–54) is a Magellanic barred spiral galaxy at a distance of $D_{\text{TRGB}} = 5.76 \pm 0.10 \text{ Mpc}$ (Tully et al. 2006). Its closest neighbour is NGC 1311 ($D_{\text{TRGB}} = 5.20 \text{ Mpc}$), more than 4° away. ESO154-G023 is similar to the galaxy ESO115-G021 in size and orientation (Koribalski 2008). When comparing the optical discs, ESO154-G023 appears to have either a thicker disc or is slightly less inclined than ESO115-G021. Our ATCA H I maps show an extended, regularly rotating H I disc with a pronounced warp on both sides. The latter appears to start at the edge of the bright stellar disc and is likely contributing to the apparent disc thickness. We measure ATCA $F_{\text{HI}} = 130.6 \text{ Jy km s}^{-1}$, within the $\sim 10\%$ uncertainty of the HIPASS F_{HI} (Koribalski et al. 2004), and derive $M_{\text{HI}} = 10^9 \text{ M}_{\odot}$. Using 3D FAT Kamphuis et al. (2015) obtain an H I rotation curve indicating $v_{\text{rot}} = 63.6 \text{ km s}^{-1}$ at $R_{\text{max}} = 15.7 \text{ kpc}$ (for $i = 79^{\circ}7$ and $PA = 218^{\circ}3$; see Table 9) and $M_{\text{dyn}} = 1.5 \times 10^{10} \text{ M}_{\odot}$. SINGG H α images reveal star formation throughout the stellar disc (Meurer et al. 2006). Furthermore, our deep ATCA H I observations reveal a dwarf galaxy at $\alpha, \delta(\text{J2000}) = 02:56:40.3, -54:35:38.8$ (see Table 7) behind the disc of ESO154-G023 at velocities of ~ 1100 to 1140 km s^{-1} . We measure $F_{\text{HI}} = 0.31 \text{ Jy km s}^{-1}$ and derive $M_{\text{HI}} = 1.2 \times 10^7 \text{ M}_{\odot}$ for $D = 12.7 \text{ Mpc}$. The newly discovered galaxy is also detected in the AAT H-band (see Kirby et al. 2008b), SINGG H α (Meurer et al. 2006) and GALEX UV images.

NGC 1313 (HIPASS J0317–66) is a late-type barred spiral galaxy at a TRGB distance of $4.07 \pm 0.22 \text{ Mpc}$ (Grise et al. 2008). For a detailed study see Ryder et al. (1995) who find a large H I disc, extending $\sim 18' \times 12'$, and measure $F_{\text{HI}} = 455 \text{ Jy km s}^{-1}$. By combining the ATCA H I data of NGC 1313 with our ATCA H I data for the dwarf

companion AM0319–662, discussed below, we create an even more sensitive mosaic of the area. We measure $F_{\text{HI}} = 491.9$ Jy km s⁻¹ for NGC 1313, in agreement with our recent H75-array HI mosaic ($F_{\text{HI}} = 496.2$ Jy km s⁻¹) and Parkes HI mosaics (Ryder et al. 1995, Barnes & de Blok 2004, Koribalski et al. 2004), and derive $M_{\text{HI}} = 1.9 \times 10^9 M_{\odot}$. Our high-resolution ATCA HI data show an extended, somewhat asymmetric HI distribution and mildly disturbed velocity field. Using 3D FAT Wang et al. (2017) obtain an HI rotation curve indicating $v_{\text{rot}} = 220$ km s⁻¹ at $R_{\text{max}} = 10.3$ kpc (see Table 9) and $M_{\text{dyn}} = 1.1 \times 10^{11} M_{\odot}$. H α imaging by Ryder & Dopita (1993) reveals the brightest H II regions in the bar and inner spiral arms of NGC 1313, surrounded by low surface brightness emission in the form of filaments, arcs and shells.

AM0319–662 (HIPASS J0321–66) is a dwarf irregular galaxy at a TRGB distance of 3.98 ± 0.36 Mpc (Karachentsev et al. 2003). It is a close companion of the large spiral galaxy NGC 1313 (HIPASS J0317–66), separated by only 20' or 23 kpc. Our ATCA data show a barely resolved HI source and no discernible rotation in the velocity field ($\sim 524 - 544$ km s⁻¹). The peak of the ATCA HI distribution is slightly offset to the south of AM0319–662's stellar body, suggesting it may be a transition dwarf galaxy (see also Makarova et al. 2005). We measure $F_{\text{HI}} \sim 0.3$ Jy km s⁻¹ and derive $M_{\text{HI}} \sim 10^6 M_{\odot}$.

NGC 1311 (HIPASS J0320–52) is a Magellanic barred spiral galaxy at distance of $D_{\text{TRGB}} = 5.22$ Mpc (Tully et al. 2013). Its closest neighbours are IC 1959 (HIPASS J0333–50) and ESO154-G023 (HIPASS J0256–54) and ESO199-G007 (HIPASS J0258–49), all separated by $\gtrsim 1$ Mpc. Eskridge et al. (2008) conduct a detailed study of ultraviolet, optical and near-infrared HST images of NGC 1311 revealing 13 candidate star clusters. NGC 1311 and IC 1959, both low-luminosity star-forming galaxies, are located in the foreground to the galaxy group LGG 93 (Pisano et al. 2011). Our ATCA HI maps show a box-shaped HI distribution, somewhat truncated on the north-eastern side where faint stellar emission is prominent. The fat inner disc suggests the presence of extra-planar HI gas; some deviations of the velocity field are observed to the north-eastern side. We measure $F_{\text{HI}} = 13.6$ Jy km s⁻¹, in agreement with HIPASS (Koribalski et al. 2004), and derive $M_{\text{HI}} = 8.7 \times 10^7 M_{\odot}$.

HIPASS J0457–42 is a nearby dwarf irregular galaxy at $D_{\text{TF}} = 7.2$ Mpc (Karachentsev et al. 2013). It is the western galaxy ($PA = 56^\circ$) of the apparent galaxy pair ESO252-IG001 (see Koribalski et al. 2004; their Appendix A). From the ATCA HI intensity map we measure a position of $\alpha, \delta(\text{J2000}) = 04:56:59.1, -42:47:58.3$ (see Table 7). The galaxy was also detected in H α , where Meurer et al. (2006) find a *curious near linear H α arc through centre along the minor axis*. Our ATCA data show an extended, regular rotating HI disc, aligned with optical appearance. We note a small HI extension or tail on the north-eastern (approaching) side. The optical properties, listed in Table 2, are of the HI-detected galaxy (ESO252-IG001 NED01). The eastern, nearly edge-on galaxy (ESO252-IG001 NED02, $PA \sim 130^\circ$) is much more distant and not a companion. The clos-

est neighbour to HIPASS J0457–42, ESO305-G002 ($v_{\text{opt}} = 259$ km s⁻¹) is more than 3° away. If the optical velocity (da Costa et al. 1991) is correct, ESO305-G002 would be a nearby dwarf spiral galaxy at a projected distance of $\sim 200'$. Inspecting HIPASS data we find HI emission at the position/velocity of ESO305-G002, but it is situated close to an HVC complex (Putman et al. 2002). At the position of 05:01:21.8, $-39:36:13$ we measure $S_{\text{peak}} = 120$ mJy, $F_{\text{HI}} = 4.3$ Jy km s⁻¹, $w_{20} = 55$ km s⁻¹ and $w_{50} = 30$ km s⁻¹.

ESO199-G007 (HIPASS J0258–49) is a dwarf spiral galaxy at a Hubble distance of $D_{\text{Ho}} = 6.6$ Mpc. Using HIPASS we measure $v_{\text{sys}} = 631$ km s⁻¹ and obtain $v_{\text{LG}} = 479$ km s⁻¹, showing this galaxy to be a member of the Local Volume. No optical velocity measurement has been reported yet. ESO199-G007's closest neighbour is NGC 1311 (HIPASS J0320–52), separated by ~ 1.5 Mpc. Our ATCA HI data show a marginally resolved, regularly rotating disc. We measure $F_{\text{HI}} = 1.6$ Jy km s⁻¹, in agreement with HIPASS (Meyer et al. 2004), and derive $M_{\text{HI}} = 1.6 \times 10^7 M_{\odot}$. Karachentsev & Kaisina (2013) derive a star formation rate of $\sim 2.3 \times 10^{-3} M_{\odot} \text{ yr}^{-1}$, and Young et al. (2014) analyse a deep *H*-band image of ESO199-G007.

IC 1959 (HIPASS J0333–50) is a Magellanic barred spiral galaxy at a distance of $D_{\text{TRGB}} = 6.05 \pm 0.14$ Mpc (Tully et al. 2006). Its nearest neighbour is NGC 1311 (HIPASS J0320–52), separated by > 1 Mpc. Deep *H*-band images of IC 1959 and NGC 1311 are analysed by Kirby et al. (2008b). Using 11HUGS Lee et al. (2009) report recent star formation with a rate of $4 - 5 \times 10^{-2} M_{\odot} \text{ yr}^{-1}$ for IC 1959. The galaxy is also detected in LVHIS 20-cm radio continuum maps (Shao et al. 2017). Our ATCA HI data show a well-resolved, symmetric and regularly rotating disc galaxy. Minor deviations in the mean HI velocity field are seen towards the north-western (approaching) side. We measure $F_{\text{HI}} = 26.0$ Jy km s⁻¹, in agreement with HIPASS (Koribalski et al. 2004), and derive $M_{\text{HI}} = 2.2 \times 10^8 M_{\odot}$. Using 3D FAT Kamphuis et al. (2015) obtain an HI rotation curve indicating $v_{\text{rot}} = 65.9$ km s⁻¹ at $R_{\text{max}} = 5.3$ kpc (for $i = 78^\circ.8$ and $PA = 149^\circ.0$; see Table 9) and $M_{\text{dyn}} = 5.3 \times 10^9 M_{\odot}$.

NGC 1705 (HIPASS J0454–53) is a well-studied BCD galaxy (type S0) at a distance of $D_{\text{TRGB}} = 5.1 \pm 0.6$ Mpc (Tosi et al. 2001). It has no known neighbours within 5° . Our high-resolution ATCA data show an extended HI distribution elongated nearly north-south ($PA \sim 20^\circ$) with a mostly regular rotation pattern. Small peculiar velocities are seen towards the north-west. We measure $F_{\text{HI}} = 12.2$ Jy km s⁻¹, $\sim 10\%$ lower than the published HIPASS F_{HI} (Koribalski et al. 2004), and derive $M_{\text{HI}} = 7.5 \times 10^7 M_{\odot}$. For a more detailed HI study see Elson et al. (2013), who improve on previous ATCA HI results by Meurer et al. (1996, 1998) and Bureau et al. (1999). The young stellar population and star clusters of NGC 1705 are studied by Annibali et al. (2009) using HST images. Extended stellar emission is seen in GALEX UV images.

ESO364-G?029 (HIPASS J0605–33) is an irregular looking barred Magellanic dwarf galaxy at a Hubble distance of $D_{\text{Ho}} = 7.6$ Mpc. Its nearest neighbour is the

dwarf galaxy ATCA J060511–332534 ($v_{\text{sys}} \sim 830 \text{ km s}^{-1}$; $F_{\text{HI}} \sim 1 \text{ Jy km s}^{-1}$), 21'.9 away, detected here (see Table 7). Other known neighbours are AM0605–341 (HIPASS J0607–34) and NGC 2188 (HIPASS J0610–34) at projected distances of 70'.2 and 82'.5, respectively. Our ATCA maps show a regularly rotating, well-resolved H I disc, encompassing the very irregular-shaped low-surface brightness stellar body. We measure $F_{\text{HI}} = 22.3 \text{ Jy km s}^{-1}$, somewhat larger than the HIPASS F_{HI} (Koribalski et al. 2004), and derive $M_{\text{HI}} = 1.2 \times 10^8 M_{\odot}$. For a detailed study of ESO364-G?029, including a comparison with the LMC and other dwarf irregular galaxies see Kouwenhoven et al. (2007).

AM0605–341 (HIPASS J0607–34) is a rather compact, barred Magellanic dwarf galaxy at a distance of $D_{\text{mem}} = 7.4 \text{ Mpc}$. Its nearest neighbours are NGC 2188 (HIPASS J0610–34) and ESO364-G?029 ((HIPASS J0605–33) at projected distances of 35'.6 and 70'.2. Our ATCA H I maps show a resolved source centred on the optical galaxy plus extended H I emission on the western (receding) side. Kirby et al. (2012) model the H I kinematics of the main component and fit a rising rotation curve. They provide a detailed discussion, including on likely tidal interactions between AM0605–341 and its eastern neighbour NGC 2188 which show opposing H I extensions. We measure $F_{\text{HI}} = 9.3 \text{ Jy km s}^{-1}$, in agreement with HIPASS (Koribalski et al. 2004), and derive $M_{\text{HI}} = 1.2 \times 10^8 M_{\odot}$.

NGC 2188 (HIPASS J0610–34) is a Magellanic barred spiral galaxy seen nearly edge-on, at a distance of $D_{\text{TF}} = 7.4 \text{ Mpc}$ (Karachentsev et al. 2013). Its nearest neighbours are AM0605–341 ((HIPASS J0607–34) and ESO364-G?029 (HIPASS J0605–33) at projected distances of 35'.6 and 82'.5 (see Kirby et al. 2012). Our ATCA data of NGC 2188 show an extended, but rather asymmetric H I distribution and somewhat peculiar velocity field. Most notably, there is significant extraplanar H I emission extending towards the east, while the western side of NGC 2188 appears compressed, resembling discs affected by ram pressure forces. This asymmetry is also, to a lesser degree, evident in the stellar disc. The mean H I velocity fields appears to show two components, a rotating disc plus peculiar motions associated with the extraplanar gas. These features were also noticed by Domgörgen et al. (1996) who analyse high-resolution VLA H I and ESO H α images. Kirby et al. (2012) model the ATCA H I velocity fields of NGC 2188's two neighbours. They suggest that tidal interactions between NGC 2188 and AM0605–341, which are separated by $\sim 77 \text{ kpc}$, may be responsible for the peculiar features. Using our ATCA H I data we measure $F_{\text{HI}} = 34.3 \text{ Jy km s}^{-1}$, in agreement with HIPASS (Koribalski et al. 2004), and derive $M_{\text{HI}} = 4.4 \times 10^8 M_{\odot}$. For comparison, Domgörgen et al. (1996) measure $F_{\text{HI}} = 20.4 \pm 0.6 \text{ Jy km s}^{-1}$, losing much of the diffuse H I emission. In a follow-up study Domgörgen & Dettmar (1997) find spectacular filaments of ionised gas extending several hundred parsecs perpendicular to the plane of the galaxy, mostly from the massive H II region in the southern (approaching) part of NGC 2188. They note that at least 24% of the H α emitting gas is diffuse. Deep H-band images are presented by Young et al. (2014).

574552 (HIPASS J0615–57) are a close dwarf galaxy pair, separated by $\sim 3'$. Karachentsev et al. (2006) obtain a distance of $D_{\text{TRGB}} = 6.05 \pm 0.49 \text{ Mpc}$ for ESO121-G020. The HIPASS detection includes H I emission from ESO121-G020 ($v_{\text{sys}} = 584 \text{ km s}^{-1}$) and its dwarf galaxy companion ATCA J061608–574552 ($v_{\text{sys}} = 540 \text{ km s}^{-1}$), which was discovered by Warren et al. (2006). No other companions are known within at least 5° . Our ATCA H I maps show two regularly rotating galaxies. We measure $F_{\text{HI}} = 7.3 \text{ Jy km s}^{-1}$ for ESO121-G020 and 2.1 Jy km s^{-1} for the companion. Assuming the above distance for both we derive $M_{\text{HI}} = 6.3$ and $1.8 \times 10^7 M_{\odot}$, respectively. Warren et al. (2006) obtain H I mass to light ratios of ~ 1.5 and $\sim 2.2 M_{\odot}/L_{\odot}$. Both galaxies are clearly detected in GALEX UV images. For a detailed analysis of ESO121-G020's H I kinematics see Kirby et al. (2012); their results are summarised in Table 9.

ESO308-G022 (HIPASS J0639–40) is a rather isolated dwarf irregular galaxy at a Hubble distance of 7.7 Mpc. Optical and infrared H-band imaging by Parodi et al. (2002) and Kirby et al. (2008b), respectively, reveal its stellar structure. Our ATCA H I maps show a resolved, regularly rotating H I disc. We measure $F_{\text{HI}} = 4.4 \text{ Jy km s}^{-1}$, in agreement with HIPASS (Meyer et al. 2004), and derive an H I mass of $6.1 \times 10^7 M_{\odot}$. A kinematic analysis of the LVHIS data by Kirby et al. (2012) results in a rising rotating curve with $v_{\text{max}} = 40 \text{ km s}^{-1}$ at a radius of $100''$ (4.1 kpc).

AM0704–582 (HIPASS J0705–58) is also known as the Argo Dwarf Irregular. It is a rather isolated, low surface brightness galaxy at a distance of $D_{\text{TRGB}} = 4.90 \pm 0.45 \text{ Mpc}$ (Karachentsev et al. 2003). Parodi et al. (2002) and Kirby et al. (2008b) measure basic optical and infrared properties, respectively. The low extremely surface brightness of AM0704–582 makes it hard to determine its shape. Using HIPASS, Koribalski et al. (2004) fit an H I systemic velocity of $564 \pm 2 \text{ km s}^{-1}$; no optical velocity measurement is available yet. Our ATCA H I maps show a well-resolved, regularly rotating disc extending well beyond the faint stellar body. We measure $F_{\text{HI}} = 33 \text{ Jy km s}^{-1}$, in agreement with HIPASS (Koribalski et al. 2004), and derive $M_{\text{HI}} = 1.9 \times 10^8 M_{\odot}$. Kirby et al. (2012) analyse the H I kinematics and discuss the galaxy in detail. Using 3D FAT Kamphuis et al. (2015) obtain an H I rotation curve indicating $v_{\text{rot}} = 38.5 \text{ km s}^{-1}$ at $R_{\text{max}} = 6.1 \text{ kpc}$ (for $i = 53^{\circ}.6$ and $PA = 275^{\circ}.9$; see Table 9) and $M_{\text{dyn}} = 2.1 \times 10^9 M_{\odot}$.

ESO059-G001 (HIPASS J0731–68) is a Magellanic barred irregular galaxy at a TRGB distance of $4.57 \pm 0.36 \text{ Mpc}$ (Karachentsev et al. 2006). It appears very isolated with no known neighbours within at least 5° . Our ATCA H I maps reveal a well-resolved, regularly rotating H I disc extending well beyond the irregular stellar disc. We measure $F_{\text{HI}} = 17.9 \text{ Jy km s}^{-1}$, in agreement with HIPASS (Koribalski et al. 2004), and derive $M_{\text{HI}} = 8.8 \times 10^7 M_{\odot}$. Using 3D FAT Kamphuis et al. (2015) obtain an H I rotation curve indicating $v_{\text{rot}} = 61.0 \text{ km s}^{-1}$ at $R_{\text{max}} = 5.4 \text{ kpc}$ (for $i = 50^{\circ}.2$ and $PA = 323^{\circ}.4$; see Table 9) and $M_{\text{dyn}} = 4.7 \times 10^9 M_{\odot}$; see also van Eymeren et al. (2009c) and Kirby et al. (2012).

NGC 2915 (HIPASS J0926–76) is a rather isolated BCD galaxy at a TRGB distance of $3.78 \pm 0.43 \text{ Mpc}$

(Karachentsev et al. 2003), much studied in HI by Meurer et al. (1996) and more recently Elson et al. (2010). No neighbouring galaxies are known within 5° . The HI cloud HIPASS J0851–75 ($v_{\text{sys}} = 482 \text{ km/s}$) west of NGC 2915 appears to be the highest velocity cloud complex near the start of the Magellanic Leading Arm. Our ATCA maps of NGC 2915 show an enormous HI disc – compared to the compact stellar body – with a mostly regular rotation pattern. Meurer et al. (1996) measured an HI extent of $\sim 20'$, i.e., $5\times$ its Holmberg radius. They note a short central bar and extended spiral arms. We measure $F_{\text{HI}} = 108.7 \text{ Jy km s}^{-1}$, in agreement with HIPASS (Koribalski et al. 2004), and derive $M_{\text{HI}} = 3.7 \times 10^8 M_\odot$. For recent HI studies of NGC 2915 see Elson et al. (2010, 2011a,b), who improve on previous ATCA HI results by Meurer et al. (1998, 1996) and Bureau et al. (1999). Elson et al. (2012) also investigate the star formation in NGC 1705 and NGC 2915.

NGC 3621 (HIPASS J1118–32) is a late-type spiral galaxy at a cepheid distance of $6.70 \pm 0.47 \text{ Mpc}$ (Ferrarese et al. 2000). To date NED shows a diverse collection of ~ 50 independent distances. Its stellar disc has a diameter of about $12' \times 7'$, while the GALEX *UV* emission extends about $20' \times 10'$ (Thilker et al. 2007). NGC 3621 appears to be rather isolated; its nearest neighbours are the newly discovered dwarf galaxies HIPASS J1131–31 and HIPASS J1132–32, both $\sim 3^\circ$ away. Our 3-pointing ATCA HI mosaic reveals the extended HI emission of NGC 3621, spanning over $40'$ (Koribalski 2017), a factor two beyond its remarkable *XUV* disc. The ATCA HI velocity field hints at a strong warp of the outer disc. Peculiar motions are also evident in the HI velocity dispersion map. Our ATCA F_{HI} estimate of $856.8 \text{ Jy km s}^{-1}$ is in good agreement with previous single-dish estimates (see Koribalski et al. 2004). We derive $M_{\text{HI}} = 9.1 \times 10^9 M_\odot$. Single-pointing VLA HI maps, taken as part of the THINGS project (Walter et al. 2008), reveal only the inner part of the galaxy ($F_{\text{HI}} = 679 \text{ Jy km s}^{-1}$), missing the peculiar extended emission towards the north and south. De Blok et al. (2008) find a slightly rising rotation curve out to a radius of 13.5 arcmin (26 kpc) with $v_{\text{rot}} = 150 \text{ km s}^{-1}$, $i \sim 65^\circ$, and $PA \approx 345^\circ$. Beyond that radius the HI distribution and kinematics change significantly, as shown in our ATCA HI maps, possibly due to the accretion of a companion. The ATCA HI maps were first analysed and discussed by Walsh (1997).

HIPASS J1131–31 is a dwarf irregular galaxy with an HI systemic velocity of 716 km s^{-1} , originally discovered in HIPASS by us. Our ATCA HI maps reveal an unresolved source, centered at $\alpha, \delta(\text{J2000}) = 11:31:34.6, -31:40:28.3$ (see Table 7). The star TYC 7215–199–1 (10.4 mag) nearly fully obscures the stellar body of this galaxy. GALEX *UV* images reveal a compact blue dwarf galaxy at the above position. Its closest neighbours are HIPASS J1132–32 ($80'$) and NGC 3621 ($182'$); projected distances are given in brackets. Based on its likely association with NGC 3621 (HIPASS J1118–32) we assign the same distance, i.e. $D_{\text{mem}} = 6.7 \text{ Mpc}$. We measure $F_{\text{HI}} = 1.13 \text{ Jy km s}^{-1}$, which corresponds to $M_{\text{HI}} = 1.2 \times 10^7 M_\odot$.

HIPASS J1132–32 is a dwarf irregular galaxy with an HI systemic velocity of $\sim 680 \text{ km s}^{-1}$, originally discovered

in HIPASS (Meyer et al. 2004). Our low-resolution ATCA data show an unresolved HI source, centered at $\alpha, \delta(\text{J2000}) = 11:33:10.6, -32:57:45.2$ (see Table 7). It coincides with a compact blue dwarf galaxy (PGC 683190) that shows a faint extension to the west. No GALEX *UV* images are available. Higher resolution ATCA data reveal a marginally resolved HI source, matching the shape of the stellar body. Doyle et al. (2005) give optical magnitudes of B_J, R , and $I = 16.28, 16.17, \text{ and } 17.22 \text{ mag}$. Its nearest neighbours are HIPASS J1131–31 ($80'$), NGC 3621 ($188'$), and ESO379-G007 ($273'$); projected distances are given in brackets. Based on its likely association with NGC 3621 (HIPASS J1118–32) we assign the same distance, i.e. $D_{\text{mem}} = 6.7 \text{ Mpc}$. We measure ATCA $F_{\text{HI}} = 1.4 \text{ Jy km s}^{-1}$, which corresponds to $M_{\text{HI}} = 1.5 \times 10^7 M_\odot$.

IC 3104 (HIPASS J1219–79) is a Magellanic barred irregular galaxy at a TRGB distance of $2.27 \pm 0.19 \text{ Mpc}$ (Karachentsev et al. 2002). Its nearest neighbour is probably HIPASS J1247–77 ($v_{\text{hel}} = 413 \text{ km s}^{-1}$) at a projected distance of $154'.3$. Our ATCA HI images show a well-resolved, regularly rotating galaxy. We measure $F_{\text{HI}} = 8.1 \text{ Jy km s}^{-1}$, consistent with the HIPASS F_{HI} (Koribalski et al. 2004), and derive $M_{\text{HI}} = 9.8 \times 10^6 M_\odot$.

HIPASS J1247–77 is a highly obscured ($A_B = 2.75$) dwarf irregular galaxy located at $\alpha, \delta(\text{J2000}) = 12:47:32.4, -77:34:53.9$ (see Table 7) as measured using our ATCA HI distribution (see also Kilborn et al. 2002). HST ACS images show a young stellar population and one bright star cluster; the galaxy’s TRGB distance is $3.16 \pm 0.25 \text{ Mpc}$ (Karachentsev et al. 2006). Our ATCA HI data reveal a resolved source, centred on the faint optical counterpart, with a regular velocity field ($PA \sim 55^\circ$). We measure $v_{\text{hel}} = 413 \text{ km s}^{-1}$ and $F_{\text{HI}} = 4.2 \text{ Jy km s}^{-1}$, in agreement with HIPASS (Koribalski et al. 2004), and derive $M_{\text{HI}} = 10^7 M_\odot$. Furthermore, our ATCA data reveal a neighbouring HI source (not shown here) at $\alpha, \delta(\text{J2000}) = 12:48:50.3, -77:49:30.6$ (see Table 7) without any obvious optical counterpart. It has a systemic velocity of $\sim 402 \text{ km s}^{-1}$ and $F_{\text{HI}} = 0.3 \text{ Jy km s}^{-1}$. We derive $M_{\text{HI}} = 7 \times 10^5 M_\odot$, assuming the same distance as above. GALEX *UV* images are not available at either position. The nearest neighbour to HIPASS J1247–77 is IC 3104.

HIPASS J1526–51, also known as HIZOA J1526–51, appears to be a dwarf irregular galaxy located in the Zone-of-Avoidance. It was first discovered in the Parkes HI multibeam survey of the Zone of Avoidance (Jurazsek et al. 2000). No optical counterpart has been identified due to the high optical extinction ($A_B = 2.30 \text{ mag}$) and high stellar density (Ryan-Weber et al. 2002). Using our ATCA HI maps we measure a centre position of $\alpha, \delta(\text{J2000}) = 15:26:22.4, -51:10:30.2$ (see Table 7). The Local Group velocity of HIPASS J1526–51 is 438 km s^{-1} which corresponds to a Hubble distance of $D_{\text{Ho}} = 5.7 \text{ Mpc}$. The ATCA data reveal an extended HI distribution and a peculiar velocity field, hinting at two distinct components. Its nearest known neighbours are ESO274-G001 (HIPASS J1514–46) and ESO223-G009 (HIPASS J1501–48), both close to 5° away. We measure $F_{\text{HI}} = 5.0 \text{ Jy km s}^{-1}$ for HIPASS J1526–51, in agreement with HIPASS (Koribalski et al. 2004), and derive M_{HI}

$$= 3.8 \times 10^7 M_{\odot}.$$

ESO137-G018 (HIPASS J1620–60) appears to be a rather isolated, Magellanic type dwarf irregular galaxy located at low Galactic latitude. Its TRGB distance is 6.40 ± 0.48 Mpc (Karachentsev et al. 2007); there are no known neighbours within 3° . Our ATCA data reveal a well-resolved, regularly rotating H I disc that extends a factor two beyond the stellar body. We measure $F_{\text{HI}} = 43.5$ Jy km s^{-1} , somewhat higher than the HIPASS F_{HI} (Koribalski et al. 2004), and derive $M_{\text{HI}} = 4.2 \times 10^8 M_{\odot}$. Bonne (2008), Kirby et al. (2012) and most recently Kamphuis et al. (2015) obtained H I rotation curves. Using 3D FAT Kamphuis et al. (2015) determine $v_{\text{rot}} = 71.2$ km s^{-1} at $R_{\text{max}} = 8.6$ kpc (for $i = 71^{\circ}5$ and $PA = 29^{\circ}2$; see Table 9) and $M_{\text{dyn}} = 1.0 \times 10^{10} M_{\odot}$. H α imaging by Kaisin et al. (2007) reveals an extended disc of clumpy and diffuse ionised gas.

IC 4662 (HIPASS J1747–64) is a barred Magellanic irregular galaxy at a distance of 2.44 ± 0.19 Mpc (Karachentsev et al. 2006). Our ATCA H I data reveal extended emission and a rather peculiar velocity field. The H I emission is brightest in the galaxy centre and along the direction of the optical minor axis. At large radii the H I envelope becomes nearly circular with a faint H I extension towards the east. Apart from irregular motions in and near the eastern extension, the H I velocity field clearly indicates rotation. The twisted iso-velocity contours highlight the disturbed nature of the kinematics in the outer disc. Van Eymeren et al. (2010) measure a total H I extent of $15^{\circ}0 \times 11^{\circ}5$, six times larger than the bright stellar body. Their deep H α images reveal a diffuse filamentary structure surrounding the box-shaped body of IC 4662 plus a detached H II region (a companion galaxy ?) $1^{\circ}5$ towards the south-east (see also Kaisin et al. 2007). Surprisingly, IC 4662 appears to be a rather isolated galaxy, with no known neighbours within 5° . Its disturbed appearance, partly due to the bar and gas outflows, could be caused by accretion of or merging with close companions. For a more detailed discussion of IC 4662 and comparison with other dwarf irregular galaxies see Janine van Eymeren’s PhD Thesis (2008) and van Eymeren et al. (2009a,b,c,d).

ESO461-G036 (HIPASS J2003–31) is a dwarf irregular galaxy at a distance of $D_{\text{TRGB}} = 7.83 \pm 0.63$ Mpc (Karachentsev et al. 2006). It appears very isolated, having no known neighbours within at least 5° . Our ATCA H I data show a remarkable, regularly rotating H I disc extending well beyond the stellar body. The HIPASS and ATCA H I observations both indicate a total H I flux density of 7.5 Jy km s^{-1} , corresponding to an H I mass of $1.1 \times 10^8 M_{\odot}$. The velocity field suggests a mild warp of the outer disc, which has a diameter of $\sim 6'$. Our H I maps show a significant swing of the position angle. While the H I emission in the inner most region is aligned with the stellar extent ($PA \sim 20^{\circ}$, the kinematic major axis suggests rotation along a different axis ($PA \sim 340^{\circ}$). Begum et al. (2008) observed ESO461-G036 as part of the FIGGS project. Their estimates of F_{HI} and D_{HI} are underestimates due to the limited observed velocity range as evident by the truncated H I spectrum in their Fig. 5. Kreckel et al. (2011) analyse VLA H I data and obtain a rotation curve showing $v_{\text{rot}} \sim 51$ km s^{-1} (for $i \sim 65^{\circ}$),

and $R_{\text{max}} = 6.8$ kpc. Without the influence of neighbouring galaxies, the kinematics of the large H I disc of ESO461-G036 reflect its intrinsic evolution. Similar to NGC 2915, the galaxy is dominated by a large dark matter halo.

IC 5052 (HIPASS J2052–69) is a barred late-type spiral galaxy at a distance of $D_{\text{TRGB}} = 6.03 \pm 0.10$ Mpc (Seth et al. 2005). It is a relatively isolated galaxy with star-formation throughout the edge-on stellar disc (Meurer et al. 2006) but no known neighbours within 5° . Our low-resolution H I maps show a large gas disc ($\sim 16' \times 8'$, corresponding to 28 kpc \times 14 kpc), i.e. about 2–3 times the size of the stellar disc. Both the H I morphology and kinematics indicate significant warping of the outer H I disc which bends symmetrically by $\sim 30^{\circ}$. As usual, the warp starts beyond the stellar disc; the PA of the outermost H I disc is $\sim 290^{\circ}$ compared to $\sim 322^{\circ}$ for the inner disc (see also Wang et al. 2017). We measure $F_{\text{HI}} = 90.0$ Jy km s^{-1} , $\sim 10\%$ less than the HIPASS F_{HI} (Koribalski et al. 2004), and derive $M_{\text{HI}} = 7.7 \times 10^8 M_{\odot}$. Using high-resolution ($9''$) ATCA H I maps O’Brien et al. (2010) study the structure of IC 5052’s inner disc. They estimate the exponential scale height of the projected minor axis to be $20^{\circ}5$ (600 pc), which is confirmed by TIRIFIC modeling. O’Brien et al. (2010) give a rotational velocity of 90 km s^{-1} for IC 5052. Rossa & Dettmar (2003) study the extraplanar diffuse ionised gas in IC 5052 as well as prominent H α filaments and shells. HST ACS images by Seth et al. (2005) reveal an intricate web of dust filaments in the edge-on, stellar disc as well as two relatively bright star forming regions. ATCA 20-cm radio continuum emission is clearly detected (see Shao et al. 2017).

6 SUMMARY & OUTLOOK

The Local Volume H I Survey (LVHIS) consists of all galaxies with Local Group velocities $v_{\text{LG}} < 550$ km s^{-1} or distances $D < 10$ Mpc that are detected in the H I Parkes All Sky Survey (HIPASS) at declinations $\delta \lesssim -30^{\circ}$. We present the results of deep ATCA H I spectral line observations of a complete sample of 82 nearby, gas-rich galaxies, including a comprehensive H I atlas (Appendix A) and online database². Furthermore, we list the optical and HIPASS properties of all LVHIS galaxies and provide information on their multi-wavelength coverage (see also Wang et al. 2017). We discuss the H I properties of each galaxy together with a brief literature overview. Members of galaxy groups, such as the Local Group, the Sculptor Group and the Cen A Group, are organised together, while the remaining LVHIS galaxies are sorted in RA order. We provide accurate ATCA H I positions for nine dwarf galaxies discovered in HIPASS and a further six dwarf galaxies discovered in our H I data cubes (either companion or background galaxies).

The LVHIS galaxy atlas includes H I moment maps and pv -diagrams for the majority of LVHIS galaxies. For each LVHIS galaxy we determine their H I flux densities and diameters, analyse their structure and kinematics, search for companions and neighbouring H I clouds and compare these

² LVHIS project page: www.atnf.csiro.au/research/LVHIS

with the stellar distribution and optical properties. The ATCA H I cubes and moment maps are made available as FITS files via our on-line LVHIS database; requests for calibrated uv -data will be considered. Scientific analysis of the LVHIS data is on-going and will be presented in subsequent papers. Recent highlights include the kinematic analysis of LVHIS galaxies (Kamphuis et al. 2015, Oh et al. 2018), investigations of the $D_{\text{HI}}-M_{\text{HI}}$ relation (Wang et al. 2016) and a comprehensive multi-wavelength study (Wang et al. 2017).

Within the LVHIS sample we identify several transition type dwarf galaxies based on their optical and H I morphologies; these are Phoenix (ESO245-G007), ESO294-G010, ESO410-G005, NGC 5237, HIPASS J1337–39, HIPASS J1348–37 and AM0319–662. Other transition type LV galaxies discussed in this paper include ESO540-G030, ESO540-G032, NGC 59, and HIDEEP J1337–3320. Their H I masses range from $\sim 10^5$ to $4 \times 10^7 M_{\odot}$, and their H I distributions are characterised by being offset and/or misaligned from the stellar body. We note that these dwarf transitional galaxies all reside in groups, apart from AM0319–662 close to NGC 1313.

The LVHIS sample contains two starburst spirals (NGC 253 and NGC 4945), a dwarf starburst galaxy (NGC 5253), an early-type post-starburst galaxy (NGC 5102) and two active galaxies with radio lobes (Cen A and Circinus). The largest H I distributions (~ 100 kpc) are found for the spiral galaxies M83, Circinus and NGC 3621. While H I warps are detected in numerous LVHIS galaxies, only one LVHIS galaxy (M83) shows strong signs of tidal interactions. We note that the most isolated galaxies in the LVHIS sample (AM0704–582, ESO215-G?009, NGC 2915, NGC 3621, ESO174-G?001, ESO308-G022, ESO461-G036, ESO149-G003, ESO223-G009, IC 5052) have typically much larger H I discs compared to their optical diameters than galaxies with many neighbours. This trend needs to be explored further.

We plan to obtain more sensitive high-resolution H I observations with the Compact Array Broadband Backend (CABB), which was installed in 2009 (Wilson et al. 2011). By using several 6-km ATCA configurations we aim to reach $10''$ angular resolution and $1\text{--}4 \text{ km s}^{-1}$ velocity resolution. The 2 GHz of bandwidth available in the new ATCA 1–3 GHz frequency band as well as high-bit sampling will allow us to also make very deep radio continuum and polarisation maps for all LVHIS galaxies and their surroundings.

Major H I surveys are planned with three new radio interferometers, which are precursors/pathfinders for the Square Kilometre Array (SKA). The Australian SKA Pathfinder (ASKAP; Johnston et al. 2008), $36 \times 12\text{-m}$ dishes forming a 6-km diameter synthesis array, is currently being equipped with chequerboard Phased Array Feeds (PAFs; Chippendale et al. 2015) operating from 0.7 to 1.8 GHz and providing 30 sq degr field of view³. First ASKAP science results were published by Serra et al. (2015). At the same time, the old WSRT is being outfitted with Vivaldi PAFs (Apertif;

Oosterloo et al. 2010), operating from 1 to 1.8 GHz and providing 8 sq degr field of view. The MeerKAT radio telescope array (Blyth et al. 2015), $64 \times 13.5\text{-m}$ dishes forming an 8-km synthesis array, located in the Northern Cape of South Africa, is currently being equipped with a range of traditional, single-horn receivers. The fast 21-cm survey speed of ASKAP and Apertif will allow a full census of nearby gas-rich galaxies, while MeerKAT is ideal for deep follow-up H I observations. In particular, the *ASKAP HI All-Sky Survey* (known as WALLABY) and its sister survey, the *Westerbork Northern Sky HI Survey* (WNSHS), together aim to cover the whole sky out to a redshift of $z = 0.26$ (Koribalski 2012, Duffy et al. 2012). For galaxies at $D = 10$ Mpc, WALLABY will have a 5σ H I mass limit of $5 \times 10^6 M_{\odot}$ and a spatial resolution of 1.5 kpc ($30''$).

LVHIS is a significant step towards the ASKAP H I All Sky Survey (WALLABY; Koribalski 2012), as it delivers similar spectral line sensitivity and resolution. With WALLABY Early Science observations and data processing under way, the LVHIS data are essential for ASKAP data verification (e.g., flux, velocity and position accuracy). Four southern fields, each 30 square degrees in size, have been observed with an array of twelve and later sixteen PAF-equipped ASKAP antennas. One of the fields currently under investigation includes the M83 galaxy group for which plenty of LVHIS data exist. Once successfully calibrated we aim to combine ASKAP and ATCA H I data.

ACKNOWLEDGEMENTS

- This research has made extensive use of the NASA/IPAC Extragalactic Database (NED) which is operated by the Jet Propulsion Laboratory, Caltech, under contract with the National Aeronautics and Space Administration.
- The Digitised Sky Survey was produced by the Space Telescope Science Institute (STScI) and is based on photographic data from the UK Schmidt Telescope, the Royal Observatory Edinburgh, the UK Science and Engineering Research Council, and the Anglo-Australian Observatory.
- We thank Janine van Eymeren, Emma Kirby, Nic Bonne, Helmut Jerjen and Igor Karachentsev for their contributions in the early stages of the LVHIS project.
- We thank the referee for suggesting the addition of major and minor axes position-velocity (pv) diagrams which enrich the LVHIS galaxy atlas.

APPENDIX A: THE LVHIS GALAXY ATLAS

The LVHIS Galaxy Atlas is published by MNRAS as online supplementary material. It contains the ATCA H I moment maps and position-velocity diagrams of all LVHIS galaxies (apart from ESO294-G010, ESO245-G007, and NGC 5128) arranged on a single page per galaxy. Each page has six figure panels, displaying — from the top left to the bottom right — the galaxy’s integrated H I distribution typically overlaid onto its DSS B -band image, the mean H I velocity field (1. moment), the integrated H I distribution (0. moment), the H I velocity dispersion (2. moment),

³ ASKAP Early Science started in Oct 2016 with an array of twelve PAF-equipped antennas.

the major-axis pv -diagram and the minor-axis pv -diagram. Some galaxy properties as well as the contour levels are given in the captions. The synthesized beam is shown in the bottom left of each panel. North is up and east to the left. Unless otherwise stated, we show the low-resolution maps obtained using ‘natural’ weighting to emphasize the large-scale HI distribution, including diffuse emission in the outer disc. The LVHIS Galaxy Atlas (incl. FITS files) is also available on the LVHIS webpages.

REFERENCES

- Annibali, F., Tosi, M., Monelli, M., Sirianni, M., Montegriffo, P., Aloisi, A., Greggio, L. 2009, *AJ* 138, 169
- Banks, G.D., Disney, M.J., Knezek, P.M., and HIPASS Team 1999, *ApJ* 524, 612 (B99)
- Barnes, D.G., et al. 2001, *MNRAS* 322, 486
- Barnes, D.G., de Blok, W.J.G. 2004, *MNRAS* 351, 333
- Beaulieu, S.F., Freeman, K.C., Carignan, C., Lockman, F.J., Jerjen, H., 2006 *AJ* 131, 325
- Begum, A., Chengalur, J.N. 2003, *A&A* 409, 879
- Begum, A., Chengalur, J.N., Karachentsev, I.D., Kaisin, S.S., Sharina, M.E. 2006, *MNRAS* 365, 1220
- Begum, A., Chengalur, J.N., Karachentsev, I.D., Sharina, M.E., Kaisin, S.S. 2008, *MNRAS* 386, 1667
- Bell, E.F., McIntosh, D.H., Katz, N., Weinberg, M.D. 2003, *ApJS* 149, 289
- Blanton, M.R., et al. 2003, *ApJ* 592, 818
- Bonne, N.J. 2008, in "Galaxies in the Local Volume", Sydney, July 2007, eds. B.S. Koribalski & H. Jerjen, Springer, p. 45
- Boomsma, R., Oosterloo, T.A., Fraternali, F., van der Hulst, J.M., Sancisi, R. 2005, *A&A* 431, 65
- Bouchard, A., Da Costa, G.S., Jerjen, H. 2004, *PASP* 116, 1032
- Bouchard, A., Jerjen, H., Da Costa, G.S., Ott, J. 2005, *AJ* 130, 205832
- Bouchard, A., Jerjen, H., Da Costa, G.S., Ott, J. 2007, *AJ* 133, 261
- Bouchard, A., Da Costa, G.S., Jerjen, H. 2009, *AJ* 137, 3038 (B09)
- Broeils, A.H. 1992, PhD Thesis, University of Groningen
- Broeils, A.H., Rhee, M.-H. 1997, *A&A* 324, 877
- Bureau, M., Freeman, K.C., Pfeitzber, D.W. 1999, *AJ* 118, 2158
- Buyle, P., Michielsen, D., de Ricke, S., Ott, J., Dejonghe, H. 2006, *MNRAS* 373, 793
- Calabretta, M.R., Staveley-Smith, L., Barnes, D.G. 2014, *PASA* 31, 7
- Cannon, J.M., Dohm-Palmer, R.C., Skillman, E.D., Bomans, D.J., Côté, S., Miller, B.W. 2003, *AJ* 126, 2806
- Cannon, J.M., McClure-Griffiths, N.M., Skillman, E.D. Côté, S. 2004, *ApJ* 607, 274
- Carignan, C., Puche D. 1990a, *AJ* 100, 394
- Carignan, C., Puche D. 1990b, *AJ* 100, 641
- Carignan, C., Beaulieu, S., Freeman, K.C. 1990, *AJ* 99, 178
- Chemlin, L., Carignan, C., Drouin, N., Freeman, K.C. 2006, *AJ* 132, 2527
- Chippendale, A.P., et al. 2015, International Symposium on Antennas and Propagation (ISAP), IEEE (astro-ph/1509.05489)
- Chung, A., van Gorkom, J.H., Kenney, J.D.P., Crawl, H., Vollmer, B. 2009, *AJ* 138, 1741
- Côté, S., Carignan, C., Freeman, K. 2000, *AJ* 120, 3027
- Côté, S., Draginda, A., Skillman E.D., Miller, B.W. 2009, *AJ* 138, 1037 (C09)
- Crnojević, D., Grebel, E.K., Cole, A.A. 2011, *A&A* 530, 59
- Crnojević, D., Grebel, E.K., Cole, A.A. 2012, *A&A* 541, 131
- Curran, S.J., Koribalski, B.S., Bains, I. 2008, *MNRAS* 389, 63
- Da Costa, G.S., Jerjen, H. Bouchard, A. 2008, in "Galaxies in the Local Volume", Sydney, July 2007, eds. B.S. Koribalski & H. Jerjen, Springer, p. 123
- Dalcanton, J.J., et al. 2009, *ApJS* 183, 67
- Dale, D.A., et al. 2009, *ApJ* 703, 517
- Davidge, T.J. 2007, *ApJ* 664, 820
- Davidge, T.J. 2008, *AJ* 135, 1636
- de Blok, W.J.G., Walter, F., Brinks, E., Trachternach, C., Oh, S.-H., Kennicutt, R.C. 2008, *AJ* 136, 2648
- Dénes, H., Kilborn, V.A., Koribalski, B.S. 2014, *MNRAS* 444, 667
- Domgörgen, H., Dettmar, R.-J. 1997, *A&A* 322, 391
- Domgörgen, H., Dahlem, M., Dettmar, R.-J. 1996, *A&A* 313, 96
- Donovan, J.L., et al. 2009, *AJ* 137, 5037
- Duffy, A.R., Meyer, M.J., Staveley-Smith, L., Bernyk, M., Croton, D.J., Koribalski, B.S., Gerstmann, D., Westerlund, S. 2012, *MNRAS* 426, 3385
- Doyle, M.T., et al. 2005, *MNRAS* 361, 34
- Elmoultie, M., Koribalski, B.S., Gordon, S., Taylor, K., Houghton, S., Lavezzi, T., Haynes, R.F. Jones, K.L. 1998a, *MNRAS* 297, 49
- Elmoultie, M., Haynes, R.F. Jones, K.L., Sadler, E.M., Ehle, M. 1998b, *MNRAS* 297, 1202
- Elson, E.C., de Blok, W.J.G., Kraan-Korteweg, R.C. 2013, *MNRAS* 429, 2550
- Elson, E.C., de Blok, W.J.G., Kraan-Korteweg, R.C. 2012, *AJ* 143, 1
- Elson, E.C., de Blok, W.J.G., Kraan-Korteweg, R.C. 2011b, *MNRAS* 415, 323
- Elson, E.C., de Blok, W.J.G., Kraan-Korteweg, R.C. 2011a, *MNRAS* 411, 200
- Elson, E.C., de Blok, W.J.G., Kraan-Korteweg, R.C. 2010, *MNRAS* 404, 2061
- Eskridge, P.B., de Grijs, R., Anders, P., Windhorst, R.A., Mager, V.A., Jansen, R.A. 2008, *AJ* 135, 120
- Ferguson, A.M.N., Wyse, R.F.G., Gallagher, J.S. 1996, *AJ* 112, 2567
- For, B.-Q., Koribalski, B.S., Jarrett, T.H. 2012, *MNRAS* 425, 1934
- Fouque, P.,ourgoulhon, E., Chamaraux, P., Paturel, G. 1992, *A&AS* 93, 211
- Freeman, K.C., Karlsson, B., Lynga, G., Burrell, J.F., van Woerden, H., Goss, W.M., Mebold, U. 1977, *A&A* 55, 445
- Gallart, C., Martín-Delgado, D., Gómez-Flechoso, M.A., Mateo, M. 2001, *AJ* 121, 2572
- Gardner, F.F., Whiteoak, J.B. 1976, *PASA* 3, 63
- Gieren, W., Pietrzyński, G., Soszyński, I., Bresolin, F., Kudritzki, R.-P. 2008, *ApJ* 672, 266
- Grise, F., Pakull, M.W., Soria, R., Motch, C., Smith, I.A., Ryder, S.D., Böttcher, M. 2008, *A&A* 486, 151
- Grossi, M., et al. 2007, *MNRAS* 374, 107
- Heald, G., et al. 1022, *A&A* 526, 118
- Heisler, C.A., Hill, T.L., McCall, M.L., Hunstead, R.W. 1997, *MNRAS* 285, 374
- Herrmann, K.A., Ciardullo, R., Feldmeier, J.J., Vinciguerra, M. 2008, *ApJ* 683, 630
- Higgs, C.R., et al. 2016, *MNRAS* 458, 1678
- Huchtmeier, W.K. 1979, *A&A* 75, 170
- Huchtmeier, W.K., Bohnenstengel, H.-D. 1981, *A&A* 100, 72
- Hunter, D.A., et al. 2012, *AJ* 144, 134
- Irwin, M., Tolstoy, E. 2002, *MNRAS* 336, 643
- Jacobs, B.A., Rizzi, L., Tully, R.B., Shaya, E.J., Makarov, D.I., Makarova, L. 2009, *AJ* 138, 332
- Jarrett, T.H. et al. 2013, *AJ* 145, 6
- Jerjen, H., Freeman, K.C., Binggeli, B. 1998, *AJ* 116, 2873
- Jerjen, H., Freeman, K.C., Binggeli, B. 2000, *AJ* 119, 166
- Johnson, M., Kamphuis, P., Koribalski, B.S., Wang, J., Oh, S.-H., Hill, A., O'Sullivan, S., Haan, S., Serra, P. 2015, *MNRAS* 451, 3192
- Johnston, S., et al. 2008, *ExA* 22, 151
- Jones, K.L., Koribalski, B.S., Elmoultie, M., Haynes, R.F. 1999, *MNRAS* 302, 649
- Józsa, G.I.G., Kenn, F., Klein, U., Oosterloo, T.A. 2007, *A&A* 468, 731
- Juraszek, S., et al. 2000, *AJ* 119, 1627
- Kaisin, S.S., Karachentsev, I.D. 2006, *Astrophysics* 49, 287
- Kaisin, S.S., Kasparova, A.V., Knyazev, A.Yu., Karachentsev, I.D. 2007, *Astronomy Letters* 33, 283
- Kamphuis, P., Józsa, G.I.G., Oh, S.-H., Spekkens, K., Urbanic, N., Serra, P., Koribalski, B.S., Dettmar, R.-J. 2015, *MNRAS* 452, 3139
- Karachentsev, I.D., et al. 2000, *ApJ* 542, 128
- Karachentsev, I.D., Sharina, M.E., Dolphin, A.E., Grebel, E.K.,

- Geisler, D., Guhathakurta, P., Hodge, P.W., Karachentseva, V.E., Sarajedini, A., Seitzer, P. 2002, *A&A* 385, 21
- Karachentsev, I.D., Makarov, M.E., Sharina, M.E., Dolphin, A.E., Grebel, E.K., Geisler, D., Guhathakurta, P., Hodge, P.W., Karachentseva, V.E., Sarajedini, A., Seitzer, P. 2003, *A&A* 398, 479
- Karachentsev, I.D., Grebel, E.K., Sharina, M.E., Dolphin, A.E., Geisler, D., Guhathakurta, P., Hodge, P.W., Karachentseva, V.E., Sarajedini, A., Seitzer, P. 2003, *A&A* 404, 93
- Karachentsev, I.D., Karachentseva, V.E., Huchtmeier, W.K., Makarov, D.I. 2004, *AJ* 127, 2031
- Karachentsev, I.D., Kaisin, S.S., Tsvetanov, Z., Ford, H. 2005, *A&A* 434, 935
- Karachentsev, I.D., et al. 2006, *AJ* 131, 1361
- Karachentsev, I.D., et al. 2007, *AJ* 133, 504
- Karachentsev, I.D., Makarov, D.I., Kaisina, E.I. 2013, *AJ* 145, 101 (K13)
- Karachentsev, I.D., Kaisina, E.I. 2013, *AJ* 146, 46
- Karachentsev, I.D., Makarov, D.I., Kaisina, E. 2013, *AJ* 145, 101
- Kennicutt, R., et al. 2003, *PASP* 115, 928
- Kennicutt, R.C. Jr., Lee, J.C., Funes, S.J., José, G., Sakai, S., Akiyama, S. 2008, *ApJS* 178, 247
- Kennicutt, R.C., et al. 2011, *PASP* 123, 1347
- Karachentsev, I.D., et al. 2008, in "Galaxies in the Local Volume", Sydney, July 2007, eds. B.S. Koribalski & H. Jerjen, Springer, p. 21
- Kilborn, V.A., et al. 2002, *AJ* 124, 690
- Kirby, E., Jerjen, H., Ryder, S., Driver, S. 2008a, in "Galaxies in the Local Volume", Sydney, July 2007, eds. B.S. Koribalski & H. Jerjen, Springer, p. 49
- Kirby, E., Jerjen, H., Ryder, S., Driver, S. 2008b, *AJ* 136, 1866
- Kirby, E.M., Koribalski, B.S., Jerjen, H., López-Sánchez, Á.R. 2012, *MNRAS* 420, 2924
- Kobulnicky, H.A., Skillman, E.D. 1995, *ApJ* 454, L121
- Koribalski, B.S., Whiteoak, J.B., Houghton, S. 1995, *PASA* 12, 20
- Koribalski, B.S., Staveley-Smith, L., + HIPASS/ZOA Teams 2004, *AJ* 128, 16
- Koribalski, B.S. 2007, in "Groups of Galaxies in the Nearby Universe", ESO workshop, eds. Savine, L., Ivanov, V.D., Borissova, J., p. 27
- Koribalski, B.S., and the LVHIS team 2008, in "Galaxies in the Local Volume", Sydney, July 2007, eds. B.S. Koribalski & H. Jerjen, Springer, p. 41
- Koribalski, B.S., López-Sánchez, Á.R. 2009, *MNRAS* 400, 1749
- Koribalski, B.S. 2010, in "Galaxies in Isolation: Exploring Nature vs Nurture", eds. L. Verdes-Montenegro, A. del Olmo, and J. Sulentic, *ASPC* 421, 137
- Koribalski, B.S. 2012, *PASA* 29, 359
- Koribalski, B.S. 2015, *Proc. IAU Symposium* 309, Cambridge University Press, eds. B. L. Ziegler, F. Combes, H. Dannerbauer, M. Verdugo, p. 39
- Koribalski, B.S. 2017, *Proc. IAU Symposium* 321, eds. A. Gil de Paz, J. Knapen & J. Lee, Cambridge University Press, p. 232
- Kouwenhoven, M.B.N., Bureau, M., Kim, S., de Zeeuw, P.T. 2007, *A&A* 470, 123
- Kraan-Korteweg, R.C., Tammann, G.A. 1979, *AN* 300, 181
- Kreckel, K., Peebles, P.J.E., van Gorkom, J.H., van de Weygaert, R., van der Hulst, J.M. 2011, *AJ* 141, 204
- Larsen, S.S., Richtler, T. 1999, *A&A* 345, 59
- Lauberts, A. 1982, ESO/Uppsala survey of the ESO(B) atlas, Garching: European Southern Observatory
- Lauberts, A., Valentijn, E.A. 1989, The surface photometry catalogue of the ESO-Uppsala galaxies, Garching: European Southern Observatory
- Lee, M.G., Byun, Y.-Ik. 1999, *AJ* 118, 817
- Lee, H., Grebel, E.K., Hodge, P.W. 2003, *A&A* 401, 141
- Lee, J.C., Kennicutt, R., Funes, S.J.J.G. Funes, Sakai, S., Akiyama, S. 2009, *ApJ* 692, 1305
- Lee, J.C., Gil de Paz, A., Kennicutt, R., et al. 2011, *ApJS* 192, 6
- Leroy, A.K., Walter, F., Bigiel, F., et al. 2009, *AJ* 137, 4670
- Lianou, S., Cole, A.A. 2013, *A&A* 549, 47
- López-Sánchez, Á.R., Koribalski, B.S., van Eymeren, J., Esteban, C., Kirby, E., Jerjen, H., Lonsdale, N. 2012, *MNRAS* 419, 1051
- López-Sánchez, Á.R., Koribalski, B.S., Esteban, C., Garcia-Rojas, J. 2008, in "Galaxies in the Local Volume", Sydney, July 2007, eds. B.S. Koribalski & H. Jerjen, Springer, p. 53
- Lucero, D., Carignan, C., Elson, E.C., Randriamampandry, T.H., Jarrett, T.H., Oosterloo, T.A., Heald, G.H. 2015, *MNRAS* 450, 3935
- Madore, B.F., Freedman, W.L., Catanzarite, J., Navarrete, M. 2009, *ApJ* 694, 1237
- Malin, D., Hadley, B. 1997, *PASA* 14, 52
- Manthey, E., Oosterloo, T. 2008, in "Galaxies in the Local Volume", Astrophysics and Space Science Proc., Springer Netherlands, eds. Koribalski & Jerjen, p. 303
- Marlowe, A.T., Meurer, G.R., Heckmann T.M. 1999, *ApJ* 522, 183
- Martínez-Delgado, D., Gallart, C., Aparicio, A. 1999, *AJ* 118, 862
- McConnachie, A.W. 2012, *AJ* 144, 4
- McKinley, B., et al. 2018, *MNRAS* 474, 4056
- Meurer, G.R., Carignan, C., Beaulieu, S.F., Freeman, K.C. 1996, *AJ* 111, 1551
- Meurer, G.R., Staveley-Smith, L., Killeen, N.E.B. 1998, *MNRAS* 300, 705
- Meurer, G.R., et al. 2006, *ApJS* 165, 307
- Meyer, M., + HIPASS Team 2004, *MNRAS* 350, 1197
- Miller, B.W. 1996, *AJ* 112, 991
- Minchin, R., et al. 2003, *MNRAS* 346, 787
- Mould, J., Sakai, S. 2008, *ApJ* 686, L75
- Müller, O., Jerjen, H., Binggeli, B. 2015, *A&A* 583, 79
- O'Brien, J.C., Freeman, K.C., van der Kruit, P.C., Bosma, A. 2010, *A&A* 515, A60
- Oh, S.-H., de Blok, W.J.G., Brinks, E., Walter, F., Kennicutt, R.C.Jr. 2011, *AJ* 141, 193
- Oh, S.-H., Staveley-Smith, L., Spekkens, K., Kamphuis, P., Koribalski, B.S. 2018, *MNRAS* 473, 3256
- Oosterloo, T., Verheijen, M., van Cappellen, W. 2010, *Proc. ISKAF2010* (astro-ph/1007.5141)
- Ott, M., Whiteoak, J.B., Henkel, C., Wielebinski, R. 2001, *A&A* 372, 463
- Ott, J., Stilp, A.M., Warren, S.R., Skillman, E., Dalcanton, J., Walter, F., de Blok, W.J.G., Koribalski, B.S., West, A. 2012, *AJ* 144, 123
- Weisz, D. 2008, in "Galaxies in the Local Volume", Sydney, July 2007, eds.
- Parodi, B.R., Barazza, F.D., Binggeli, B. et al. 2002, *A&A* 388, 29
- Parodi, B.R., Binggeli, B. 2003, *A&A* 398, 501
- Phillips, M.M., Jenkins, C.R., Dopita, M.A., Sadler, E.M., Biette, L. 1986, *AJ* 91, 1062
- Pritzl, B.J., et al. 2003, *ApJ* 596, L47
- Puche, D., et al. 1991, *AJ* 101, 456
- Radburn-Smith, D.J., et al. 2012, *ApJ* 753, 138
- Radburn-Smith, D.J., et al. 2014, *ApJ* 780, 105
- Rejkuba, M. 2004, *A&A* 413, 903
- Roberts, M.S., Haynes, M.P. 1994, *ARA&A* 32, 115
- Rogstad, D.H., Lockhart, I.A., Wright, M.C.H. 1974, *ApJ* 193, 309
- Rossa, J., Dettmar, R.-J. 2003, *A&A* 406, 505
- Ryan-Weber, E., et al. 2002, *AJ* 124, 1954
- Ryan-Weber, E., et al. 2004, *AJ* 127, 1431
- Ryan-Weber, E., et al. 2008, *MNRAS* 384, 535
- Ryder, S.D., Staveley-Smith, L., Malin, D.F., Walsh, W. 1995, *AJ* 109, 1592
- Ryder, S.D., Dopita, M. 1993, *ApJS* 88, 415
- Sault, R.J., Teuben, P.J., Wright, M.C.H. 1995, *ASPC* 77, 433

- Saviane, I. & Jerjen, H. 2007, *AJ* 133, 1756
- Schiminovich, D., van Gorkom, J.H., van der Hulst, J.M., Kasow, S. 1994, *ApJ* 423, L101
- Schlafly, E.F., Finkbeiner, D. P. 2011, *ApJ* 737, 103
- Serra, P., et al. 2012, *MNRAS* 422, 1835
- Serra, P., Koribalski, B.S., Kilborn, V., et al. 2015, *MNRAS* 452, 2680
- Seth, A.C., Dalcanton, J.J., de Jong, R.C. 2005, *AJ* 129, 1331
- Shao, L., Koribalski, B.S., Wang, J., et al. 2017, *MNRAS*, submitted
- Simpson, C.E., Gottesman, S.T. 2000, *AJ* 120, 2975
- Skillman, E.D., Terlevich, R., Teuben P.J., van Woerden, H. 1988, *A&A* 198, 33
- Stanimirovic, S. Staveley-Smith, L., Dickey, J.M., Sault, R.J., Snowden, S.L. 1999, *MNRAS* 302, 417
- Staveley-Smith, L., Kim, S., Calabretta, M.R., Haynes, R.F., Kesteven, M.J. 2003, *MNRAS* 339, 87
- Staveley-Smith, L., Kraan-Korteweg, R.C., Schröder, A.C., Henning, P.A., Koribalski, B.S., Stewart, I.M., Heald, G. 2016, *AJ* 151, 52
- St. Germain, J., Carignan, C., Côté, S., Oosterloo, T. 1999, *AJ* 118, 1235
- Struve, C., Oosterloo, T.A., Morganti, R., Saripalli, L. 2010, *A&A* 515, 67
- Thim, F., Tammann, G.A., Saha, A., Dolphin, A., Sandage, A., Tolstoy, E., Labhardt, L. 2003, *ApJ* 590, 256
- Thilker, D., et al. 2007, *ApJS* 173, 538
- Thomson, R.C. 1992, *MNRAS* 257, 689
- Tosi, M., et al. 2001, *AJ* 122, 1271
- Tüllmann, R., Rosa, M.R., Elwert, T., Bomans, D.J., Ferguson, A.M.N., Dettmar, R.-J. 2003, *ESO Messenger* 114, 39
- Tully, B.R., et al. 2006, *AJ* 132, 729
- Tully, B.R., et al. 2013, *AJ* 146, 86
- van der Hulst, J.M., van Albada, T.S., Sancisi, R. 2001, *ASP Conf. Proc.*, eds. J.E. Hibbard, M. Rupen and J.H. van Gorkom, Vol. 240, p. 451
- van Eymeren, J., Marcelin, M., Bomans, D.J. 2008, in "Galaxies in the Local Volume", Sydney, July 2007, eds. B.S. Koribalski & H. Jerjen, Springer, p. 341
- van Eymeren, J. 2008, PhD Thesis, University of Bochum
- van Eymeren, J., Marcelin, M., Koribalski, B.S., Dettmar, R.-J., Bomans, D.J., Gach, J.-L., Balard, P. 2009a, *A&A* 493, 511
- van Eymeren, J., Marcelin, M., Koribalski, B., Dettmar, R.-J., Bomans, D.J., Gach, J.-L., Balard, P. 2009b, *A&A* 505, 105
- van Eymeren, J., Trachternach, C., Koribalski, B., Dettmar, R.-J. 2009c, *A&A* 505, 1
- van Eymeren, J., Koribalski, B.S., López-Sánchez, Á.R., Dettmar, R.-J., Bomans, D.J. 2010, *MNRAS* 407, 113
- van Gorkom, J.H., van der Hulst, J.M., Haschick, A.S., Tubbs, A.D. 1990, *AJ* 99, 1781
- van Woerden, H., van Driel, W., Braun, R., Rots, A.H. 1993, *A&A* 269, 15
- Verdes-Montenegro, L., Bosma A., Athanassoula E. 2002, *A&A* 389, 825
- de Vaucouleurs, G., de Vaucouleurs, A., Corwin, H.G., Jr., Buta, R.J., Paturel, G., Fouque, P. 1991, *Third Reference Catalogue of Bright Galaxies*, Springer, New York [RC3]
- Wang, J., et al. 2013, *MNRAS* 433, 270
- Wang, J., Serra, P., Józsa, G.I.G., Koribalski, B.S., van der Hulst, T., Kamphuis, P., Cheng, L., Fu, J., Xiao, T., Overzier, R., Wieringa, M., Wang, E. 2015, *MNRAS* 453, 2399
- Wang, J., Koribalski, B.S., Serra, P., van der Hulst T., Roychowdhury, S., Kamphuis, P., Chengalur, J.N. 2016, *MNRAS* 460, 2143
- Wang, J., Koribalski, B.S., et al. 2017, *MNRAS* 472, 3029
- Walsh, W. 1997, PhD Thesis, University of NSW
- Walter, F., Brinks, E., de Blok, E., Bigiel, F., Kennicutt, R. C., Thornley, M.D., Leroy, A.K. 2008, *AJ* 136, 2563
- Warren, B., Jerjen, H., Koribalski, B. 2004, *AJ* 128, 1152
- Warren, B., Jerjen, H., Koribalski, B. 2006, *AJ* 131, 2056
- Warren, B., Jerjen, H., Koribalski, B. 2007, *AJ* 134, 1849
- Westmeier, T., Braun, R., Koribalski, B.S. 2011, *MNRAS* 410, 2217
- Westmeier, T., Koribalski, B.S., Braun, R. 2013, *MNRAS* 434, 3511
- Westmeier, T., Staveley-Smith, L., Calabretta, M., Jurek, R., Koribalski, B.S., Meyer, M., Popping, A., Wong, O.I. 2015, *MNRAS* 453, 338
- Westmeier, T., et al. 2017, *MNRAS* 472, 4832
- Wilcots, E.M., Miller, B.W. 1998, *AJ* 116, 2363
- Wilson, W.E., et al. 2011, *MNRAS* 416, 832
- Wong, O.I., et al. 2006, *MNRAS* 371, 1855
- Wong, O.I., Meurer, G.R., Zheng, Z., Heckman, T.M., Thilker, D.A., Zwaan, M.A. 2016, *MNRAS* 460, 1106
- Woodley, K.A. 2006, *AJ* 132, 2424
- Young, L.M., Lo, K.Y. 1997, *ApJ* 490, 710
- Young, L.M., Skillman, E.D., Weisz, D.R., Dolphin, A.E. 2007, *ApJ* 659, 331
- Young, T., Jerjen, H., López-Sánchez, Á.R., Koribalski, B.S. 2014, *MNRAS* 444, 3052
- Yun, M.S., Ho, P.T.P., Lo, K.Y. 1993, *ApJ* 411, L17
- Zwaan, M., Staveley-Smith, L., Koribalski, B.S., et al. 2003, *AJ* 125, 2842

